Sensor Array Processing: Localisation of Wireless Sources

by

Zexi Fang

A Thesis submitted in fulfillment of requirements for
the degree of Doctor of Philosophy (PhD)
and
the Diploma of Imperial College London (DIC)

March 2018

Supervisor: Prof. A. Manikas

Imperial College London
Department of Electrical and Electronic Engineering

Abstract

In this thesis, various subspace array processing techniques for wireless source localisation are presented and investigated in the following three aspects.

First, in the environment of indoor optical wireless communications, the paths of different sources and/or from different reflectors may impinge on the receiver from closely spaced directions with a high probability. In this case, the ranges of the paths, together with their directions, are important especially for isolating the desired source from the interferers. A blind multi-source localisation approach, which can be used as a channel estimator in the receiver of a communication system, is proposed for direction, range, and path gain estimation. Utilising the above channel parameter estimates, two subspace multibeam beamformers are also presented to achieve complete interference cancellation.

Second, in applications such as wireless sensor networks and ubiquitous computing, both the location and orientation of an array are important parameters of interest to be estimated. Hence, array localisation and orientation estimation approaches are proposed for two cases. In the first case, a number of sources of known locations are employed to estimate these parameters of a receiver array. In the second case, a receiver array is utilised to estimate these parameters of multiple sources with each one being a transmitter array.

Last, when sources operate in the near field of an array, the spherical wave propagation model needs to be considered. A problem associated with such a scenario is source localisation under the wideband assumption, where the wavefront of a baseband signal varies when traversing through the sensors of the array. Two novel approaches with the employment of the subcovariance of the received signal and the rotation of the array reference point are proposed to localise multiple sources under the wideband assumption.

Throughout the thesis, computer simulation studies are presented for evaluating the performance of the proposed approaches.

Declaration of Originality

I hereby declare that this thesis is my own work. Where other sources of information have been used, they have been acknowledged.

Copyright Declaration

Acknowledgements

First, I would like to express my gratitude to my supervisor Professor Athanassios Manikas, who has given me an insight into the field of array processing. Throughout my PhD research, he has given me his expert advice and extraordinary support, without which my work would not have been possible.

Next, I would like to thank my colleagues and friends in the Communications and Signal Processing Group. Especially, I would thank Hamdi, He, Thibaud, and Vidhya for all the technical discussions we had and for their great friendship over the past four years.

Also, I am particularly grateful to my friends Alireza and Yifan, who are always willing to help me overcome the difficulties I have encountered and provide me with invaluable suggestions.

Last but not least, I would like to acknowledge my parents for showing faith in me. They have always been patient, encouraging, and supportive over my life. I would not have reached this far without them.

Table of Contents

List of Figures

List of Tables

Notation

a, A	Scalar
$\underline{a}, \underline{A}$	Column vector
$\mathbb{A}$	Matrix
$(\cdot)^*$	Complex conjugate
$(\cdot)^T$	Transpose
$(\cdot)^H$	Hermitian transpose
$(\cdot)^\#$	Moore–Penrose pseudoinverse
$\lvert\cdot\rvert$	Absolute value
$\lVert\cdot\rVert$	Euclidean norm
$\lfloor\cdot\rfloor$	Floor function
$\odot$	Hadamard product
$\oslash$	Hadamard division
$\otimes$	Kronecker product
$\boxtimes$	Khatri–Rao product
$\underline{A}^b$	Element-wise b-th power of $\underline{A}$
$\mathbb{A}^{\odot b}$	Element-wise b-th power of $\mathbb{A}$
$\mathrm{diag}(\underline{A})$	Diagonal matrix formed from $\underline{A}$
$\underline{\mathrm{diag}}(\mathbb{A})$	Column vector formed from the diagonal of $\mathbb{A}$
$\mathrm{eig}_i(\mathbb{A})$	i-th eigenvalue of $\mathbb{A}$
$\exp(\underline{A})$	Element-wise exponential of $\underline{A}$

$\text{rank}(\mathbb{A})$	Rank of $\mathbb{A}$
$\text{rect}(\cdot)$	Rectangular function
$\text{tr}(\mathbb{A})$	Trace of $\mathbb{A}$
$\text{vec}(\mathbb{A})$	Column-wise vectorisation of $\mathbb{A}$
$\mathcal{E}\{\cdot\}$	Expectation operator
$\underline{1}_N$	Column vector of N ones
$\underline{0}_N$	Column vector of N zeros
$\mathbb{I}_N$	$N \times N$ identity matrix
$\mathbb{O}_{M\times N}$	$M \times N$ zero matrix
$\mathcal{Z}$	Set of integers
$\mathcal{R}$	Set of real numbers
$\mathcal{C}$	Set of complex numbers

Abbreviations

AIC	Akaike information criterion
AWGN	additive white Gaussian noise
CCI	co-channel interference
DAC	digital-to-analogue converter
DOA	direction of arrival
DOD	direction of departure
ESPRIT	estimation of signal parameters via rotational invariance techniques
EVB	eigenvalue-based
ISI	intersymbol interference
LOS	line-of-sight
MAI	multiple access interference
MDL	minimum description length
MIMO	multiple-input multiple-output
MISO	multiple-input single-output
ML	maximum likelihood
MMSE	minimum mean squared error
MUSIC	multiple signal classification
NBA	narrowband assumption
NLOS	non-line-of-sight
OWC	optical wireless communications

RF	radio frequency
RMSE	root mean squared error
RRB	reference-rotation-based
RSS	received signal strength
Rx	receiver
SCB	subcovariance-based
SIMO	single-input multiple-output
SISO	single-input single-output
SNIR	signal-to-noise-plus-interference ratio
SNR	signal-to-noise ratio
STAR	spatiotemporal array
TDL	tapped delay line
TDOA	time difference of arrival
TOA	time of arrival
Tx	transmitter
WBA	wideband assumption

Chapter 1

Introduction

An array is a collection of sensors spatially distributed in three-dimensional real space with a common array reference point [1]. The signals received at the array convey the spatial and temporal information of the signal environment, and array processing is mainly concerned with extracting and exploiting this information to solve problems of interest. In general, there exist three major problems in array processing, which are the detection of the number of sources, estimation of their parameters, and reception of desired signals. They have been extensively studied in the literature for various applications such as wireless communications [2, 3], sonars [4, 5], radars [6, 7], and wireless sensor networks [8–13].

A key concept in array processing is the array manifold vector, which represents the complex array response to a source [1]. It maps the signal of the source to a one-dimensional subspace embedded in a multidimensional complex observation space. Such subspaces of all the sources in the environment constitute the signal subspace, which is completely determined by their corresponding array manifold vectors. Along with the concept of the array manifold vector is subspace array processing techniques, which exploit the information of the signal subspace (or its complementary noise subspace) to solve the detection, estimation, and reception

problems.

In theory, the number of sources can be inferred from the multiplicity of the minimum eigenvalue of the covariance matrix of the received signal vector, as these eigenvalues correspond to the noise subspace. In practice, since the covariance matrix is estimated from a finite number of samples, the smallest eigenvalues, which are theoretically identical, generally differ. In this case, a subjunctive threshold can be utilised to distinguish the most significant eigenvalues from the least significant ones based on a sequence of hypothesis tests [14, 15]. Besides, objective detection can be achieved by minimising information criteria such as the Akaike information criterion (AIC) or minimum description length (MDL) principle [16–18].

In terms of parameter estimation, a widely employed subspace approach is the multiple signal classification (MUSIC) algorithm, which searches over parameter space the array manifold vectors that are orthogonal to the noise subspace [19]. This superresolution algorithm advantages over other estimation algorithms such as maximum likelihood (ML) and maximum entropy in its high estimation precision. There are also many variants of the MUSIC algorithm. One of them is the root-MUSIC algorithm, which transforms the cost function to a polynomial and estimates the parameters by finding its roots closest to the complex unit circle [20–22]. Another widely used subspace estimation method is the estimation of signal parameters via rotational invariance techniques (ESPRIT), which exploits the rotational invariance of signal subspaces using an array of a translational invariance structure; i.e., sensor doublets [23].

In addition, with regards to the reception problem, various beamforming algorithms are present in the literature, including the steering vector beamformer [24], Wiener–Hopf beamformer [25], Capon's beamformer [26, 27], and subspace beamformer [28]. In particular, the subspace beamformer steers nulls towards interferers by projecting the received signal vector onto the subspace orthogonal to the inter-

ference subspace to achieve complete interference cancellation.

Commonly, in many applications where the above approaches are utilised to solve the detection, estimation, and reception problems, source ranges are not taken into consideration in the signal model. By contrast, source localisation involves both source directions and ranges, and is a problem of significant interest in array processing. For instance, in array communications, localisation approaches can be utilised as channel estimators for estimating source locations, which can then be employed to design beamformers that better isolate desired signals from interferers. Besides, when sources operate in the near field of an array, the spherical wave propagation model needs to be considered, which essentially incorporates both source directions and ranges. To this end, various problems associated with source localisation will be scrutinised in the thesis. Specifically, Chapter 2 is concerning arrayed indoor optical wireless communications (OWC) where the environment is heavily interfered, while Chapters 3 to 5 are regarding localisation and orientation estimation problems (mainly) brought by spherical wave propagation.

The rest of this chapter is organised as follows. In Section 1.1, the state of the art of the topics that will be studied in this thesis is detailed in four aspects. In Section 1.2, the challenges and gaps posed in wireless source localisation are presented. Last, in Section 1.3, the scope and structure of the thesis are given.

1.1 State of the Art

1.1.1 Optical Wireless Communications

An OWC system is generally an electrical–optical–electrical chain: Information is first carried by electrical signals, which are then converted to electromagnetic waves (optical signals) using photoemitters. The optical signals are radiated to free space, received by photosensors, and converted back to electrical signals. The

reception can be either incoherent by directly counting the number of photons, or coherent by using beamsplitters and optical local oscillators. The received electrical signals are further processed for information recovery [29].

The spectrum used in an OWC system has a broad range and includes both the visible and invisible (i.e., infrared and ultraviolet) optical bands. Particularly, if visible signals are utilised, such a system is referred to as a visible light communication system. In contrast to invisible signals that carry information only, visible signals can provide illumination at the same time. Since optical signals cannot penetrate opaque obstacles due to their high frequency, OWC is well suited for indoor communications. However, optical access points (namely, photoemitters and photosensors) can be connected to wired backbones for inter-room communications.

The configuration of an indoor OWC system is classified according to two criteria as shown in Figure 1.1 [30]. The first criterion is the directionality of the photoemitter and photosensor. If a directional photoemitter and photosensor that are aimed towards each other are employed as in Figure 1.1(a) or 1.1(b), then such a configuration is a directed system. Directed systems maximise signal power efficiency as path loss is minimised; however, they are less flexible, especially when mobile terminals are present in the environment, the directionality of which cannot be easily controlled. On the other hand, if a wide-angle photoemitter and photosensor that are not aimed towards each other are utilised as in Figure 1.1(e) or 1.1(f), then it is a nondirected system. Nondirected systems suffer from the loss in signal-to-noise ratio (SNR) but are more convenient for mobile terminals. Moreover, a mix of directed and nondirected links can also be exploited as in Figure 1.1(c) or 1.1(d); such a configuration is a hybrid system.

The second criterion is the existence of the line-of-sight (LOS) path between the photoemitter and photosensor. If there exists the LOS path as in Figure 1.1(a),

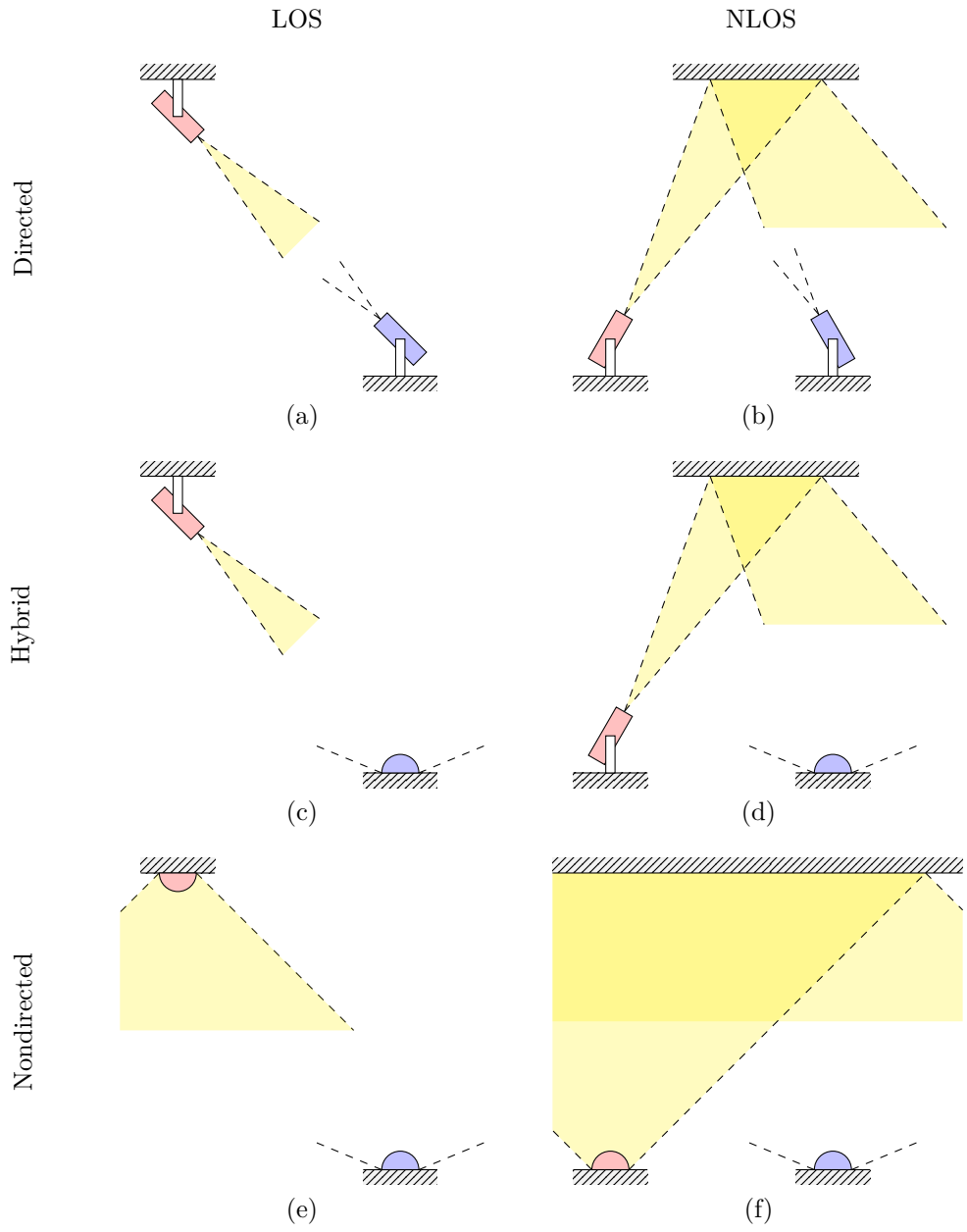

Figure 1.1: Classification of OWC configurations. The classification criteria are the directionality of the photoemitter (red) and photosensor (blue) as well as the existence of the LOS path. (a) Directed–LOS system. (b) Directed–NLOS system. (c) Hybrid–LOS system. (d) Hybrid–NLOS system. (e) Nondirected–LOS system. (f) Nondirected–NLOS system.

1.1(c) or 1.1(e), then this configuration is an LOS system. Similarly, this configuration maximises power efficiency due to the existence of the LOS path. Otherwise, if there only exist non-line-of-sight (NLOS) paths due to the reflections from the walls, ceiling, and floor of the indoor environment as in Figure 1.1(b), 1.1(d) or 1.1(f), then it is an NLOS system. This configuration advantages in the ease of use at the cost of the loss in power efficiency. Based on the above criteria, six common configurations of an indoor OWC system can be formed, among which the nondirected–LOS system as shown in Figure 1.1(e) will be studied in this thesis.

The above configurations are generally concerning single-input single-output (SISO) systems, but can also be extended to single-input multiple-output (SIMO), multiple-input single-output (MISO), and multiple-input multiple-output (MIMO) systems. In SIMO systems, an array of photosensors is utilised at the receiver and spatial diversity is achieved by efficiently combining (e.g., through equal gain combining) the signals received at all the photosensors for the mitigation of channel fading and the improvement in system performance [31–34]. Spatial diversity can also be achieved at the transmitter in MISO systems by repetition coding or path selection, for reducing the scintillation of optical signals [35–37]. In addition, both transmit and receive diversity can be achieved in MIMO systems, which are extensively studied in the literature [38–49]. In contrast to SISO systems that may suffer from huge path loss, the systems involving photoemitter and/or photosensor arrays advantage in the improvement in transmission rate and the reduction in power loss.

Due to the signal confinement of the indoor OWC system, especially a multi-source MIMO OWC system, the signal environment generally has huge interference and the channel impulse response has a long delay spread [30, 50, 51]. Hence, a major challenge posed in indoor OWC is the mitigation of interference, including intersymbol interference (ISI) induced from multipaths and multiple access inter-

ference (MAI) or co-channel interference (CCI) brought by multiple photoemitters.

There are two approaches to alleviating the effect of interference in OWC. The first approach is to physically adjust the configuration of photoemitters and photosensors. The positions of the photoemitters and photosensors can be carefully chosen with respect to the reflectors to avoid multipaths to a certain degree [44, 52–54]. Further, the directionality of the photoemitters and photosensors can be tuned to reduce misalignment between them, and, therefore, to mitigate MAI or CCI [55, 56]. However, the above physical adjustment approaches are inflexible for mobile terminals and inapplicable to nondirected systems.

The second approach is to cancel interference using beamforming schemes (in SIMO, MISO, and MIMO systems) with full awareness of channel knowledge. In this case, channel information needs to be estimated at the receiver side. In a fixed environment where there are no relative motions among the photoemitters, photosensors, and reflectors, the channel can be estimated using the known positions and directionality of the above elements, together with their physical properties such as the emission angle and field of view [44, 57, 58]. However, this method is only applicable to a static environment with a limited number of multipaths. On the other hand, known pilot signals are commonly utilised to estimate and update channel information intermittently. Although pilot-aided channel estimation schemes proposed for radio frequency (RF) systems may be suitable for the optical field, novel estimation algorithms are also proposed and tailored for OWC systems. In [59], channel information is estimated using either a least squares method that minimises the distortion between the pilot and the received signal, or a correlation bank based on the cross-correlation between the pilot and the received signal. In [60], a minimum mean squared error (MMSE) estimator is presented, which utilises the variable statistic window (i.e., a sliding window that incorporates past channel information) to improve the robustness and stability of the estimation

performance.

With the channel knowledge estimated, interference cancellation approaches including zero forcing, MMSE, and ML sequence detection at the receiver [59, 61, 62], and spatial modulation at the transmitter [47, 55] can be employed to improve the system performance. In addition, channel estimation and interference cancellation can be jointly carried out as in [63], where pilot signals are used to train an artificial neural network, and the mitigation of interference becomes a classification problem. However, the above approaches depend on full channel awareness estimated using pilot signals, at the cost of the loss in transmission rate. Thus, novel blind channel estimation and reception algorithms that can address the issue of heavy interference in OWC systems are much sought after.

1.1.2 Localisation

In applications such as ubiquitous computing [64] and wireless sensor networks [12], which are not restricted in the optical band, a problem that has drawn extensive attention is the localisation of wireless sources or targets. Generally, the localisation procedure is executed in two phases: the association phase and the metric fusion phase. In the association phase, the spatial relations between sources and sensors are estimated using received signals. Subsequently, source locations are inferred using these spatial relations (i.e., metrics) in the metric fusion phase.

Typically, the metrics employed in the localisation procedure can be either the ranges or directions of sources [65]; consequently, localisation techniques can be categorised into three groups: range-based, direction-based, and hybrid [11,66–69].

In range-based techniques as shown in Figure 1.2, multiple sensors are employed to measure source ranges individually, rather than collaboratively as an array. With the estimates of the source ranges and the known sensor locations, source locations can be estimated using, for example, the method of least squares.

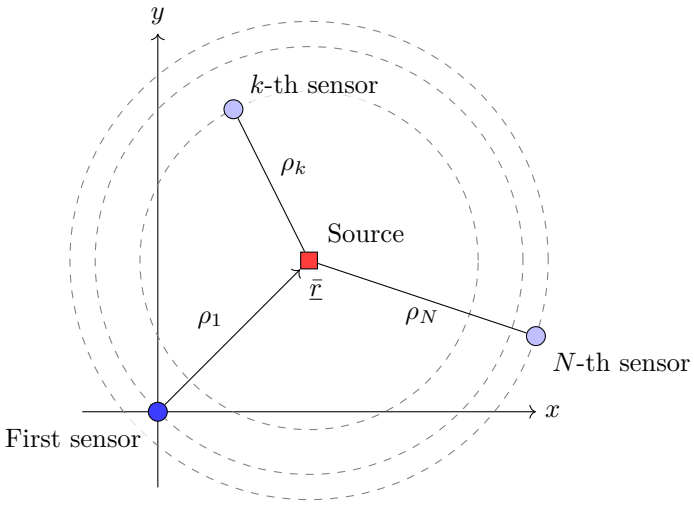

Figure 1.2: Range-based localisation. Individual sensors are utilised to estimate the ranges between the source and the sensors. The source location is then inferred from the estimated ranges.

The ranges can be acquired via two common approaches. One is based on the received signal strength (RSS), which is inversely proportional to (the power of) the propagation distance [70–75]. However, the accuracy of RSS-based approaches can be impaired due to the noise, fading, path loss, and shadowing effect in the environment [76]. The other method is based on the times of arrival (TOAs) from the sources to the sensors [77–79]. This approach requires the sources and sensors to be synchronised. There also exists a variant of the TOA-based approaches that relies on the measurement of the time differences of arrival (TDOAs) [77, 80–88]. By contrast, the TDOA-based approaches require the synchronisation among the sensors only.

In addition, in direction-based techniques as shown in Figure 1.3, multiple sensor arrays are used to estimate the directions of arrival (DOAs) of sources with respect to a global direction reference [89–92]. Direction estimation can be achieved using various aforementioned techniques such as the ML estimator, MUSIC, and ESPRIT. Source locations can then be derived from the DOAs and the known sensor array locations. Moreover, the performance of direction-based localisation

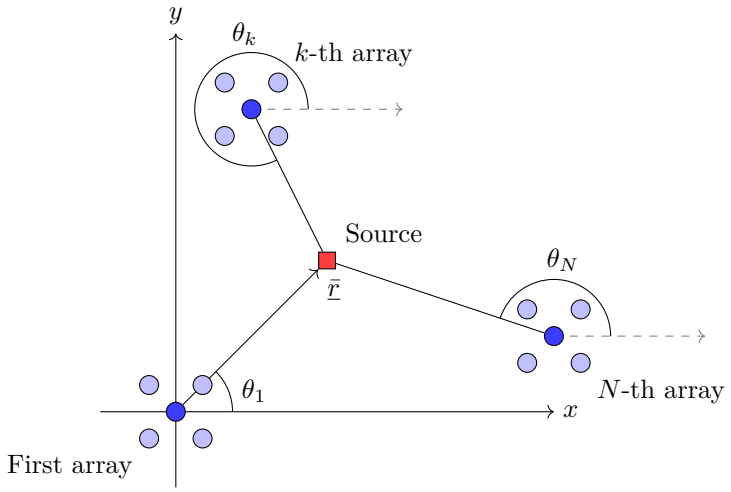

Figure 1.3: Direction-based localisation. Multiple arrays are exploited to estimate the source directions with respect to a common direction reference. The source location is then calculated from the estimated directions.

approaches is restricted by that of the direction finding techniques, and is degraded by low SNR, a finite number of observation snapshots, and a small number of array elements [93].

Apart from these range- and direction-based techniques, hybrid DOA–TOA localisation approaches can be found in the literature [85, 94].

1.1.3 Orientation Estimation

Along with the above localisation problem, an interesting and important problem is the estimation of the orientation of an array, especially in directional systems. The orientation of an array is defined as the rotation from a global coordinate system to the local coordinate system of the array. It is governed by three Euler angles; thus, the objective of the orientation estimation process is finding these Euler angles.

In the literature, there are two major approaches to estimating the orientation of a receiver array. If the array consists of distributed sensors with a relatively large aperture, then the ranges between a single source and the array elements can

be utilised to estimate the Euler angles. The ranges can be inferred by tracking the locations of the array elements [95] or by measuring the carrier phase difference between array elements [96]. On the other hand, if the array is compact, then the Euler angles can be estimated using the DOAs and ranges of multiple sources of known locations. In this case, the ranges are commonly inferred from the TOAs of the sources, which are estimated using decorrelation or matched filtering with the transmitted waveforms known at the receiver array [97, 98].

1.1.4 Wideband Assumption

An assumption that is commonly made in many applications of array processing is the narrowband assumption (NBA), which means that the wavefront of a baseband signal does not vary significantly when traversing through the sensors of an array [99]. This assumption may not be valid with a high probability in a distributed array of sensors as shown in Figure 1.4, since the ranges between the source and all the sensors may differ hugely. In such a case, the wideband assumption (WBA), where the baseband signal varies significantly when traversing

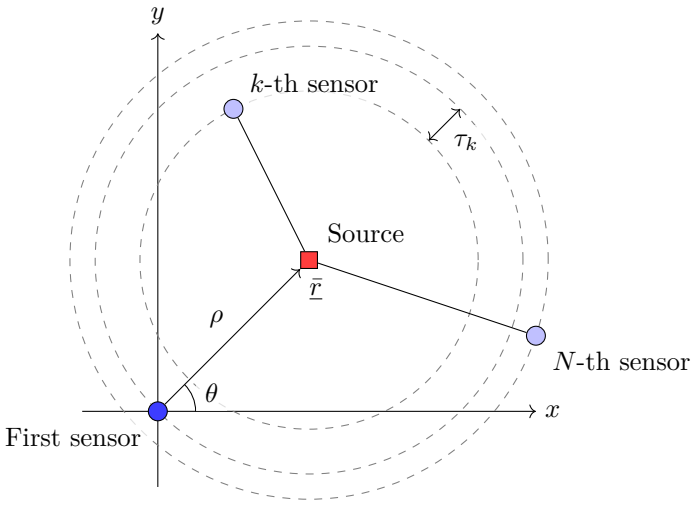

Figure 1.4: Distributed array of sensors and WBA. If the relative delay τ_k between the first and the k-th sensors from the source becomes significant such that the baseband signal varies significantly, then the signal model follows the WBA.

through the sensors of the array, needs to be considered. When the WBA is valid, subspace estimation algorithms proposed under the NBA such as MUSIC may fail to operate and deliver correct results.

One approach to solving the estimation problem under the WBA is to exploit the concept of the rotation of the array reference point [13]. When the array reference point changes from one sensor to another, the array manifold vector is scaled by a factor that is a function of the ranges between the source and the two array reference points. This range information can then be recovered by calculating the second order statistics of the signals received with different array reference points. Therefore, the source location can be inferred using range-based localisation approaches. Nevertheless, when this approach is applied to localise multiple sources, orthogonality needs to be introduced among the sources, and the estimation procedure needs to be performed for every source with all the interferers suppressed.

1.2 Challenges and Gaps

There exist a number of challenges and gaps posed in wireless source localisation problems. Following is a list of problems that have not been fully addressed in the literature and are to be examined in the thesis.

Channel estimation and interference cancellation. In applications such as indoor multi-source MIMO OWC systems, a key challenge is to estimate channel information and eliminate interference from undesired sources. In nonparametric OWC systems, this is usually achieved by physically adjusting the positions of the sources and sensors with respect to the reflectors, or by using beamforming algorithms at the transmitter and/or receiver with full channel awareness through pilot signals. The first method is infeasi-

ble to some system configurations like a nondirected–LOS system, while the second method suffers from the loss in transmission rate. To this end, a parametric approach that achieves blind channel estimation using localisation approaches and complete interference cancellation using subspace beamforming is needed.

Localisation problem. There exist a lot of multi-source localisation algorithms using sensor arrays in the literature. However, they suffer from pseudo location estimates when fusing the source ranges and/or directions estimated from multiple sensors and/or sensor arrays together. Localisation approaches that can estimate the locations of multiple sources without the pseudo location problem are desired to be investigated.

Orientation estimation problem. Alongside the localisation problem is the orientation estimation problem. The existing approaches generally rely on the TOA estimation using pilot signals, of which the receiver array needs to have full knowledge. Additionally, the existing approaches are concerning the estimation of the orientation of a receiver array using the signals of multiple sources. There lack techniques that estimate the orientation of transmitter arrays apart from localising all the array elements. Hence, the above two problems will be researched in the thesis as well.

Wideband assumption. Subspace estimation techniques such as MUSIC enjoy outstanding estimation accuracy. However, these algorithms may fail to estimate source parameters under the WBA, where the wavefront of a baseband signal varies when traversing through the sensors of an array. Therefore, new subspace approaches that address the issues under the WBA are much sought after.

1.3 Thesis Scope and Organisation

The aim of the thesis is to analyse and address various localisation problems in array processing. Subspace localisation techniques will be scrutinised in the thesis to solve such problems in many communications and signal processing applications. The rest of the thesis is organised as follows.

In Chapter 2, a novel parametric model is presented for indoor multi-source MIMO OWC with the incorporation of the geometries of photoemitter and photosensor arrays. A localisation approach, which is employed as a blind channel estimator for estimating the azimuth, elevation, range, and path gain, is proposed as a three-step procedure, with the employment of cone angle parameterisation. Moreover, two subspace multibeam beamformers are presented; they constructively combine all the paths of the desired source and achieve complete interference elimination, without the requirement of full channel awareness.

From Chapters 3 to 5, various wireless source localisation problems are studied in a more general sense, without being limited to the optical band only. Particularly, in Chapter 3, the localisation and orientation estimation of a receiver array are examined. A sensor array is utilised to estimate the location and orientation of its own with respect to a global coordinate system using the signals of multiple sources of known locations. By using subspace direction finding techniques and three systems of quadratic and linear equations, the location and orientation can be accurately estimated.

In Chapter 4, the localisation and orientation estimation of multiple transmitter arrays are investigated. A sensor array comprising distributed groups of small aperture arrays is employed to estimate the locations and orientations of multiple sources with each one being an emitter array. The source directions are estimated using subspace techniques and the source ranges are estimated by solving a system

of equations. Moreover, the orientations are estimated by making use of the source beamforming weight vectors.

In Chapter 5, the localisation of wireless sources is studied under the WBA. Specifically, two approaches are proposed for solving the localisation problem. The first approach utilises the subcovariance matrix of the received signal vector and its singular value decomposition to estimate the source locations. The second approach employs the rotation/change of the array reference point to translate the WBA problem into its NBA counterpart so that NBA subspace techniques can be readily applied to solve the localisation problem.

In all technical chapters from Chapters 2 to 5, computer simulation studies are carried out using MATLAB for evaluating the performance of the proposed approaches.

Finally, in Chapter 6, the conclusions of the thesis are drawn, the list of contributions is given, and the suggestions for further work are presented.

Chapter 2

Parametric Indoor Optical Wireless Communications

The study of OWC has given fresh impetus to the recent development of solid state lighting technologies. Considered as a potential alternative to the conventional but congested RF band, the optical band advantages in terms of its unlicensed spectrum, large bandwidth, low energy consumption, affordability, and high security. It can be exploited in applications where RF signals are not accessible (e.g., in basements or tunnels), or not permitted for private communications due to safety regulations (e.g., in airplanes or hospitals). Owing to the above benefits, OWC has become a complementary technique to the current RF communication systems and a promising candidate for the future.

In this chapter, a parametric approach to indoor multi-source MIMO OWC is presented, with the incorporation of the array geometries of photoemitters and photosensors. In addition, a localisation approach is proposed as a blind channel estimator for estimating the source locations and path gains, which are then employed to design beamformers that better isolate desired sources from interferers. With the employment of this parametric approach, complete interference

cancellation in OWC systems can be outstandingly achieved.

The rest of this chapter is organised as follows. In Section 2.1, the signal model of indoor MIMO OWC is presented. In Section 2.2, a blind subspace channel estimator is proposed to estimate the parameters of interest including the azimuth, elevation, range bin, and path gain in a three-step procedure. In addition, two spatiotemporal multibeam beamformers are presented, which effectively receive all the paths of the desired source and provide complete interference cancellation. In Section 2.3, the performance of the proposed channel estimator and beamformers is evaluated through computer simulation studies. Last, in Section 2.4, the chapter is summarised.

2.1 Signal Model of Optical Wireless Communications

With reference to Figure 2.1, consider an array of N photosensors in the presence of M sources with each source being an array of $\bar{N}$ photoemitters. Hereafter, the terms "sensor" and "emitter" are used in place of "photosensor" and "photoemitter" unless otherwise noted. The sensor array geometry is described as

$$[\underline{r}_1, \underline{r}_2, \ldots, \underline{r}_N] = \left[\underline{r}_x, \underline{r}_y, \underline{r}_z\right]^T \in \mathcal{R}^{3\times N} \tag{2.1}$$

where $\underline{r}_k \in \mathcal{R}^{3\times 1}$ denotes the Cartesian coordinates of the k-th sensor while $\underline{r}_x$, $\underline{r}_y$ and $\underline{r}_z \in \mathcal{R}^{N\times 1}$ contain the coordinates of the x-, y-, and z-axis of all the sensors, respectively. Without loss of generality, the array centroid (represented as the dark blue element in Figure 2.1) is the origin of the coordinate system and is selected as the array reference point. Besides, the photosensitive direction of a sensor is defined as the direction along which the impinging signal can be

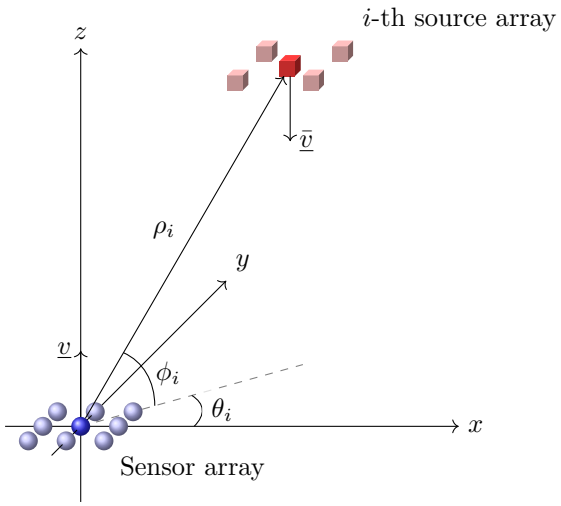

Figure 2.1: Geometry of the sensor array and i-th source array. The elements of the sensor array are represented by the blue spheres with the array reference point denoted by the darker one. The elements of the i-th source array is represented by the red cubes. The location of the source is parameterised by its azimuth θ_i, elevation ϕ_i, and range ρ_i.

maximally detected. The photosensitive direction of all the sensors is assumed to be in the direction of the positive z-axis for simplicity and is denoted as a unit vector $\underline{v} \in \mathcal{R}^{3\times 1}$. Similarly, the array geometry of the i-th source is described as

$$[\underline{\bar{r}}_1, \underline{\bar{r}}_2, \ldots, \underline{\bar{r}}_{\bar{N}}] = \left[\underline{\bar{r}}_x, \underline{\bar{r}}_y, \underline{\bar{r}}_z\right]^T \in \mathcal{R}^{3\times \bar{N}}. \tag{2.2}$$

The photoemissive direction is defined as the direction along which the transmitted signal power is the maximum. The photoemissive direction of all the emitters is assumed to be in the direction of the negative z-axis and is denoted as a unit vector $\underline{\bar{v}} \in \mathcal{R}^{3\times 1}$.

With reference to Figure 2.2, suppose that the i-th source transmits a sequence of channel symbols with the channel symbol period T_{cs}. The q-th channel symbol is denoted as $\mathrm{a}_i[q]$ for $q \in \mathcal{Z}$. The channel symbols are coded using a unique Gold sequence of length N_c and chip period $T_c = T_{\text{cs}}/N_c$. The ℓ-th element of the code is denoted as $c_i[\ell]$ for $\ell = 0, 1, \ldots, N_c - 1$. The coded channel symbols are sent to

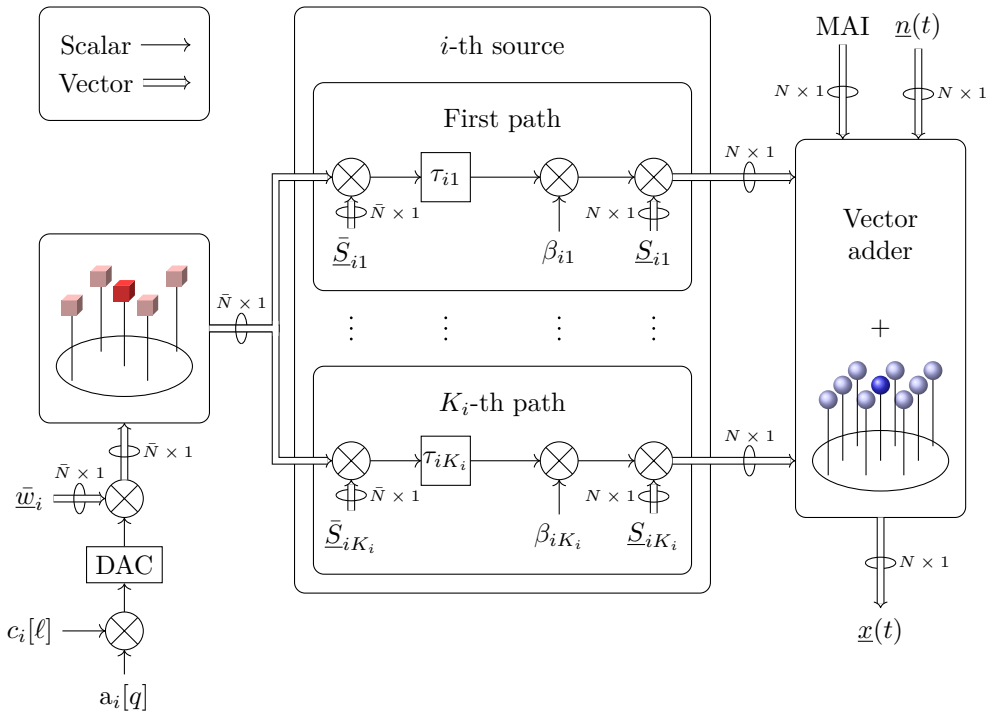

Figure 2.2: Baseband representation of the MIMO OWC system. Each path of the source is modelled using the sensor and source array geometries, path fading coefficient, DOA, DOD, and range in terms of delay.

a digital-to-analogue converter (DAC) and the output continuous waveform is denoted as $m_i(t)$. The output waveform is then weighted using a source beamforming weight vector $\underline{\bar{w}}_i \in \mathcal{C}^{\bar{N}\times 1}$ before being radiated to free space by $\bar{N}$ emitters.

Assume that the signal of the i-th source arrives at the sensor array via K_i paths. The baseband signal received at the sensor array can be modelled as [1, 30, 44]

$$\underline{x}(t) = \sum_{i=1}^{M} \sum_{p=1}^{K_i} \beta_{ip} \underline{S}_{ip} \underline{\bar{S}}_{ip}^{H} \underline{\bar{w}}_i m_i(t - \tau_{ip}) + \underline{n}(t) \tag{2.3}$$

where, for the p-th path of the i-th source, β_{ip} is its complex path fading coefficient, $\underline{S}_{ip} \in \mathcal{C}^{N\times 1}$ is its sensor array manifold vector, $\underline{\bar{S}}_{ip} \in \mathcal{C}^{\bar{N}\times 1}$ is its source array manifold vector, and $\tau_{ip} = \rho_{ip}/c$ is its delay with ρ_{ip} denoting the range of this path and c being the speed of light. Note that the delay is assumed to be smaller than a channel symbol period due to the short range of the indoor environment;

i.e., $0 \leq \tau_{ip} < T_{\text{cs}}$. The vector $\underline{n}(t)$ denotes the complex additive white Gaussian noise (AWGN) of zero mean and covariance $\sigma_n^2 \mathbb{I}_N$.

In particular, the sensor array manifold vector associated with this path is given as

$$\underline{S}_{ip} \triangleq \underline{S}(\theta_{ip}, \phi_{ip}) = \underline{g}(\theta_{ip}, \phi_{ip}) \odot \exp\Big(-j2\pi \frac{F_c}{c} \left[\underline{r}_x, \underline{r}_y, \underline{r}_z\right] \underline{u}_{ip}\Big) \tag{2.4}$$

where $\underline{g}(\theta_{ip}, \phi_{ip}) \in \mathcal{R}^{N\times 1}$ is the directional gain vector, F_c is the optical carrier frequency, and $\underline{u}_{ip} \in \mathcal{R}^{3\times 1}$ is a unit vector pointing from the sensor array reference point towards the direction of this path; the unit vector is defined as

$$\underline{u}_{ip} \triangleq \underline{u}(\theta_{ip}, \phi_{ip}) = [\cos\theta_{ip} \cos\phi_{ip}, \sin\theta_{ip} \cos\phi_{ip}, \sin\phi_{ip}]^T \tag{2.5}$$

with θ_{ip} and ϕ_{ip} being its azimuth and elevation, respectively. Additionally, all the sensors are assumed to be identical; thus, the directional gain vector is simplified to

$$\underline{g}(\theta_{ip}, \phi_{ip}) = g(\theta_{ip}, \phi_{ip})\, \underline{1}_N = \underline{1}_N \sqrt{\sin\phi_{ip}}. \tag{2.6}$$

Similarly, the source array manifold vector $\bar{\underline{S}}_{ip}$ is defined as

$$\bar{\underline{S}}_{ip} \triangleq \bar{\underline{S}}\big(\bar{\theta}_{ip}, \bar{\phi}_{ip}\big) = \bar{\underline{g}}\big(\bar{\theta}_{ip}, \bar{\phi}_{ip}\big) \odot \exp\Big(j2\pi \frac{F_c}{c} \left[\bar{\underline{r}}_x, \bar{\underline{r}}_y, \bar{\underline{r}}_z\right] \bar{\underline{u}}_{ip}\Big) \tag{2.7}$$

with $\bar{\underline{g}}\big(\bar{\theta}_{ip}, \bar{\phi}_{ip}\big) \in \mathcal{R}^{\bar{N}\times 1}$ being the directional gain vector and $\bar{\underline{u}}_{ip} \in \mathcal{R}^{3\times 1}$ denoting the direction of departure (DOD) of this path. The emission of the signal follows Lambert's cosine law. Assuming that the order of emission is one for simplicity, the directional gain vector is given as

$$\bar{\underline{g}}\big(\bar{\theta}_{ip}, \bar{\phi}_{ip}\big) = \bar{g}\big(\bar{\theta}_{ip}, \bar{\phi}_{ip}\big)\, \underline{1}_{\bar{N}} = \underline{1}_{\bar{N}} \sqrt{\sin\bar{\phi}_{ip}}. \tag{2.8}$$

The received signal is sampled at the sampling frequency $1/T_c$ and is collected using N tapped delay lines (TDLs) of length $2N_c$. The snapshots of the received signal can be represented by a data cube as illustrated in Figure 2.3(a), where the q-th page is denoted as $\mathbb{X}[q] \in \mathcal{C}^{N\times 2N_c}$. The output of the TDLs is shown in Figure 2.3(b), where the q-th column is a column-wise vectorisation of $\mathbb{X}^T[q]$ and can be modelled as

$$\begin{aligned}\underline{x}[q] &= \mathrm{vec}\Big(\mathbb{X}^T[q]\Big) \\ &= \sum_{i=1}^{M}\sum_{p=1}^{K_i} \underbrace{\beta_{ip}\bar{\underline{S}}_{ip}^H\bar{\underline{w}}_i}_{=\gamma_{ip}} \Big[\underline{h}_{ip}^-, \underline{h}_{ip}, \underline{h}_{ip}^+\Big] \begin{bmatrix} \mathrm{a}_i[q-1] \\ \mathrm{a}_i[q] \\ \mathrm{a}_i[q+1] \end{bmatrix} + \underline{n}[q]\end{aligned}$$

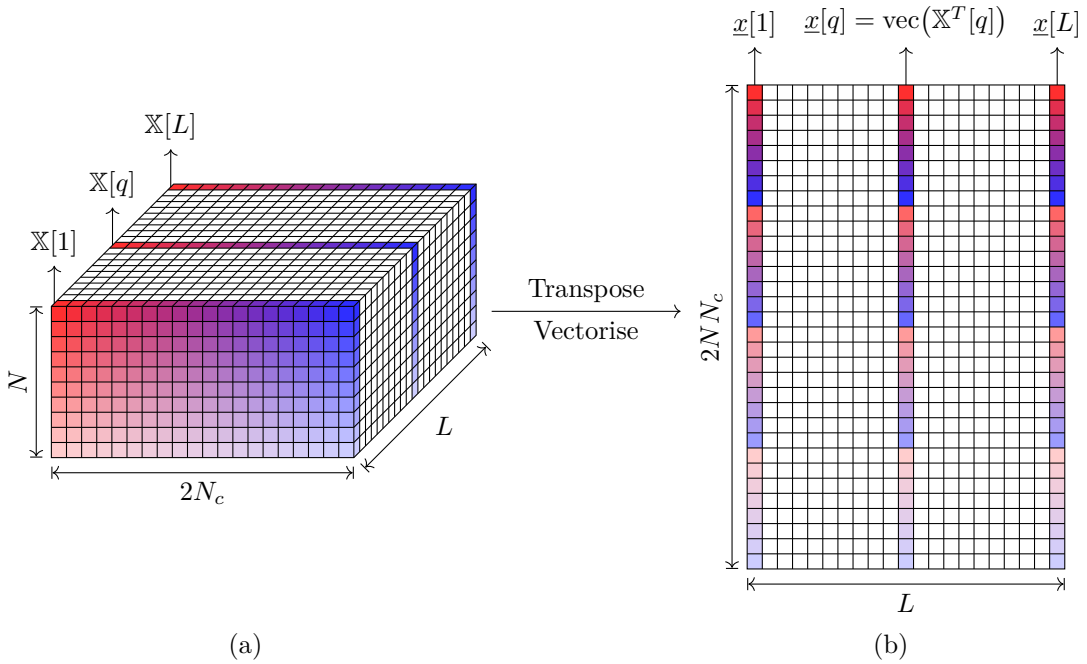

Figure 2.3: Signal rearrangement. (a) Received data cube. The q-th page $\mathbb{X}[q]$ consists of $2N_c$ snapshots received at N sensors. (b) Rearranged signal matrix. The q-th column $\underline{x}[q]$ is the transposed and column-wise vectorised version of $\mathbb{X}[q]$.

$$= \sum_{i=1}^{M} \sum_{p=1}^{K_i} \gamma_{ip} \left[\underline{h}_{ip}^{-}, \underline{h}_{ip}, \underline{h}_{ip}^{+} \right] \begin{bmatrix} \mathrm{a}_i[q-1] \\ \mathrm{a}_i[q] \\ \mathrm{a}_i[q+1] \end{bmatrix} + \underline{n}[q] \in \mathcal{C}^{2NN_c \times 1}. \tag{2.9}$$

In Equ. (2.9), the spatiotemporal array (STAR) manifold vector associated with the current channel symbol of the p-th path of the i-th source is defined as

$$\underline{h}_{ip} \triangleq \underline{h}(\theta_{ip}, \phi_{ip}, \ell_{ip}) = \underline{S}_{ip} \otimes \mathbb{J}_{2N_c}^{\ell_{ip}} \underline{c}_i \in \mathcal{C}^{2NN_c \times 1} \tag{2.10}$$

where

$$\mathbb{J}_{2N_c} = \begin{bmatrix} \underline{0}_{2N_c-1}^{T}, & 0 \\ \mathbb{I}_{2N_c-1}, & \underline{0}_{2N_c-1} \end{bmatrix} \in \mathcal{Z}^{2N_c \times 2N_c} \tag{2.11}$$

is the $2N_c$-dimensional lower shift matrix,

$$0 \leq \ell_{ip} = \left\lfloor \frac{\tau_{ip}}{T_c} \right\rfloor = \left\lfloor \frac{\rho_{ip}}{cT_c} \right\rfloor \leq N_c - 1 \tag{2.12}$$

denotes the index of the range bin, and

$$\underline{c}_i = \left[c_i[0], c_i[1], \ldots, c_i[N_c-1], \underline{0}_{N_c}^{T} \right]^{T} \in \mathcal{Z}^{2N_c \times 1} \tag{2.13}$$

contains the Gold sequence of the i-th source padded with N_c zeros. The STAR manifold vectors of the previous and next channel symbols are given as

$$\underline{h}_{ip}^{-} = \left(\mathbb{I}_N \otimes \left(\mathbb{J}_{2N_c}^{T} \right)^{N_c} \right) \underline{h}_{ip}; \tag{2.14a}$$

$$\underline{h}_{ip}^{+} = \left(\mathbb{I}_N \otimes \mathbb{J}_{2N_c}^{N_c} \right) \underline{h}_{ip}. \tag{2.14b}$$

Moreover, $\mathrm{a}_i[q-1]$, $\mathrm{a}_i[q]$, and $\mathrm{a}_i[q+1]$ represent the previous, current, and next channel symbols, respectively. The term γ_{ip} incorporates both the path fading

coefficient β_{ip} and the source array gain $\underline{\bar{S}}_{ip}^{H}\underline{\bar{w}}_i$, and is referred to as the (overall) path gain for the sake of simplicity unless otherwise noted.

Without loss of generality, assume that the first source is the desired source to be estimated and recovered. Then, Equ. (2.9) can be rewritten as

$$\underline{x}[q] = \underbrace{\mathbb{H}_1\underline{\gamma}_1\mathrm{a}_1[q]}_{\text{desired}} + \underbrace{\left[\mathbb{H}_1^{-}\underline{\gamma}_1, \mathbb{H}_1^{+}\underline{\gamma}_1\right]\begin{bmatrix}\mathrm{a}_1[q-1]\\ \mathrm{a}_1[q+1]\end{bmatrix}}_{\text{ISI}} + \underbrace{\sum_{i=2}^{M}\left[\mathbb{H}_i^{-}\underline{\gamma}_i, \mathbb{H}_i\underline{\gamma}_i, \mathbb{H}_i^{+}\underline{\gamma}_i\right]\begin{bmatrix}\mathrm{a}_i[q-1]\\ \mathrm{a}_i[q]\\ \mathrm{a}_i[q+1]\end{bmatrix}}_{\text{MAI}} + \underbrace{\underline{n}[q]}_{\text{noise}} \quad (2.15)$$

where, for all the paths of the i-th source, $\mathbb{H}_i^{-}$, $\mathbb{H}_i$, and $\mathbb{H}_i^{+} \in \mathcal{C}^{2NN_c\times K_i}$ contain the STAR manifold vectors associated with the previous, current, and next channel symbols, respectively, and $\underline{\gamma}_i = [\gamma_{i1}, \gamma_{i2}, \ldots, \gamma_{iK_i}]^T \in \mathcal{C}^{K_i\times 1}$ comprises their path gains. In Equ. (2.15), the first term is the current channel symbol from all the paths of the desired source; the second term, referred to as the ISI, is the contribution of the previous and next channel symbols from all the paths of the desired source; the third term, referred to as the MAI, is the channel symbols from all the paths of all the undesired sources (interferers); the fourth term is the noise.

Suppose that L snapshots of $\underline{x}[q]$ are collected; the spatiotemporally rearranged snapshots (i.e., the output of the TDLs) can be written in a matrix format as

$$\mathbb{X} = [\underline{x}[1], \underline{x}[2], \ldots, \underline{x}[L]] \in \mathcal{C}^{2NN_c\times L}. \quad (2.16)$$

The covariance matrix of $\mathbb{X}$ can be constructed as

$$\mathbb{R}_{xx} = \frac{1}{L}\mathbb{X}\mathbb{X}^H = \mathbb{R}_{dd} + \mathbb{R}_{jj} + \mathbb{R}_{nn} \in \mathcal{C}^{2NN_c \times 2NN_c} \tag{2.17}$$

where the three summands correspond to the covariance matrices of the desired signal, interference (ISI and MAI), and noise, respectively.

2.2 Localisation and Beamforming

2.2.1 Location and Path Gain Estimation

There are four parameters of interest to be estimated: the azimuth θ, elevation ϕ, range bin ℓ, and path gain γ. The estimation procedure is divided into three steps: the range bin estimation, joint azimuth and elevation estimation, and path gain estimation.

Joint Cone Angle and Range Bin Estimation

The initial step is to jointly estimate the cone angles (which will be defined later) and range bins of all the paths of the desired source.

Suppose that there exist N_A sensors in the array that form a linear array as shown in Figure 2.4. (Note that in an arbitrary array, a linear array can always be formed by any two sensors at least.) For convenience, assume that they are the first N_A sensors and one of them is the array reference point. The coordinates of the elements of the linear array can be expressed in a new x'-axis, which is rotated from the original x-axis by Θ on the azimuth plane and then by Φ on the elevation plane; namely,

$$\underline{r}'_k = [x'_k, y'_k, z'_k]^T = \mathbb{Q}\underline{r}_k \in \mathcal{R}^{3\times 1} \tag{2.18}$$

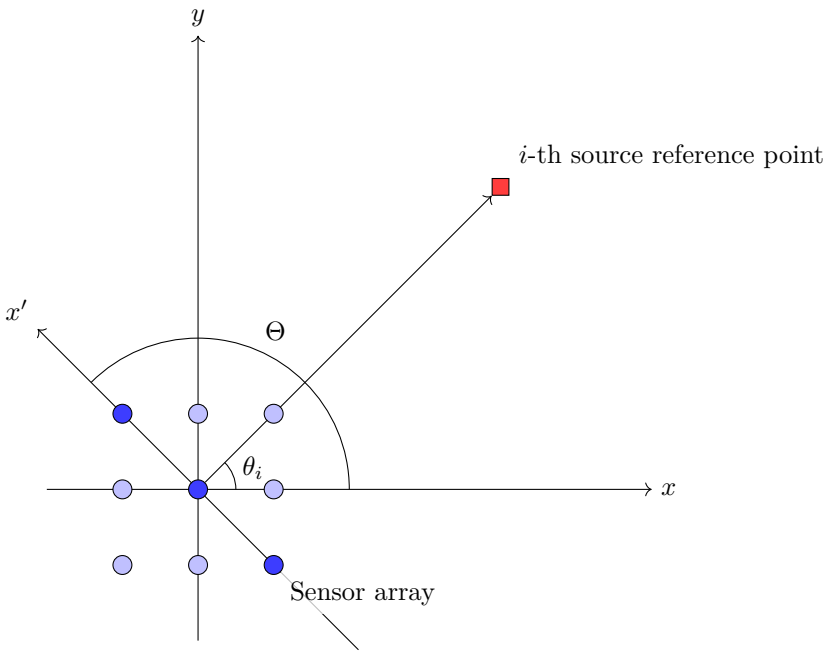

Figure 2.4: Rotation angle of the linear array. The selected N_A sensors are represented by the dark blue circles. Only the rotation Θ on the azimuth plane is shown for simplicity. The rotation Φ on the elevation plane can be similarly defined and is not shown here.

for $k = 1, 2, \ldots, N_A$ where

$$\mathbb{Q} = \mathbb{Q}_\Phi \mathbb{Q}_\Theta \in \mathcal{R}^{3\times 3} \tag{2.19}$$

is the rotation matrix consisting of

$$\mathbb{Q}_\Theta = \begin{bmatrix} \cos\Theta, & \sin\Theta, & 0 \\ -\sin\Theta, & \cos\Theta, & 0 \\ 0, & 0, & 1 \end{bmatrix} \in \mathcal{R}^{3\times 3}; \tag{2.20a}$$

$$\mathbb{Q}_\Phi = \begin{bmatrix} \cos\Phi, & 0, & \sin\Phi \\ 0, & 1, & 0 \\ -\sin\Phi, & 0, & \cos\Phi \end{bmatrix} \in \mathcal{R}^{3\times 3}. \tag{2.20b}$$

Since the selected elements lie on the x'-axis only, their coordinates can be specified by a vector $\underline{r}'_{xA} = \left[x'_1, x'_2, \ldots, x'_{N_A}\right]^T \in \mathcal{R}^{N_A\times 1}$.

Moreover, define the cone angle α_{ip} for the p-th path of the i-th source using its azimuth θ_{ip}, elevation ϕ_{ip}, and the rotation angles Θ and Φ as

$$\alpha_{ip} = \arccos(\cos\theta_{ip}\cos\phi_{ip}\cos\Theta\cos\Phi + \sin\theta_{ip}\cos\phi_{ip}\sin\Theta\cos\Phi + \sin\phi_{ip}\sin\Phi) \tag{2.21}$$

such that the STAR manifold vector associated with the N_A sensors can be rewritten as

$$\begin{aligned}\underline{h}_{ipA} &\triangleq \underline{h}_A(\alpha_{ip}, \ell_{ip}) \\ &= \underline{S}_A(\alpha_{ip}) \otimes \mathbb{J}_{2N_c}^{\ell_{ip}} \underline{c}_i \\ &= \exp\left(-\jmath 2\pi \frac{F_c}{c} \underline{r}'_{xA} \cos\alpha_{ip}\right) \otimes \mathbb{J}_{2N_c}^{\ell_{ip}} \underline{c}_i \in \mathcal{C}^{2N_A N_c \times 1},\end{aligned} \tag{2.22}$$

which is parameterised by the cone angle and range bin only $[1, 100]$. Therefore, a two-dimensional search can be performed to jointly estimate the cone angle and range bin, as described as follows.

Define a selection matrix that selects the subcovariance matrix associated with the N_A sensors from Equ. (2.17) as

$$\mathbb{F}_A = \left[\mathbb{I}_{N_A}, \mathbb{O}_{N_A \times (N - N_A)}\right] \in \mathcal{Z}^{N_A \times N}. \tag{2.23}$$

Note that all the paths of the same source are linearly combined by the path gains after the spatiotemporal rearrangement. Therefore, a preprocessing matrix needs to be applied to the covariance matrix $\mathbb{R}_{xx}$ to suppress all the paths except the desired one to be estimated [101]. The preprocessing matrix of the desired source corresponding to a path of range bin ℓ is defined as

$$\mathbb{P}_\ell = \mathbb{P}^{\perp}_{\mathbb{C}_{1\ell}} = \mathbb{I}_{2N_c} - \mathbb{C}_{1\ell}\left(\mathbb{C}_{1\ell}^H \mathbb{C}_{1\ell}\right)^{-1} \mathbb{C}_{1\ell}^H \in \mathcal{R}^{2N_c \times 2N_c}. \tag{2.24}$$

It is the projection matrix onto the complementary subspace of the one spanned by the columns of $\mathbb{C}_{1\ell} \in \mathcal{R}^{2N_c \times (N_c-1)}$, which contains the shifted versions of the desired Gold sequence except for the range bin ℓ; i.e.,

$$\mathbb{C}_{1\ell} = \left[\mathbb{J}^0_{2N_c}\underline{c}_1, \mathbb{J}^1_{2N_c}\underline{c}_1, \ldots, \mathbb{J}^{\ell-1}_{2N_c}\underline{c}_1, \mathbb{J}^{\ell+1}_{2N_c}\underline{c}_1, \mathbb{J}^{\ell+2}_{2N_c}\underline{c}_1, \ldots, \mathbb{J}^{N_c-1}_{2N_c}\underline{c}_1\right]. \tag{2.25}$$

Using the covariance matrix $\mathbb{R}_{xx}$ given in Equ. (2.17), construct the preprocessed subcovariance matrix corresponding to the N_A sensors as

$$\mathbb{R}_{x_{A\ell}x_{A\ell}} = \left(\mathbb{F}_A \otimes \mathbb{P}_\ell\right) \mathbb{R}_{xx} \left(\mathbb{F}_A \otimes \mathbb{P}_\ell\right)^H \in \mathcal{C}^{2N_A N_c \times 2N_A N_c}. \tag{2.26}$$

Subsequently, the cone angle and range bin of the path can be estimated by a two-dimensional search of

$$\xi(\alpha, \ell) = \frac{\bar{\underline{h}}^H_A(\alpha, \ell)\, \bar{\underline{h}}_A(\alpha, \ell)}{\bar{\underline{h}}^H_A(\alpha, \ell)\, \mathbb{E}_{n_{A\ell}} \mathbb{E}^H_{n_{A\ell}} \bar{\underline{h}}_A(\alpha, \ell)} \tag{2.27}$$

where

$$\bar{\underline{h}}_A(\alpha, \ell) = \left(\mathbb{I}_{N_A} \otimes \mathbb{P}_\ell\right) \left(\underline{S}_A(\alpha) \otimes \mathbb{J}^\ell_{2N_c}\underline{c}_1\right) \in \mathcal{C}^{2N_A N_c \times 1} \tag{2.28}$$

is the preprocessed STAR manifold vector and $\mathbb{E}_{n_{A\ell}} \in \mathcal{C}^{2N_A N_c \times (2N_A N_c - 3M)}$ denotes the noise subspace of $\mathbb{R}_{x_{A\ell}x_{A\ell}}$.

Joint Azimuth and Elevation Estimation

On completion of the estimation of the cone angles $\hat{\alpha}$ and range bins $\hat{\ell}$ of all the paths of the desired source, their azimuths θ and elevations ϕ are to be estimated. Likewise, based on the estimated range bins $\hat{\ell}$, the preprocessed covariance matrix can be obtained as

$$\mathbb{R}_{x_{\hat{\ell}}x_{\hat{\ell}}} = \left(\mathbb{I}_N \otimes \mathbb{P}_{\hat{\ell}}\right) \mathbb{R}_{xx} \left(\mathbb{I}_N \otimes \mathbb{P}_{\hat{\ell}}\right)^H \in \mathcal{C}^{2NN_c \times 2NN_c} \tag{2.29}$$

and its noise subspace is denoted as $\mathbb{E}_{n_{\hat{\ell}}} \in \mathcal{C}^{2NN_c \times (2NN_c - 3M)}$. By employing the estimated cone angles $\hat{\alpha}$ as well, the azimuth and elevation can then be jointly estimated by a one-dimensional search of

$$\xi(\theta, \phi) = \frac{\bar{\underline{h}}^H\left(\phi, \hat{\alpha}, \hat{\ell}\right) \bar{\underline{h}}\left(\phi, \hat{\alpha}, \hat{\ell}\right)}{\bar{\underline{h}}^H\left(\phi, \hat{\alpha}, \hat{\ell}\right) \mathbb{E}_{n_{\hat{\ell}}} \mathbb{E}_{n_{\hat{\ell}}}^H \bar{\underline{h}}\left(\phi, \hat{\alpha}, \hat{\ell}\right)} \tag{2.30}$$

where

$$\bar{\underline{h}}\left(\phi, \hat{\alpha}, \hat{\ell}\right) = \left(\mathbb{I}_N \otimes \mathbb{P}_{\hat{\ell}}\right) \left(\underline{S}(\phi, \hat{\alpha}) \otimes \mathbb{J}_{2N_c}^{\hat{\ell}} \underline{c}_1\right) \in \mathcal{C}^{2NN_c \times 1}. \tag{2.31}$$

Note that for a particular combination of ϕ and $\hat{\alpha}$, there exist two possible values of the azimuth θ, which are

$$\theta = \pm \left(\arccos\left(\frac{\cos\hat{\alpha} - \sin\phi \sin\Phi}{\cos\phi \cos\Phi} \right) + \Theta \right) \bmod 360^\circ. \tag{2.32}$$

Thus, the cost function needs to be executed twice at the two azimuths to resolve ambiguity. Since θ is a derived parameter of ϕ and $\hat{\alpha}$, this algorithm merely requires a one-dimensional search over the elevation.

Path Gain Estimation

In order to constructively combine all the paths of the desired source for recovering the desired information, their path gains need to be estimated. Assume that the transmitted information is encoded as the phase difference between consecutive channel symbols. Therefore, one only needs to estimate a vector that is collinear with the path gain vector $\underline{\gamma}_1$ (i.e., the relative path gains for the sake of combining all the paths), rather than all of its actual elements, for information recovery.

From Equ. (2.17), it is easy to know that the rank of $\mathbb{R}_{xx} - \mathbb{R}_{nn}$ contains the contribution of the desired signal of rank one and interference of rank $3M - 1$.

Define a covariance matrix as

$$\mathbb{R}_{jj}\left(\underline{\gamma}\right) = \mathbb{R}_{xx} - \hat{\mathbb{R}}_{nn} - \mathbb{H}_1 \underline{\gamma}\, \underline{\gamma}^H \mathbb{H}_1^H \tag{2.33}$$

where $\hat{\mathbb{R}}_{nn}$ denotes the estimate of the noise covariance matrix, which can be constructed from the least significant eigenvalues of $\mathbb{R}_{xx}$. The rank of $\mathbb{R}_{jj}\left(\underline{\gamma}\right)$ will be lowered by one if the argument $\underline{\gamma}$ and the path gain $\underline{\gamma}_1$ are collinear. Hence, define a cost function as [102]

$$\xi\left(\underline{\gamma}\right) = \sum_{\substack{b=1 \\ \mathrm{eig}_b>0}}^{2NN_c} \left(1 + \mathrm{eig}_b\left(\mathbb{R}_{jj}\left(\underline{\gamma}\right)\right)\right) + 10\log_{10}\left(\sum_{\substack{b=1 \\ \mathrm{eig}_b<0}}^{2NN_c} \left|\mathrm{eig}_b\left(\mathbb{R}_{jj}\left(\underline{\gamma}\right)\right)\right|\right), \tag{2.34}$$

the minimisation of which lowers the rank of $\mathbb{R}_{jj}\left(\underline{\gamma}\right)$ by one and delivers the estimate of $\underline{\gamma}_1$.

In conclusion, the proposed source location and path gain estimation algorithm can be summarised as the following steps.

Step 1: Construct the covariance matrix of the spatiotemporally rearranged signal matrix using Equ. (2.17).

Step 2: Preprocess a subcovariance matrix of the signal that corresponds to a linear array using Equ. (2.26). Jointly estimate the cone angles and range bins of all the paths of the desired source by a two-dimensional search of Equ. (2.27).

Step 3: Preprocess the covariance matrix of the signal using Equ. (2.29). Based on the estimated cone angles and range bins from Step 2, jointly estimate the azimuths and elevations by a one-dimensional search of Equ. (2.31) over the elevation. Derive the azimuth from the estimated elevation using Equ. (2.32).

Step 4: Construct the desired signal subspace using all the estimated parameters. Estimate the path gain vector by minimising Equ. (2.34).

2.2.2 Subspace Multibeam Beamforming

After estimating the source locations and path gains, beamforming techniques are applied to recover the transmitted signals. Since the enclosed signal environment with multiple sources contains huge interference, there is a high probability that some paths are closely located in space (directions). Thus, the source locations, which involve both directions and ranges, are utilised to design beamformers to isolate the desired signal from the interferers.

Two subspace beamformers are provided to resolve all the paths of the desired source, combine them using the path gains and suppress the interference [103]. With reference to Equ. (2.15), the weight vectors of the beamformers are given as

$$\underline{w}_A = \mathbb{P}^{\perp}_{\mathbb{E}_j} \mathbb{H}_1 \left(\mathbb{H}_1^H \mathbb{P}^{\perp}_{\mathbb{E}_j} \mathbb{H}_1 \right)^{-1} \underline{\gamma}_1; \tag{2.35}$$

$$\underline{w}_B = \mathbb{P}^{\perp}_{\mathbb{E}_j} \mathbb{H}_1 \underline{\gamma}_1 \tag{2.36}$$

where $\mathbb{E}_j$ spans the interference (ISI and MAI) subspace and $\mathbb{P}^{\perp}_{\mathbb{E}_j}$ denotes the projection matrix onto the complementary subspace of the interference subspace. In order to construct the weight vector, the matrices $\mathbb{H}_1$ and $\mathbb{E}_j$ need to be constructed. The matrix $\mathbb{H}_1$ can be directly recovered from the channel parameter estimates in the previous steps, while $\mathbb{E}_j$ can be estimated by taking the eigenvectors of

$$\mathbb{R}_{jj} = \mathbb{R}_{xx} - \mathbb{H}_1 \underline{\gamma}_1 \underline{\gamma}_1^H \mathbb{H}_1^H \tag{2.37}$$

associated with its most significant eigenvalues. Note that these subspace beamformers require the channel knowledge of the desired source only.

2.3 Computer Simulation Studies

In this section, the performance of the localisation approach and beamformers for the indoor multi-source MIMO OWC system is assessed through computer simulation studies. In the simulations, a nine-element grid array of half-wavelength intersensor spacing is utilised at the receiver side. The sensor array operates in the presence of three sources with each one being a nine-element grid array of half-wavelength intersensor spacing. The first source is the desired source while the rest are the interferers. The signal of each source arrives at the array along three paths; their parameters are listed in Table 2.1. Additionally, other simulation parameters are listed in Table 2.2.

2.3.1 Evaluation of the Localisation Approach

First, the joint cone angle and range bin estimation is shown in Figure 2.5, where three peaks at the cone angles and range bins $(74°, 10)$, $(87°, 12)$, and $(115°, 8)$ can be observed, indicating a correct estimation of the range bins. With the

Table 2.1: Simulation Parameters

Source	Path	Azimuth θ	Elevation ϕ	Range ρ	Bin ℓ	Path gain γ	
						Magnitude	Phase
1	1	297°	53°	6.9 m	10	8.63	198.35°
	2	80°	73°	8.5 m	12	3.30	86.17°
	3	143°	58°	5.6 m	8	7.21	302.87°
2	1	296°	48°	5.3 m	7	1.91	63.75°
	2	127°	50°	6.2 m	9	5.44	149.08°
	3	61°	79°	9.4 m	14	1.42	289.49°
3	1	45°	33°	5.9 m	8	7.30	226.92°
	2	9°	37°	8.7 m	13	7.42	180.75°
	3	288°	39°	5.1 m	7	0.62	220.11°

Table 2.2: Array System Parameters

Parameter	Value
Carrier frequency	600 THz
Channel symbol frequency	30 MHz
Code length	15
Number of snapshots	200
SNR	20 dB

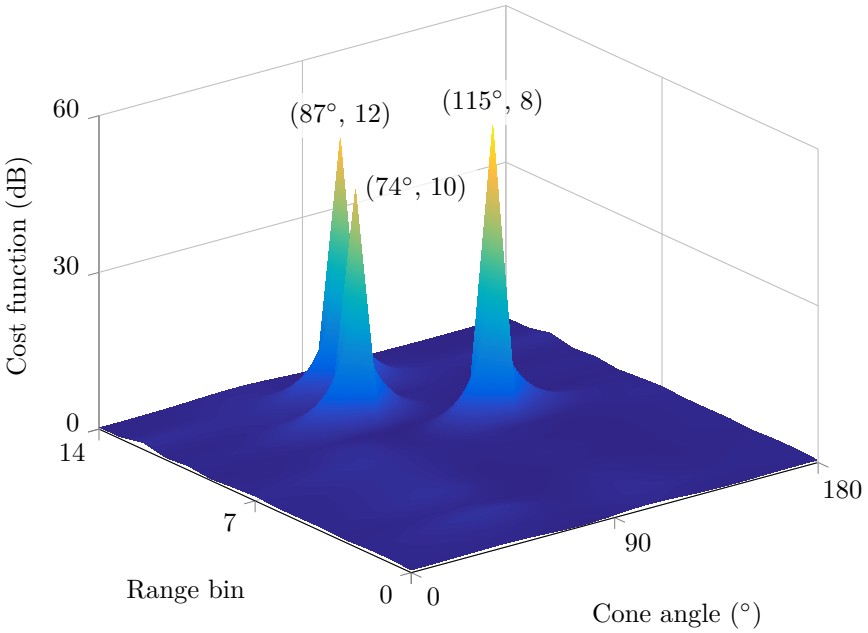

Figure 2.5: Cone angle and range bin estimation.

knowledge of the cone angle and range bin estimates, the azimuths and elevations are jointly estimated. The estimation result is shown in Figure 2.6, where three peaks at the azimuths and elevations $(297°, 53°)$, $(80°, 73°)$, and $(143°, 58°)$ can be observed; this means that the azimuths and elevations are correctly estimated as well. In addition, the path gains of the three paths of the desired source are estimated as $25.02\exp(j189.65°)$, $9.19\exp(j77.49°)$ and $21.00\exp(j294.08°)$. Note that they are different from the true path gains; however, the vector consisting of the true path gains and that consisting of the estimated path gains are collinear,

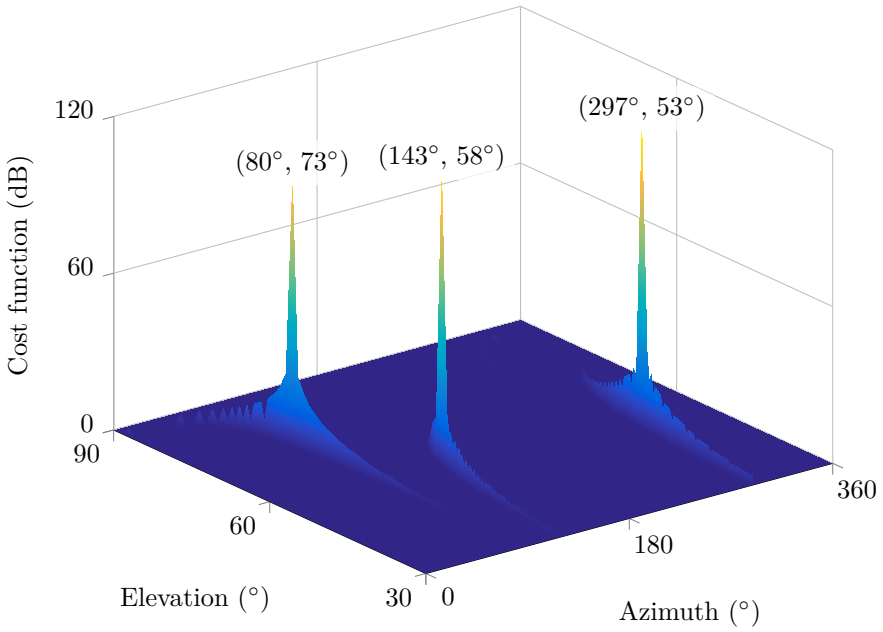

Figure 2.6: Azimuth and elevation estimation.

with a projection residual of 1.29×10^{-4}. Therefore, the channel parameters (i.e., azimuths, elevations, range bins, and path gains) of all the paths of the desired source are correctly estimated.

The performance of the estimators is also analysed in terms of the estimation root mean squared error (RMSE) using Monte Carlo simulations. The RMSEs of the azimuth, elevation, and path gain estimates with respect to the product of the SNR and number of snapshots[1] are shown in Figure 2.7. As can be observed, even at low SNR or with a small number of snapshots, the RMSEs of the three estimates are small, with the azimuth and elevation below $(1 \times 10^{-3})^\circ$ and the path gain below 1×10^{-2}. This indicates that the channel parameters can be estimated with excellent precision using the proposed localisation approach. In addition, the RMSEs decline as SNR $\times$ L increases. This is the expected result of the subspace estimators: the noise subspace can be more accurately estimated in practice with either higher SNR or more number of snapshots.

[1]Note that the RMSE Cramér–Rao bound is inversely proportional to SNR $\times$ L [1].

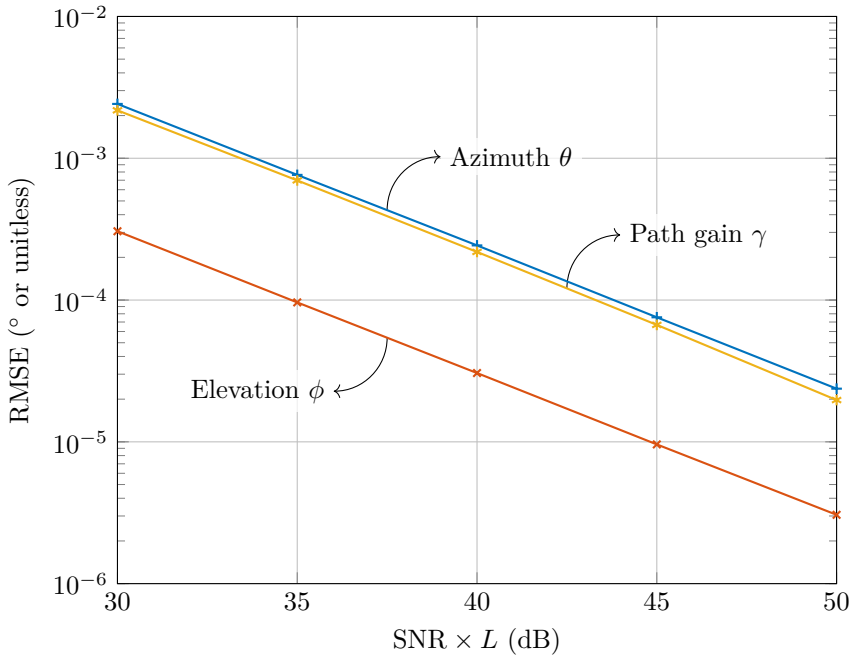

Figure 2.7: Estimation RMSE versus SNR and number of snapshots. The RMSEs of the azimuth θ, elevation ϕ, and path gain γ decrease as SNR $\times$ L increases. The results are averaged over 10 000 simulations.

2.3.2 Evaluation of the Beamformer

The performance of the two subspace beamformers are compared with the beamformer using the strongest and weakest paths, decorrelating receiver, and MMSE equaliser. The latter two are commonly employed in nonparametric OWC systems and their weight vectors are given, respectively, as [101, 104]

$$\underline{w}_D = \mathrm{col}_2\left(\mathbb{H}^H\left(\mathbb{H}^H\mathbb{H}\right)^{-1}\right); \tag{2.38}$$

$$\underline{w}_M = \mathrm{col}_2\left(\mathbb{H}^H\left(\mathbb{H}^H\mathbb{H} + \sigma_n^2\mathbb{I}_{3M}\right)^{-1}\right) \tag{2.39}$$

where

$$\mathbb{H} = \left[\mathbb{H}_1^-\underline{\gamma}_1, \mathbb{H}_1\underline{\gamma}_1, \mathbb{H}_1^+\underline{\gamma}_1, \mathbb{H}_2^-\underline{\gamma}_2, \mathbb{H}_2\underline{\gamma}_2, \mathbb{H}_2^+\underline{\gamma}_2, \ldots, \mathbb{H}_M^-\underline{\gamma}_M, \mathbb{H}_M\underline{\gamma}_M, \mathbb{H}_M^+\underline{\gamma}_M\right] \tag{2.40}$$

denotes the full channel knowledge these two receivers require.

The performance of the beamformers/receivers is investigated in terms of the output signal-to-noise-plus-interference ratio (SNIR), which is given as

$$\text{SNIR} = \frac{\underline{w}^H \mathbb{R}_{dd} \underline{w}}{\underline{w}^H \mathbb{R}_{uu} \underline{w}} \tag{2.41}$$

where $\mathbb{R}_{dd}$ and $\mathbb{R}_{uu}$ are the covariance matrices of the desired signal and undesired signal (interference and noise). The output SNIR with respect to the increasing input SNR is shown in Figure 2.8. All the beamformers/receivers have proportional increment in the output SNIR. This is the expected performance of the subspace beamformers since the interference is completely eliminated and the output SNIR only depends on the desired signal power and noise power. It can also be clearly observed that the two subspace beamformers maintain a comparable performance with the decorrelating receiver and MMSE multiuser receiver, and outperforms the

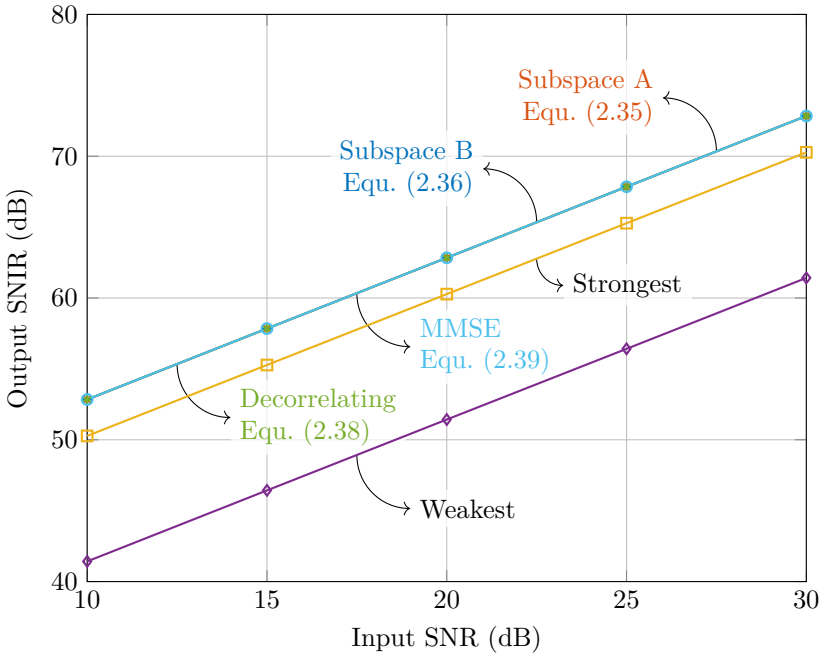

Figure 2.8: Output SNIR versus SNR. The results are averaged over 10 000 simulations.

other two beamformers. In addition, the output SNIR with respect to increasing number of sources is shown in Figure 2.9, with the input SNR fixed at 20 dB. All the beamformers/receivers have a constant output SNIR. From Figures 2.8 and 2.9, it can be concluded that, unlike the optimal decorrelating receiver and MMSE equaliser that require the channel knowledge of all signals (i.e., both the desired signal and the interferers), the two subspace beamformers only require that of the desired signal. However, they achieve comparable performance in terms of the output SNIR with the decorrelating receiver and MMSE, which are multiuser and thus very complex receivers.

2.4 Summary

In this chapter, a novel parametric model that incorporates the geometry of the photosensor and photoemitter arrays is studied for the indoor multi-source MIMO

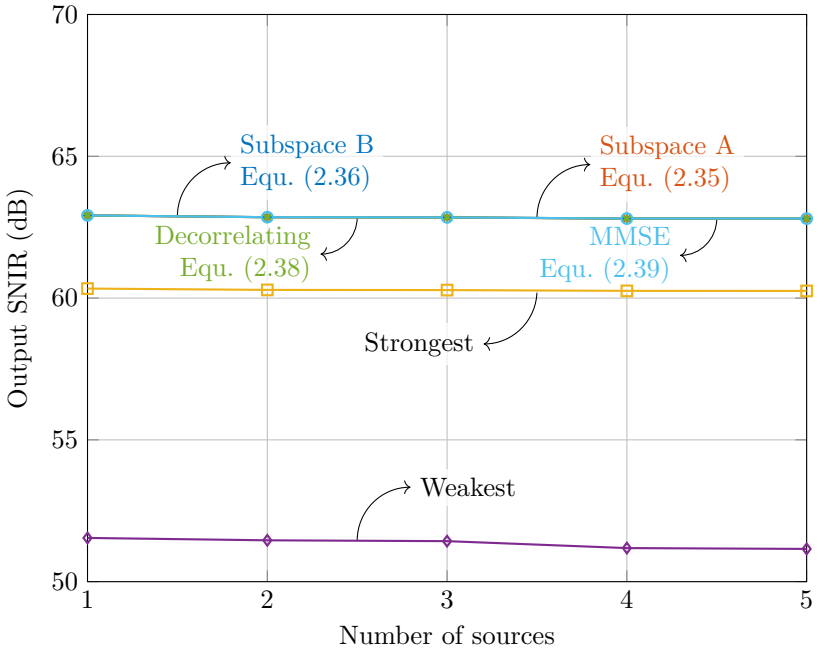

Figure 2.9: Output SNIR versus number of sources. The results are averaged over 10 000 simulations.

OWC system. A localisation approach, which is utilised as a blind spatiotemporal channel estimator to estimate the azimuth, elevation, range, and path gain, is presented as a three-step procedure, with the employment of the cone angle parameterisation. In addition, two multibeam beamformers that effectively combine all the paths of the desired source and completely eliminate ISI and MAI are presented. In contrast to the traditional OWC system where the interference is generally reduced by adjusting the locations and directions of the photoemitters and photosensors, the beamformers presented in this chapter achieve complete interference cancellation without the requirement of a precise physical configuration. Its system performance is comparable to the optimal decorrelating receiver in terms of the output SNIR, without full channel awareness.

Chapter 3

Localisation and Orientation Estimation of Receiver Arrays

The estimation of the location and orientation of an array of a known geometry has gained increasing interest in various research areas where the spatial information of the array plays a significant role for performance enhancement. For instance, in a large number of military and civil applications, wireless sensor networks are deployed to detect and track targets in their neighbourhood [105]. However, in many cases, the locations and orientations of the sensor arrays in the networks are not accurately known, which degrades the detection and tracking performance. Hence, localising and orienting the sensor arrays precisely are the essentials leading to better performance of the sensor networks [98].

In this chapter, the localisation and orientation estimation of a receiver array is studied. A sensor array of a known array geometry is utilised to estimate its own location and orientation with respect to a global coordinate system based on the signals transmitted from multiple sources of known locations. The estimation approach proposed in this chapter is carried out in a four-phase procedure: The DOAs of the sources are estimated first using subspace techniques. Based on the

DOA estimates, the ranges of the sources can be directly derived by solve a system of quadratic equations, without knowing the transmitted signals. Finally, the location and orientation of the sensor array are estimated by solving two systems of linear equations in the last two steps. Hereafter, the term "receiver estimation" is used to refer to this scenario unless otherwise noted.

The rest of this chapter is organised as follows. In Section 3.1, the signal model of the receiver estimation scenario is explained. In Section 3.2 the receiver estimation approach is detailed as a four-step procedure. In Section 3.3, the performance of the proposed approaches is evaluated using computer simulation studies. Last, in Section 3.4, the chapter is summarised.

3.1 Signal Model of Receiver Estimation

Consider an array of N sensors of a known array geometry. The array receives the signals from M sources with $M < N$ via the LOS paths only. Note that each source can consist of multiple emitters; however, it is assumed that each source is a single emitter for the sake of simplicity. (The generalisation to multi-emitter sources is fairly straightforward and is not explained in this chapter.) The geometry of the sensor array and sources is shown in Figure 3.1, where the sensors are represented by the blue spheres and the sources are represented by the red cubes. With reference to Figure 3.1, the locations of the sensors and sources can be specified in two distinct Cartesian coordinate systems: the local coordinate system (blue and lower case) and the global coordinate system (red and upper case). Hereafter, the terms "local system" and "global system" are used to refer to the local and global coordinate systems, respectively, for convenience unless otherwise noted.

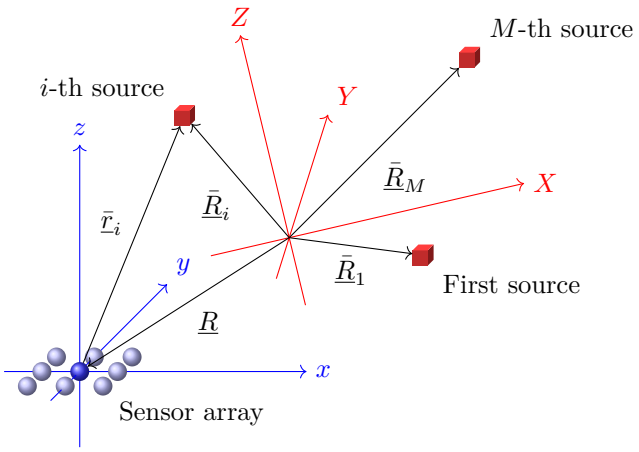

Figure 3.1: Geometry of the sensor array and sources. The sensors of the array are represented by the blue spheres with the array reference point denoted by the darker one. The sources are represented by the red cubes. Their locations can be specified in both the local (blue and lower case) and global (red and upper case) coordinate systems.

Specifically, in the local system, the known array geometry is described as

$$[\underline{r}_1, \underline{r}_2, \ldots, \underline{r}_N] = \left[\underline{r}_x, \underline{r}_y, \underline{r}_z\right]^T \in \mathcal{R}^{3\times N} \tag{3.1}$$

where $\underline{r}_k = [x_k, y_k, z_k]^T \in \mathcal{R}^{3\times 1}$ is the Cartesian coordinates of the k-th sensor while $\underline{r}_x$, $\underline{r}_y$, and $\underline{r}_z \in \mathcal{R}^{N\times 1}$ contain the coordinates of the x-, y-, and z-axis of all the sensors, respectively. Without loss of generality, assume that the array centroid $\underline{r} = [x, y, z]^T \in \mathcal{R}^{3\times 1}$ is the origin of the local system and the array reference point. It is also defined as the location of the array in the local system. Further, the unknown location of the i-th source is parameterised by its unknown azimuth θ_i, elevation ϕ_i, and range ρ_i as

$$\bar{\underline{r}}_i \triangleq \bar{\underline{r}}(\theta_i, \phi_i, \rho_i) = \rho_i \underline{u}_i = [\bar{x}_i, \bar{y}_i, \bar{z}_i]^T \in \mathcal{R}^{3\times 1} \tag{3.2}$$

where

$$\underline{u}_i \triangleq \underline{u}(\theta_i, \phi_i) = [\cos\theta_i \cos\phi_i, \sin\theta_i \cos\phi_i, \sin\phi_i]^T \in \mathcal{R}^{3\times 1} \tag{3.3}$$

is the unit vector pointing from the array reference point towards the i-th source. In addition, note that $\rho_i = \|\bar{\underline{r}}_i\|$.

On the other hand, in the global system, the unknown location of the sensor array (i.e., the array reference point) is denoted as $\underline{R} = [X, Y, Z]^T \in \mathcal{R}^{3\times 1}$. In addition, the known location of the i-th source in the global system is denoted as $\bar{\underline{R}}_i = \left[\bar{X}_i, \bar{Y}_i, \bar{Z}_i\right]^T \in \mathcal{R}^{3\times 1}$.

Furthermore, the unknown mapping from the local system to its global counterpart is governed by a transformation matrix defined as

$$\mathbb{T} = \begin{bmatrix} \mathbb{Q}, & \underline{R} \\ \underline{0}_3^T, & 1 \end{bmatrix} \tag{3.4}$$

where $\mathbb{Q} \in \mathcal{R}^{3\times 3}$ is the orthogonal rotation matrix and $\underline{R}$, the location of the sensor array in the global system, also serves as the translation vector. Using this transformation matrix $\mathbb{T}$ and its inverse $\mathbb{T}^{-1}$, a vector $\underline{v} \in \mathcal{R}^{3\times 1}$ in the local system can be mapped to and from its global counterpart $\underline{V} \in \mathcal{R}^{3\times 1}$ as

$$\left[\underline{V}^T, 1\right]^T = \mathbb{T}\left[\underline{v}^T, 1\right]^T; \tag{3.5a}$$

$$\left[\underline{v}^T, 1\right]^T = \mathbb{T}^{-1}\left[\underline{V}^T, 1\right]^T \tag{3.5b}$$

or, equivalently, as

$$\underline{V} = \mathbb{Q}\underline{v} + \underline{R}; \tag{3.6a}$$

$$\underline{v} = \mathbb{Q}^{-1}\underline{V} - \mathbb{Q}^{-1}\underline{R}. \tag{3.6b}$$

In particular, the rotation matrix $\mathbb{Q}$ can be written in terms of the product of three rotation matrices as

$$\mathbb{Q} = \mathbb{Q}_x\mathbb{Q}_y\mathbb{Q}_z \tag{3.7}$$

where

$$\mathbb{Q}_x = \begin{bmatrix} 1, & 0, & 0 \\ 0, & \cos\alpha, & \sin\alpha \\ 0, & -\sin\alpha, & \cos\alpha \end{bmatrix} \in \mathcal{R}^{3\times 3}; \tag{3.8a}$$

$$\mathbb{Q}_y = \begin{bmatrix} \cos\beta, & 0, & -\sin\beta \\ 0, & 1, & 0 \\ \sin\beta, & 0, & \cos\beta \end{bmatrix} \in \mathcal{R}^{3\times 3}; \tag{3.8b}$$

$$\mathbb{Q}_z = \begin{bmatrix} \cos\gamma, & \sin\gamma, & 0 \\ -\sin\gamma, & \cos\gamma, & 0 \\ 0, & 0, & 1 \end{bmatrix} \in \mathcal{R}^{3\times 3} \tag{3.8c}$$

are the rotation matrices about the x-, y-, and z-axis with the respective unknown Euler angles α (a.k.a., roll), β (a.k.a., pitch), and γ (a.k.a., yaw), as shown in Figure 3.2. By convention, $0° \leq \alpha \leq 360°$, $0° \leq \beta \leq 180°$, and $0° \leq \gamma \leq 360°$.

In summary, only the array geometry in the local system and the locations of the sources in the global system are known. The rest are unknown, including the location of the sensor array in the global system $\underline{R}$ and the orientation $\mathbb{Q}$ (or the Euler angles α, β, and γ), which are to be estimated. The knowns and unknowns are also summarised in Table 3.1.

As the sensors form a compact array, the plane wave propagation model is considered. In addition, the NBA is generally valid under this circumstance. Therefore, the signal received at the sensor array can be modelled as

$$\underline{x}(t) = \sum_{i=1}^{M} \underline{S}_i m_i(t) + \underline{n}(t) \in \mathcal{C}^{N\times 1} \tag{3.9}$$

where, for the i-th source, $\underline{S}_i \in \mathcal{C}^{N\times 1}$ is the plane wave array manifold vector given

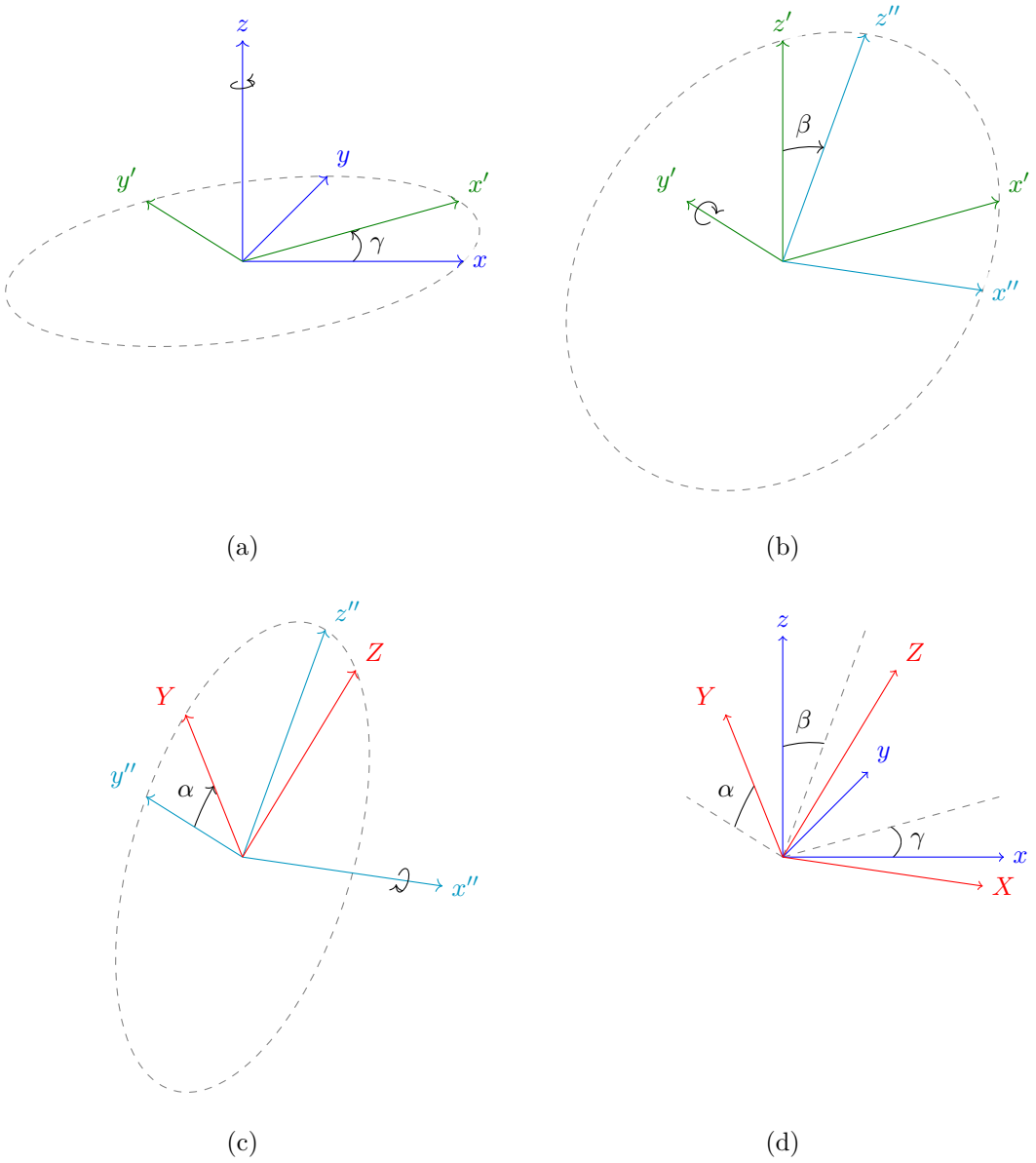

Figure 3.2: Transformation from the local system to the global system. (a) Yaw γ. The local coordinate system xyz is rotated around the z-axis for γ to the coordinate system $x'y'z'$. (b) Pitch β. The coordinate system $x'y'z'$ is rotated around the y'-axis for β to the coordinate system $x''y''z''$. (c) Roll α. The coordinate system $x''y''z''$ is rotated around the x''-axis for α to the global coordinate system XYZ. (d) Euler angles α, β, and γ. The coordinate transformation is dictated by the three Euler angles.

Table 3.1: Summary of the Knowns and Unknowns

Parameter	Local system		Global system	
	Symbol	Status	Symbol	Status
Sensor array geometry	$\underline{r}_k$	known	—	
Sensor array location	$\underline{r}$	known	$\underline{R}$	unknown*
Source locations	$\bar{\underline{r}}_i$	unknown	$\bar{\underline{R}}_i$	known
Source parameters	θ_i, ϕ_i, and ρ_i	unknown	—	
Transformation matrix	$\mathbb{T}$	unknown	—	
Rotation matrices	$\mathbb{Q}_x$, $\mathbb{Q}_y$, and $\mathbb{Q}_z$	unknown	—	
Euler angles	α, β, and γ	unknown*	—	

*These unknowns are to be estimated.

as

$$\underline{S}_i \triangleq \underline{S}(\theta_i, \phi_i) = \exp\Big(-j2\pi \frac{F_c}{c} \left[\underline{r}_x, \underline{r}_y, \underline{r}_z\right] \underline{u}_i\Big), \tag{3.10}$$

$m_i(t)$ is the message signal, and $\underline{n}(t) \in \mathcal{C}^{N\times 1}$ is the complex AWGN of zero mean and covariance $\sigma_n^2 \mathbb{I}_N$. The received signal vector can be rewritten in a matrix format as

$$\underline{x}(t) = \mathbb{S}\underline{m}(t) + \underline{n}(t) \tag{3.11}$$

where

$$\mathbb{S} = [\underline{S}_1, \underline{S}_2, \ldots, \underline{S}_M] \in \mathcal{C}^{N\times M}; \tag{3.12}$$

$$\underline{m}(t) = [m_1(t), m_2(t), \ldots, m_M(t)]^T \in \mathcal{C}^{N\times 1}. \tag{3.13}$$

3.2 Design of the Estimation Approach

The objective of the estimation problem is to find the location of the array reference point of the receiver array in the global system as well as the orientation of the local system with respect to the global system. The estimation procedure is carried out

in the following four phases: First, the azimuths and elevations (i.e., directions) of all the sources are estimated in the local system using subspace techniques. Next, based on the direction estimates, the ranges of the sources in the local system are estimated by solving a system of quadratic equations. Subsequently, with the range estimates available, the sensor array location in the global system as well as its orientation can be estimated by solving two systems of linear equations in the final two phases. The four-phase estimation procedure is detailed as follows.

3.2.1 Direction Estimation

Initially, the directions of the sources are estimated based on the second order statistics of the received signal vector given in Equ. (3.11) in the local system. In particular, the covariance matrix of the received signal vector is

$$\begin{aligned}\mathbb{R}_{xx} &= \mathcal{E}\Big\{\underline{x}(t)\,\underline{x}^H(t)\Big\} \\ &= \mathbb{S}\,\underbrace{\mathcal{E}\Big\{\underline{m}(t)\,\underline{m}^H(t)\Big\}}_{=\mathbb{R}_{mm}}\mathbb{S}^H + \underbrace{\mathcal{E}\Big\{\underline{x}(t)\,\underline{x}^H(t)\Big\}}_{=\mathbb{R}_{nn}} \\ &= \mathbb{S}\mathbb{R}_{mm}\mathbb{S}^H + \mathbb{R}_{nn} \in \mathcal{C}^{N\times N} \end{aligned} \tag{3.14}$$

where $\mathbb{R}_{mm} \in \mathcal{C}^{M\times M}$ and $\mathbb{R}_{nn} = \sigma_n^2\mathbb{I}_N \in \mathcal{R}^{N\times N}$ are the covariance matrices of the messages and noise, respectively. Using subspace techniques like MUSIC, the azimuths and elevations of the sources can be estimated by a two-dimensional search of

$$\xi(\theta,\phi) = \frac{\underline{S}^H(\theta,\phi)\,\underline{S}(\theta,\phi)}{\underline{S}^H(\theta,\phi)\,\mathbb{E}_n\mathbb{E}_n^H\,\underline{S}(\theta,\phi)} \tag{3.15}$$

where $\mathbb{E}_n \in \mathcal{C}^{N\times(N-M)}$ represents the noise subspace of $\mathbb{R}_{xx}$.

3.2.2 Range Estimation

After estimating the azimuths θ_i and elevations ϕ_i of all the sources, their directional unit vectors $\underline{u}_i$ can be derived. Define the matrix containing the estimates of the directional unit vectors of all the sources as

$$\mathbb{U} = [\underline{\hat{u}}_1, \underline{\hat{u}}_2, \ldots, \underline{\hat{u}}_M] \in \mathcal{R}^{3\times M} \tag{3.16}$$

where $\underline{\hat{u}}_i$ is the estimate of the i-th directional unit vector. In addition, a vector comprising the unknown ranges of all the sources can be defined as

$$\underline{\rho} = [\rho_1, \rho_2, \ldots, \rho_M]^T \in \mathcal{R}^{M\times 1}. \tag{3.17}$$

Recall that the location of the i-th source in the local system is given as $\bar{\underline{r}}_i = \rho_i \underline{u}_i$. This location vector $\bar{\underline{r}}_i$ is variant with respect to the change of the coordinate system; i.e., its global counterpart $\bar{\underline{R}}_i$, given as

$$\bar{\underline{R}}_i = \mathbb{Q}\bar{\underline{r}}_i + \underline{R}, \tag{3.18}$$

is not equal to $\bar{\underline{r}}_i$ in general. Nevertheless, the distance between any two location vectors $\bar{\underline{r}}_i$ and $\bar{\underline{r}}_j$ (assume that $i < j$) is invariant with respect to the coordinate transformation. Specifically, the difference between $\bar{\underline{r}}_i$ and $\bar{\underline{r}}_j$ is given as

$$\bar{\underline{R}}_i - \bar{\underline{R}}_j = (\mathbb{Q}\bar{\underline{r}}_i + \underline{R}) - \left(\mathbb{Q}\bar{\underline{r}}_j + \underline{R}\right) = \mathbb{Q}\left(\bar{\underline{r}}_i - \bar{\underline{r}}_j\right) \tag{3.19}$$

and the squares of the Euclidean norms of its both sides can be expressed as

$$\left\|\bar{\underline{R}}_i - \bar{\underline{R}}_j\right\|^2 = \left(\bar{\underline{r}}_i - \bar{\underline{r}}_j\right)^T \mathbb{Q}^T\mathbb{Q}\left(\bar{\underline{r}}_i - \bar{\underline{r}}_j\right). \tag{3.20}$$

Since $\mathbb{Q}$ is an orthogonal matrix, $\mathbb{Q}^T\mathbb{Q} = \mathbb{I}_3$. Hence,

$$\begin{aligned}\left\|\underline{\bar{R}}_i - \underline{\bar{R}}_j\right\|^2 &= \left(\underline{\bar{r}}_i - \underline{\bar{r}}_j\right)^T \left(\underline{\bar{r}}_i - \underline{\bar{r}}_j\right) \\ &= \left\|\underline{\bar{r}}_i\right\|^2 - 2\underline{\bar{r}}_i^T \underline{\bar{r}}_j + \left\|\underline{\bar{r}}_j\right\|^2 \\ &= \rho_i^2 - 2\underline{\bar{u}}_i^T \underline{\bar{u}}_j \rho_i \rho_j + \rho_j^2. \end{aligned} \tag{3.21}$$

This is a bivariate quadratic equation and can be rewritten as

$$\left\|\underline{\bar{R}}_i - \underline{\bar{R}}_j\right\|^2 = \underline{\rho}^T \mathbb{F}_{ij} \mathbb{U}^T \mathbb{U} \mathbb{F}_{ij} \underline{\rho} \tag{3.22}$$

where $\mathbb{F}_{ij} \in \mathcal{Z}^{M \times M}$ is the selection matrix of the i-th and j-th sources defined as

$$\mathbb{F}_{ij} = \mathrm{diag}\Big(\left[\underline{0}_{i-1}^T, 1, \underline{0}_{j-i-1}^T, -1, \underline{0}_{M-j}^T\right]^T\Big). \tag{3.23}$$

Equation (3.22) expresses the invariance of the distance between a pair of sources. Taking all the $J = \binom{M}{2}$ pairs into account, the invariance can be represented as

$$\left(\mathbb{I}_J \otimes \underline{\rho}\right)^T \mathbb{A}_\rho \underline{\rho} = \underline{B}_\rho \tag{3.24}$$

where

$$\mathbb{A}_\rho = \begin{bmatrix} \mathbb{F}_{12}\mathbb{U}^T\mathbb{U}\mathbb{F}_{12} \\ \mathbb{F}_{13}\mathbb{U}^T\mathbb{U}\mathbb{F}_{13} \\ \vdots \\ \mathbb{F}_{(M-1)M}\mathbb{U}^T\mathbb{U}\mathbb{F}_{(M-1)M} \end{bmatrix} \in \mathcal{R}^{JM \times M}; \tag{3.25a}$$

$$\underline{B}_{\rho} = \begin{bmatrix} \left\|\bar{\underline{R}}_1 - \bar{\underline{R}}_2\right\|^2 \\ \left\|\bar{\underline{R}}_1 - \bar{\underline{R}}_3\right\|^2 \\ \vdots \\ \left\|\bar{\underline{R}}_{M-1} - \bar{\underline{R}}_M\right\|^2 \end{bmatrix} \in \mathcal{R}^{J\times 1}. \tag{3.25b}$$

Equation (3.24) is a system of multivariate quadratic equations of M unknowns and J equations. The ranges $\underline{\rho}$ can then be estimated by solving Equ. (3.24) if $J \geq M$; i.e., $M > 2$ [106].

3.2.3 Location Estimation

After estimating the directions and ranges of the sources in the local system, the location of the receiver array in the global system should be estimated next. Based on Equ. (3.18) and [13], the location $\underline{R}$ can be estimated by solving the following system of linear equations

$$\mathbb{A}_R \underline{R} = \underline{B}_R \Rightarrow \hat{\underline{R}} = \mathbb{A}_R^{\#} \underline{B}_R \tag{3.26}$$

where

$$\mathbb{A}_R = \begin{bmatrix} 2\left(\bar{\underline{R}}_1 - \bar{\underline{R}}_2\right) \\ 2\left(\bar{\underline{R}}_1 - \bar{\underline{R}}_3\right) \\ \vdots \\ 2\left(\bar{\underline{R}}_1 - \bar{\underline{R}}_M\right) \end{bmatrix} \in \mathcal{R}^{(M-1)\times 3}; \tag{3.27a}$$

$$\underline{B}_R = \begin{bmatrix} \left(\left\|\bar{\underline{R}}_1\right\|^2 - \left\|\bar{\underline{R}}_2\right\|^2\right) - (\hat{\rho}_1^2 - \hat{\rho}_2^2) \\ \left(\left\|\bar{\underline{R}}_1\right\|^2 - \left\|\bar{\underline{R}}_3\right\|^2\right) - (\hat{\rho}_1^2 - \hat{\rho}_3^2) \\ \vdots \\ \left(\left\|\bar{\underline{R}}_1\right\|^2 - \left\|\bar{\underline{R}}_M\right\|^2\right) - (\hat{\rho}_1^2 - \hat{\rho}_M^2) \end{bmatrix} \in \mathcal{R}^{(M-1)\times 1} \tag{3.27b}$$

with $M - 1 \geq 3$; i.e., $M > 3$.

3.2.4 Orientation Estimation

The final step is to estimate the orientation of the receiver array. Equation (3.18) can be rewritten as

$$(\bar{\underline{r}}_i \otimes \mathbb{I}_3)^T \operatorname{vec}(\mathbb{Q}) = \bar{\underline{R}}_i - \hat{\underline{R}} \tag{3.28}$$

where $\operatorname{vec}(\mathbb{Q})$ is the only unknown to be estimated. Likewise, $\operatorname{vec}(\mathbb{Q})$ can also be determined by solving the following system of linear equations

$$\mathbb{A}_Q \operatorname{vec}(\mathbb{Q}) = \underline{B}_Q \Rightarrow \operatorname{vec}\Big(\hat{\mathbb{Q}}\Big) = \mathbb{A}_Q^{\#} \underline{B}_Q \tag{3.29}$$

where

$$\mathbb{A}_Q = [\bar{\underline{r}}_1, \bar{\underline{r}}_2, \ldots, \bar{\underline{r}}_M]^T \otimes \mathbb{I}_3 \in \mathcal{R}^{3M \times 9}; \tag{3.30a}$$

$$\underline{B}_Q = \Big[\bar{\underline{R}}_1^T, \bar{\underline{R}}_2^T, \ldots, \bar{\underline{R}}_M^T\Big]^T - \underline{1}_M \otimes \underline{R} \in \mathcal{R}^{3M \times 1} \tag{3.30b}$$

with $3M \geq 9$; i.e., $M > 2$ [106]. Further, the Euler angles α, β, and γ can be derived from $\hat{\mathbb{Q}}$ as

$$\hat{\alpha} = \arctan\left(\frac{\underline{F}_2^T \hat{\mathbb{Q}} \underline{F}_3}{\underline{F}_3^T \hat{\mathbb{Q}} \underline{F}_3}\right); \tag{3.31a}$$

$$\hat{\beta} = -\arcsin\Big(\underline{F}_1^T \hat{\mathbb{Q}} \underline{F}_3\Big); \tag{3.31b}$$

$$\hat{\gamma} = \arctan\left(\frac{\underline{F}_1^T \hat{\mathbb{Q}} \underline{F}_2}{\underline{F}_1^T \hat{\mathbb{Q}} \underline{F}_1}\right) \tag{3.31c}$$

where $\underline{F}_p = \Big[\underline{0}_{p-1}^T, 1, \underline{0}_{3-p}^T\Big]^T \in \mathcal{Z}^{3\times 1}$ for $p = 1, 2, 3$. Furthermore, it is clear that at least four sources are needed to successfully estimate the location and orientation of the receiver array.

In conclusion, the proposed localisation and orientation estimation algorithm is summarised as the following steps.

Step 1: Construct the covariance matrix of the received signal vector and estimate the azimuths and elevations of all the sources in the local system by a two-dimensional search of Equ. (3.15).

Step 2: Based on the estimated directions from Step 1, estimate the ranges of the sources by solving a system of equations given in Equ. (3.24).

Step 3: Based on the estimated ranges from Step 2, estimate the location of the sensor array in the global system by solving a system of equations using Equ. (3.26).

Step 4: Estimate the orientation of the sensor array by solving a system of equations using Equ. (3.29). Subsequently, derive the Euler angles from the rotation matrix using Equs. (3.31a) to (3.31c).

In addition, note that if the source elevations are negligible, the range estimation step can be circumvented; i.e., the location and orientation of the receiver array can be estimated without solving the system of quadratic equations. This simplified approach is detailed in Appendix 3.A.

Besides, if NLOS paths are in existence in addition to the LOS paths, then the received signal is firstly preprocessed to remove the NLOS paths before any LOS localisation algorithm is employed [107]. Nevertheless, for the sake of simplicity, the NLOS paths are not considered in this chapter.

3.3 Computer Simulation Studies

In this section, the performance of the location and orientation estimators of the receiver array in the three- and two-dimensional scenarios is assessed through

computer simulation studies.

In the simulations, a nine-element grid array of 0.05 m (half-wavelength) intersensor spacing is utilised. First, the three-dimensional scenario is investigated. In this case, the array operates in the presence of four sources; their parameters in the local system are listed in Table 3.2. The parameters of the sensor array in the global system, together with the Euler angles, are also listed in Table 3.2. Additionally, other array system parameters are listed in Table 3.3.

The joint azimuth and elevation estimation result in the three-dimensional scenario is shown in Figure 3.3, where four peaks at the azimuths and elevations $(58°, 39°)$, $(331°, 28°)$, $(110°, 22°)$, and $(273°, 64°)$ can be observed, indicating a successful estimation of the source directions. Based on the source direction estimates, the source ranges and the sensor array location and orientation in the global system can be estimated. The estimation errors of the four phases are listed

Table 3.2: Simulation Parameters of Three-Dimensional Receiver Estimation

Item		**Azimuth** θ	**Elevation** ϕ	**Range** ρ	**Roll** α	**Pitch** β	**Yaw** γ
Local	**Source 1**	58°	39°	810 m	60°	77°	20°
	Source 2	331°	28°	773 m			
	Source 3	110°	22°	537 m			
	Source 4	273°	64°	377 m			
Global	**Sensor array**	40°	38°	900 m			

Table 3.3: Array System Parameters

Parameter	**Value**
Carrier frequency	3 GHz
Sampling frequency	30 MHz
Number of snapshots	200
SNR	20 dB

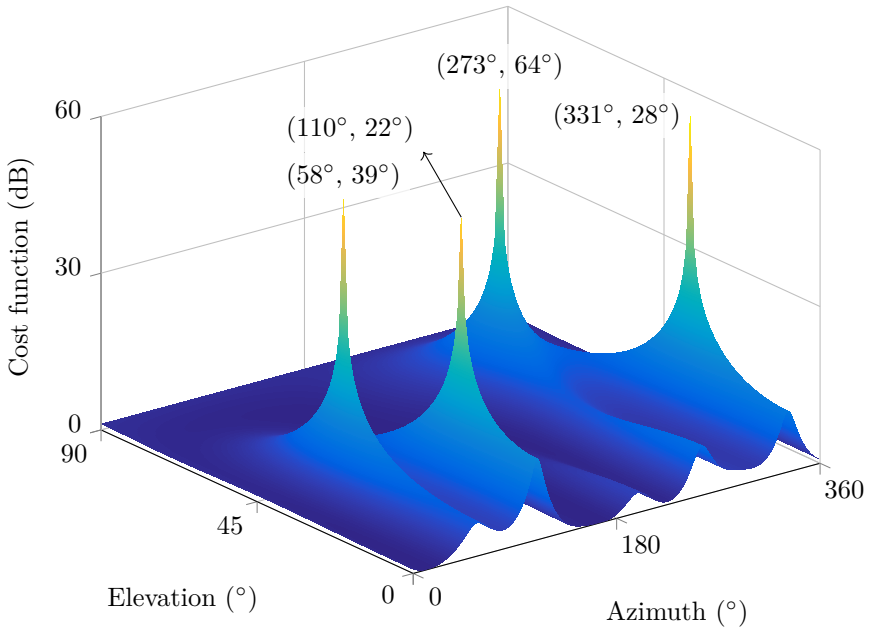

Figure 3.3: Three-dimensional receiver azimuth and elevation estimation.

in Table 3.4. The estimation errors of the azimuths and elevations are in the order of $(1 \times 10^{-2})°$, which is as expected since MUSIC is a superresolution algorithm. Based on these estimation errors, the errors of the ranges and the location of the sensor array are in the order of 1×10^{-1} m, and those of the Euler angles are in the order of $(1 \times 10^{-1})°$, which suggests that the location and orientation of the sensor array are very accurately estimated.

Furthermore, the performance of the estimators in the three-dimensional scenario is assessed in terms of the estimation RMSE. As shown in Figure 3.4, the RMSE curves of the sensor array location and Euler angles decline as SNR $\times$ L increases for the proposed approach. Moreover, the RMSE reaches the order of magnitude of 1 m for the location displacement and 1° for the Euler angles even at low SNR or with a small number of snapshots.

Another common localisation approach is based on the TOA of sources. The comparison of the DOA- and TOA-based approaches can be found in [13]. Note that the performance of the TOA-based approach is dependent on the bandwidth

Table 3.4: Estimation Errors of Three-Dimensional Receiver Estimation

Source	**Azimuth θ**	**Elevation ϕ**	**Range ρ**
1	$(0.77 \times 10^{-2})^\circ$	$(1.76 \times 10^{-2})^\circ$	2.01×10^{-1} m
2	$(1.29 \times 10^{-2})^\circ$	$(0.65 \times 10^{-2})^\circ$	1.28×10^{-1} m
3	$(2.05 \times 10^{-2})^\circ$	$(0.70 \times 10^{-2})^\circ$	3.11×10^{-1} m
4	$(1.19 \times 10^{-2})^\circ$	$(1.82 \times 10^{-2})^\circ$	5.94×10^{-1} m
Sensor array	***X***	***Y***	***Z***
	7.52×10^{-1} m	7.04×10^{-1} m	1.94×10^{-1} m
Euler angle	**Roll α**	**Pitch β**	**Yaw γ**
	$(1.30 \times 10^{-1})^\circ$	$(0.40 \times 10^{-1})^\circ$	$(0.83 \times 10^{-1})^\circ$

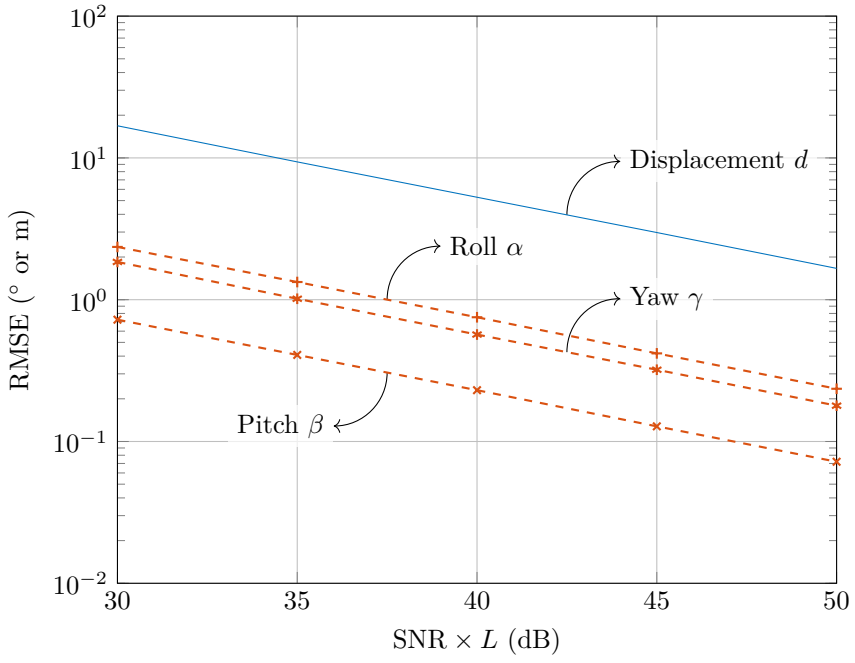

Figure 3.4: Three-dimensional receiver estimation RMSE versus SNR and number of snapshots. The RMSEs of the displacement d and Euler angles α, β, and γ decrease as SNR $\times$ L increases. The results are averaged over 10 000 simulations.

of the signal: the estimation is erroneous if the bandwidth is too narrow, in spite of the increase in the SNR or the number of snapshots.

In addition, similar simulations are carried out in the two-dimensional scenario using the simplified approach explained in Appendix 3.A. The parameters that are different from the three-dimensional case are listed in Table 3.5. The azimuth estimation result is shown in Figure 3.5, where three peaks at the azimuths 154°, 253°, and 82° can be observed, indicating a successful estimation of the azimuths. Based on the azimuth estimates, the sensor array location and orientation in the global system can be directly estimated, without the estimation of the source

Table 3.5: Simulation Parameters of Two-Dimensional Receiver Estimation

Item		**Azimuth θ**	**Range ρ**	Yaw γ
Local	**Source 1**	154°	580 m	$-16°$
	Source 2	253°	22 m	
	Source 3	82°	993 m	
Global	**Sensor array**	125°	782 m	

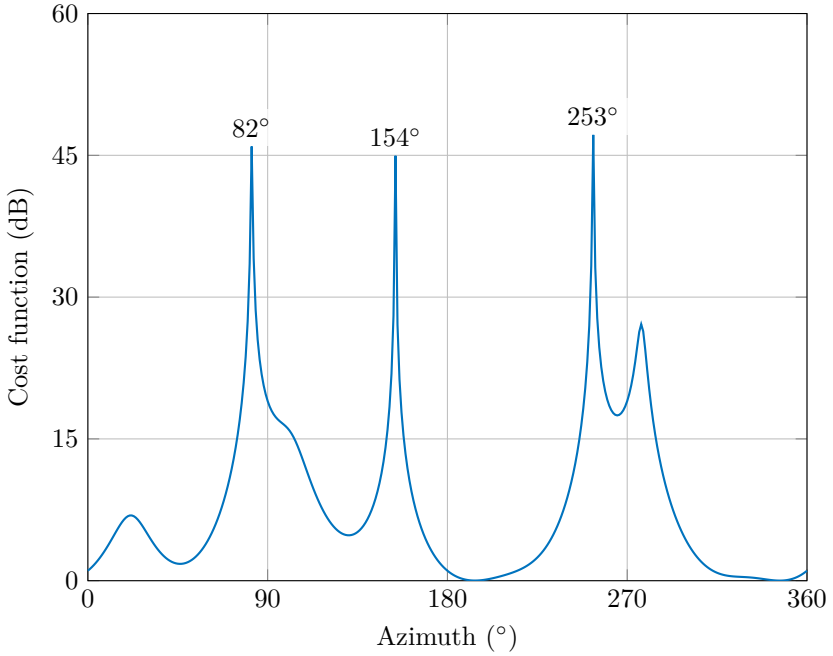

Figure 3.5: Two-dimensional receiver azimuth estimation.

ranges. The estimation errors of the source directions and sensor array location and orientation are listed in Table 3.6. On top, the estimation RMSE is shown in Figure 3.6. Similar conclusions to the three-dimensional scenario can be drawn from the estimation results.

Table 3.6: Estimation Errors of Two-Dimensional Receiver Estimation

Source	**Azimuth θ**	
1	$(4.87 \times 10^{-2})^\circ$	
2	$(4.67 \times 10^{-2})^\circ$	
3	$(0.14 \times 10^{-2})^\circ$	
Sensor array	***X***	***Y***
	$0.09 \times 10^{-1}\,\mathrm{m}$	$5.26 \times 10^{-1}\,\mathrm{m}$
Euler angle	**Yaw γ**	
	$(3.46 \times 10^{-2})^\circ$	

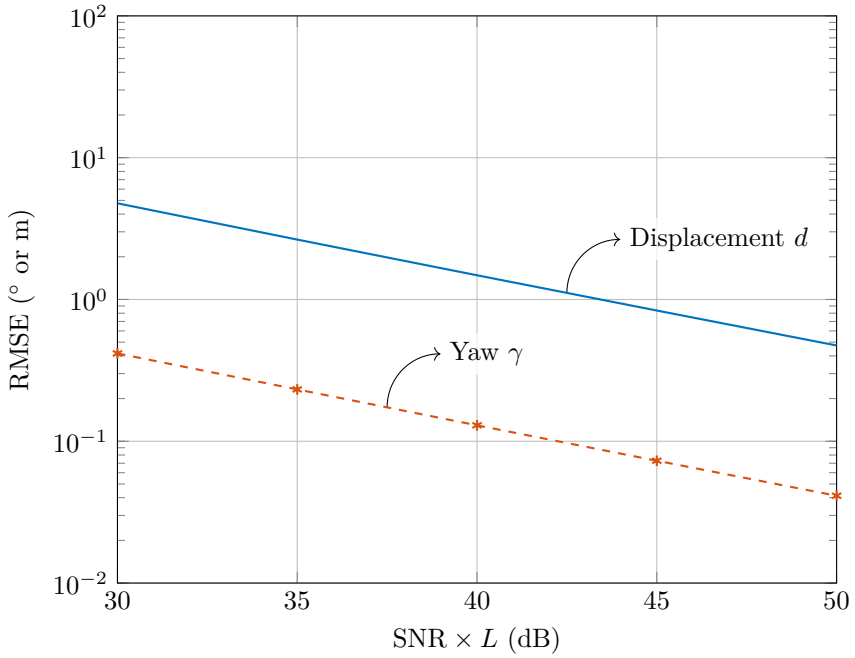

Figure 3.6: Two-dimensional receiver estimation RMSE versus SNR and number of snapshots. The RMSEs of the displacement d and yaw γ decrease as SNR $\times$ L increases. The results are averaged over 10 000 simulations.

3.4 Summary

In this chapter, the approach to the estimation the location and orientation of a receiver array is proposed. A sensor array is utilised to estimate the location and orientation of its own in a global coordinate system based on the signals transmitted from multiple sources. First, the directions of the sources are estimated using subspace techniques like MUSIC. Subsequently, with the estimated directions, the location and orientation of the receiver array are estimated by solving three systems of equations, without the knowledge of the transmitted signals. In addition, a simplified approach is proposed for the two-dimensional case. From the computer simulation results, the approaches presented in this chapter are shown to estimate the location and orientation with exceeding accuracy, compared to the DOA–TOA estimation approach.

Appendix 3.A Simplification with Negligible Elevations

The receiver location and orientation estimation approach described in Section 3.2 can be hugely simplified when the elevations of the sources are negligible.

In two-dimensional space, the elevations of all the sources are zeros; i.e., $\phi_i = 0^\circ$ for $i = 1, 2, \ldots, M$. This implies that the z-coordinates of all the sources are zeros in both the local and global systems; i.e., $\underline{\bar{r}}_z = \underline{\bar{R}}_z = \underline{0}_M$. In addition, the Euler angles $\alpha = \beta = 0^\circ$ since the global system is simply a rotated (and displaced) version of the local system about the z-axis only; this indicates that $\mathbb{Q} = \mathbb{Q}_z$. Under this circumstance, the estimation approach can be carried out as the following three-phase procedure.

The first phase is the same as the approach in three-dimensional space. Using

subspace techniques like MUSIC, the azimuths of the sources can be estimated by a one-dimensional search of

$$\xi(\theta) = \frac{\underline{S}^H(\theta)\,\underline{S}(\theta)}{\underline{S}^H(\theta)\,\mathbb{E}_n\mathbb{E}_n^H\,\underline{S}(\theta)} \tag{3.32}$$

where $\mathbb{E}_n \in \mathcal{C}^{N\times(N-M)}$ denotes the noise subspace.

The location of the receiver array is estimated upon completion of the direction estimation. Recall that the location of the i-th source in the local system can be mapped to its global counterpart using Equ. (3.18), which can be rewritten as

$$\begin{aligned}
\begin{bmatrix} \bar{X}_i \\ \bar{Y}_i \\ 0 \end{bmatrix} &= \begin{bmatrix} \cos\gamma, & \sin\gamma, & 0 \\ -\sin\gamma, & \cos\gamma, & 0 \\ 0, & 0, & 1 \end{bmatrix} \begin{bmatrix} \bar{x}_i \\ \bar{y}_i \\ 0 \end{bmatrix} + \begin{bmatrix} X \\ Y \\ 0 \end{bmatrix} \\
&= \begin{bmatrix} \cos\gamma, & \sin\gamma, & 0 \\ -\sin\gamma, & \cos\gamma, & 0 \\ 0, & 0, & 1 \end{bmatrix} \rho_i \begin{bmatrix} \cos\theta_i \\ \sin\theta_i \\ 0 \end{bmatrix} + \begin{bmatrix} X \\ Y \\ 0 \end{bmatrix} \\
&= \rho_i \begin{bmatrix} \cos\gamma\cos\theta_i + \sin\gamma\sin\theta_i \\ -\sin\gamma\cos\theta_i + \cos\gamma\sin\theta_i \\ 0 \end{bmatrix} + \begin{bmatrix} X \\ Y \\ 0 \end{bmatrix}
\end{aligned} \tag{3.33}$$

in a two-dimensional scenario. This implies that

$$\frac{\bar{Y}_i - Y}{\bar{X}_i - X} = \frac{-\sin\gamma\cos\theta_i + \cos\gamma\sin\theta_i}{\cos\gamma\cos\theta_i + \sin\gamma\sin\theta_i} = \frac{-\tan\gamma + \tan\theta_i}{1 + \tan\gamma\tan\theta_i}. \tag{3.34}$$

Rearranging the above equation yields

$$\tan\gamma = \frac{\left(\bar{X}_i - X\right)\tan\theta_i - \left(\bar{Y}_i - Y\right)}{\left(\bar{X}_i - X\right) + \left(\bar{Y}_i - Y\right)\tan\theta_i}. \tag{3.35}$$

Note that the above equality holds for any source. Therefore, with a pair of distinct sources (e.g., the i-th and j-th sources), the following equation can be constructed

$$\frac{\left(\bar{X}_i - X\right)\tan\theta_i - \left(\bar{Y}_i - Y\right)}{\left(\bar{X}_i - X\right) + \left(\bar{Y}_i - Y\right)\tan\theta_i} = \frac{\left(\bar{X}_j - X\right)\tan\theta_j - \left(\bar{Y}_j - Y\right)}{\left(\bar{X}_j - X\right) + \left(\bar{Y}_j - Y\right)\tan\theta_j}. \tag{3.36}$$

Rearranging the above equation yields

$$\begin{aligned} X^2 + Y^2 + \left(\left(-\bar{X}_i - \bar{X}_j\right) + \left(\bar{Y}_i - \bar{Y}_j\right)\cot(\theta_i - \theta_j)\right) X \\ + \left(\left(-\bar{X}_i + \bar{X}_j\right)\cot(\theta_i - \theta_j) + \left(-\bar{Y}_i - \bar{Y}_j\right)\right) Y \\ + \left(\left(\bar{X}_i\bar{X}_j + \bar{Y}_i\bar{Y}_j\right) + \left(\bar{X}_i\bar{Y}_j + \bar{X}_j\bar{Y}_i\right)\right)\cot(\theta_i - \theta_j) = 0, \end{aligned} \tag{3.37}$$

which can be rewritten as

$$\underline{1}_3^T \underline{R}^2 + \underline{A}_{ij}^T \underline{R} + B_{ij} = 0 \tag{3.38}$$

where

$$\underline{A}_{ij} = -\left[\mathbb{G}\left(\underline{\bar{R}}_i + \mathbb{G}\underline{\bar{R}}_j\right), \mathbb{F}\left(\underline{\bar{R}}_i - \mathbb{G}\underline{\bar{R}}_j\right), \underline{0}_3\right]^T \underline{K}_{ij} \in \mathcal{R}^{3\times 1}; \tag{3.39a}$$

$$B_{ij} = \left[\underline{\bar{R}}_i^T \underline{\bar{R}}_j, -\underline{\bar{R}}_i^T \mathbb{F}\mathbb{G}\underline{\bar{R}}_j, 0\right] \underline{K}_{ij} \tag{3.39b}$$

with

$$\mathbb{F} = \begin{bmatrix} 0, & 1, & 0 \\ 1, & 0, & 0 \\ 0, & 0, & 0 \end{bmatrix} \in \mathcal{Z}^{3\times 3}; \tag{3.40a}$$

$$\mathbb{G} = \begin{bmatrix} 1, & 0, & 0 \\ 0, & -1, & 0 \\ 0, & 0, & 0 \end{bmatrix} \in \mathcal{Z}^{3\times 3}; \tag{3.40b}$$

$$\underline{K}_{ij} = \left[1, \cot(\theta_i - \theta_j), 0\right]^T \in \mathcal{R}^{3\times 1}. \tag{3.40c}$$

Note that the terms $\underline{A}_{ij}$ and B_{ij} are determined by the known locations of the i-th and j-th sources in the global system and their estimated directions in the local system. In addition, there exist $J = \binom{M}{2}$ distinct pairs from the M sources. Define a group as a set of two distinct pairs; i.e., the first pair consists of the i-th and j-th sources with $i < j$, the second pair consists of the p-th and q-th sources with $p < q$, and $i \neq p \vee j \neq q$. Therefore, there exist $G = \binom{J}{2}$ distinct groups from the J pairs. Taking the difference between Equ. (3.38) of two distinct groups yields

$$\left(\underline{A}_{ij} - \underline{A}_{pq}\right)^T \underline{R} + (B_{ij} - B_{pq}) = 0. \tag{3.41}$$

Utilising all the groups, the location of the receiver array $\underline{R}$ can be estimated by solving the following system of linear equations

$$\mathbb{A}_R \underline{R} = \underline{B}_R \Rightarrow \hat{\underline{R}} = \mathbb{A}_R^{\#} B_R \tag{3.42}$$

where

$$\mathbb{A}_R = \left[\underline{A}_{12} - \underline{A}_{13}, \underline{A}_{12} - \underline{A}_{14}, \ldots, \underline{A}_{(M-2)M} - \underline{A}_{(M-1)M}\right]^T \in \mathcal{R}^{G\times 3}; \tag{3.43a}$$

$$\underline{B}_R = \left[B_{13} - B_{12}, B_{14} - B_{12}, \ldots, B_{(M-1)M} - B_{(M-2)M}\right]^T \in \mathcal{R}^{G\times 1} \tag{3.43b}$$

with $G \geq 2$ (as there are only two unknowns X and Y); i.e., $M > 2$.

Next, the orientation of the receiver array is estimated. Equation (3.35) can be rewritten as

$$\tan\gamma = \frac{\left(\bar{X}_i - X\right)\sin\theta_i - \left(\bar{Y}_i - Y\right)\cos\theta_i}{\left(\bar{X}_i - X\right)\cos\theta_i + \left(\bar{Y}_i - Y\right)\sin\theta_i} = \frac{\left(\underline{\bar{R}}_i - \underline{R}\right)^T \mathbb{GF}\underline{u}_i}{\left(\underline{\bar{R}}_i - \underline{R}\right)^T \underline{u}_i}. \tag{3.44}$$

Therefore, the receiver array orientation, or the yaw γ, can be estimated subsequently with the location estimate $\hat{\underline{R}}$ as

$$\hat{\gamma} = \frac{1}{M}\underline{1}_M^T \arctan\Big(\underline{\text{diag}}\Big(\bar{\mathbb{R}}\mathbb{G}\mathbb{F}\mathbb{U}\Big) \oslash \underline{\text{diag}}\Big(\bar{\mathbb{R}}\mathbb{U}\Big)\Big) \tag{3.45}$$

where

$$\bar{\mathbb{R}} = \Big[\underline{\bar{R}}_1, \underline{\bar{R}}_2, \ldots, \underline{\bar{R}}_M\Big]^T - \underline{1}_M \hat{\underline{R}}^T \in \mathcal{R}^{M\times 3}. \tag{3.46}$$

Furthermore, it is clear that at least three sources are required in order to successfully estimate the location and orientation of the receiver array in two-dimensional space. Additionally, the procedure of solving the system of quadratic equations is circumvented in this case, which considerably simplifies the estimation algorithm.

In conclusion, the proposed estimation algorithm for two-dimensional space is summarised as the following steps.

Step 1: Construct the covariance matrix of the received signal vector and estimate the azimuths and elevations of all the sources in the local system by a one-dimensional search of Equ. (3.32).

Step 2: Based on the estimated directions from Step 1, estimate the location of the sensor array in the global system by solving a system of equations using Equ. (3.42).

Step 3: Based on the estimated location from Step 2, estimate the Euler angle (yaw) using Equ. (3.45).

Chapter 4

Localisation and Orientation Estimation of Transmitter Arrays

The previous chapter is concerning the localisation and orientation estimation of receiver arrays. On the contrary, localising and orienting arrayed sources/targets using distributed sensor arrays have seen many applications in ubiquitous computing [64], personal communications [108], and military missions [109]. Localisation is generally achieved using range- or direction-based methods, while orientation is estimated based on the location estimates of all the elements of the transmitter arrays. However, these algorithms suffer from pseudo locations when applied to multi-source scenarios.

In this chapter, a distributed receiver array consisting of groups of small aperture sensor arrays is employed to estimate the locations and orientations of multiple sources with each source being a transmitter array of a known geometry. The estimation is carried out in a three-phase procedure: The DOAs of the sources are estimated using subspace techniques in the first step. The ranges are estimated by solving a system of equations. Subsequently, two subspace approaches are proposed to estimate their orientations with the exploitation of the beamforming

weight vectors of the sources. Hereafter, the term "transmitter estimation" is used to refer to this scenario unless otherwise noted.

The rest of this chapter is organised as follows. In Section 4.1, the signal model of the transmitter estimation scenario is explained. In Section 4.2, the transmitter estimation approach is detailed as a three-step procedure. In Section 4.3, the performance of the proposed approaches is evaluated using computer simulation studies. Last, in Section 4.4, the chapter is summarised.

4.1 Signal Model of Transmitter Estimation

With reference to Figure 4.1, consider an array of N distributed sensors of a known array geometry. The array can be divided into B groups where the b-th

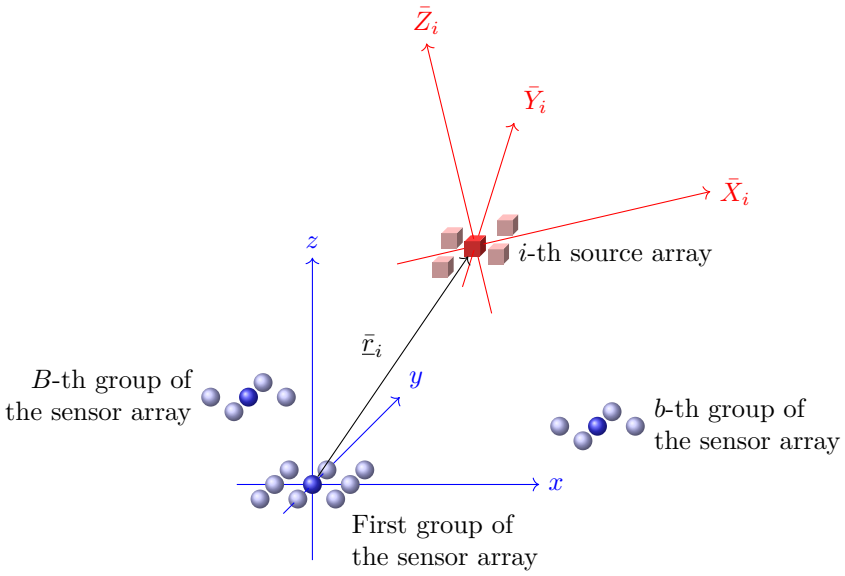

Figure 4.1: Geometry of the sensor array and i-th source. The sensors of the sensor array are represented by the blue spheres with the primary and secondary array reference points denoted by the darker ones. The emitters of the i-th source array are represented by the red cubes with the array reference point denoted by the darker one. Their locations can be specified in both the sensor (blue and lower case) and i-th source (red and upper case) coordinate systems.

one comprises N_b sensors of small intersensor spacing for $b = 1, 2, \ldots, B$ with

$$\sum_{b=1}^{B} N_b = N. \tag{4.1}$$

For simplicity, a two-dimensional representative geometry of the first and the b-th groups is shown in Figure 4.2. With reference to Figure 4.2, the array geometry of the b-th group is described as

$$\underline{r}_b \underline{1}_{N_b}^T + \left[\underline{r}_{b1}, \underline{r}_{b2}, \ldots, \underline{r}_{bN_b}\right] = \left[\underline{r}_{xb}, \underline{r}_{yb}, \underline{r}_{zb}\right]^T \in \mathcal{R}^{3\times N_b} \tag{4.2}$$

where $\underline{r}_b = [x_b, y_b, z_b]^T \in \mathcal{R}^{3\times 1}$ denotes the Cartesian coordinates of the array reference point of this group in the sensor coordinate system (blue and lower case in Figure 4.1), and $\underline{r}_{bk} \in \mathcal{R}^{3\times 1}$ represents the location of the k-th sensor of the

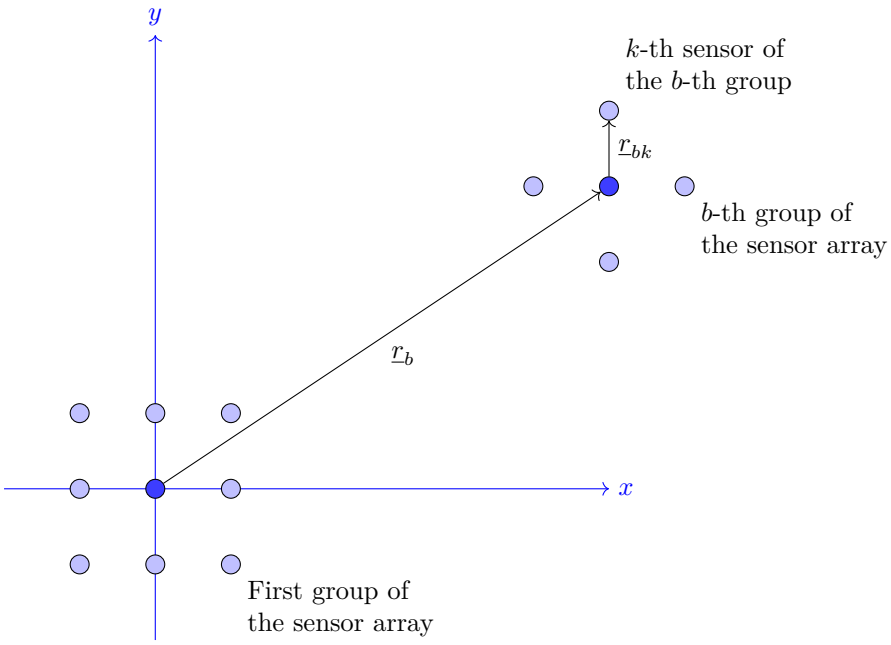

Figure 4.2: Two-dimensional representation of the array geometry. The vector $\underline{r}_b$ represents location of the array reference point of the b-th group (i.e., the b-th secondary array reference point) with respect to the primary array reference point. The vector $\underline{r}_{bk}$ represents the location of the k-th sensor of the b-th group with respect to the b-th secondary array reference point.

b-th group with respect to its own array reference point. The array geometry of the overall system is the concatenation of those of all the groups and is given as

$$\left[\underline{r}_x, \underline{r}_y, \underline{r}_z\right] = \begin{bmatrix} \underline{r}_{x1}, & \underline{r}_{y1}, & \underline{r}_{z1} \\ \underline{r}_{x2}, & \underline{r}_{y2}, & \underline{r}_{z2} \\ \vdots & \vdots & \vdots \\ \underline{r}_{xB}, & \underline{r}_{yB}, & \underline{r}_{zB} \end{bmatrix} \in \mathcal{R}^{N\times 3}. \tag{4.3}$$

In addition, define the array reference point of the first group as the primary array reference point and that of the b-th group as the b-th secondary array reference point.

The sensor array receives signals from M sources via LOS paths only, where the i-th source is an array of $\bar{N}$ emitters. With reference to Figure 4.1, the unknown location of the i-th source (i.e., the location of its array reference point) in the sensor coordinate system is parameterised by its unknown azimuth θ_i, elevation ϕ_i, and range ρ_i as

$$\underline{\bar{r}}_i \triangleq \underline{\bar{r}}(\theta_i, \phi_i, \rho_i) = \rho_i \underline{u}_i \in \mathcal{R}^{3\times 1} \tag{4.4}$$

where

$$\underline{u}_i \triangleq \underline{u}(\theta_i, \phi_i) = [\cos\theta_i \cos\phi_i, \sin\theta_i \cos\phi_i, \sin\phi_i]^T \in \mathcal{R}^{3\times 1} \tag{4.5}$$

is the unit vector pointing from the sensor primary array reference point towards the i-th source array reference point. In addition, the known array geometry of the i-th source can be described as

$$\left[\underline{\bar{R}}_{i1}, \underline{\bar{R}}_{i2}, \ldots, \underline{\bar{R}}_{i\bar{N}}\right] = \left[\underline{\bar{R}}_{Xi}, \underline{\bar{R}}_{Yi}, \underline{\bar{R}}_{Zi}\right]^T \in \mathcal{R}^{3\times \bar{N}} \tag{4.6}$$

with respect to a coordinate system associated with the source itself; that is, the i-th source coordinate system (red and upper case in Figure 4.1). The DOD of

the i-th source is denoted as $\bar{\theta}_i$ and $\bar{\phi}_i$ in the i-th source coordinate system. Its corresponding directional unit vector pointing from the source array reference point towards the sensor primary array reference point is given as

$$\underline{\bar{u}}_i \triangleq \underline{\bar{u}}\left(\bar{\theta}_i, \bar{\phi}_i\right) = \left[\cos\bar{\theta}_i \cos\bar{\phi}_i, \sin\bar{\theta}_i \cos\bar{\phi}_i, \sin\bar{\phi}_i\right]^T \in \mathcal{R}^{3\times 1}. \tag{4.7}$$

Hereafter, the terms "sensor system" and "i-th source system" are used to refer to the sensor and i-th source coordinate systems, respectively, unless otherwise noted.

Moreover, the unknown mapping from the sensor system to the i-th source system is dictated by a transformation matrix given as

$$\mathbb{T}_i = \begin{bmatrix} \mathbb{Q}_i, & -\mathbb{Q}_i\underline{\bar{r}}_i \\ \underline{0}_3^T, & 1 \end{bmatrix} \tag{4.8}$$

where $\mathbb{Q}_i \in \mathcal{R}^{3\times 3}$ is the orthogonal rotation matrix and $-\mathbb{Q}_i\underline{\bar{r}}_i$ is the translation vector. The rotation matrix $\mathbb{Q}_i$ can be written as the product of three rotation matrices as

$$\mathbb{Q}_i = \mathbb{Q}_{xi}\mathbb{Q}_{yi}\mathbb{Q}_{zi} \tag{4.9}$$

where

$$\mathbb{Q}_{xi} = \begin{bmatrix} 1, & 0, & 0 \\ 0, & \cos\alpha_i, & \sin\alpha_i \\ 0, & -\sin\alpha_i, & \cos\alpha_i \end{bmatrix} \in \mathcal{R}^{3\times 3}; \tag{4.10a}$$

$$\mathbb{Q}_{yi} = \begin{bmatrix} \cos\beta_i, & 0, & -\sin\beta_i \\ 0, & 1, & 0 \\ \sin\beta_i, & 0, & \cos\beta_i \end{bmatrix} \in \mathcal{R}^{3\times 3}; \tag{4.10b}$$

$$\mathbb{Q}_{zi} = \begin{bmatrix} \cos\gamma_i, & \sin\gamma_i, & 0 \\ -\sin\gamma_i, & \cos\gamma_i, & 0 \\ 0, & 0, & 1 \end{bmatrix} \in \mathcal{R}^{3\times 3} \tag{4.10c}$$

are the rotation matrices about the x-, y-, and z-axis with the unknown Euler angles α_i, β_i, and γ_i, respectively. More information about the Euler angles can be found in Chapter 3.

In summary, only the receiver array geometry in the sensor system and the transmitter array geometries in the source systems are known. The rest are unknown, including the locations $\underline{\bar{r}}_i$ and the orientations $\mathbb{Q}_i$ (or the Euler angles α_i, β_i, and γ_i) of all the sources, which are to be estimated. The knowns and unknowns are also summarised in Table 4.1.

Now, consider the received signal model of the sensor array. Suppose that the i-th source transmits a sequence of channel symbols with the channel symbol period T_{cs}. The q-th channel symbol is denoted as $\mathrm{a}_i[q]$ for $q \in \mathcal{Z}$. The channel symbol period T_{cs} is segmented into $\bar{N}$ chip periods with each chip period having the duration of $\bar{T} = T_{\text{cs}}/\bar{N}$. Within the ℓ-th chip period for $\ell = 0, 1, \ldots, \bar{N}-1$,

Table 4.1: Summary of the Knowns and Unknowns

Parameter	**Sensor system**		**Source system**	
	Symbol	**Status**	**Symbol**	**Status**
Sensor array geometry	$\underline{r}_{bk}$	known	—	
Source array geometries	—		$\underline{\bar{R}}_{i\bar{k}}$	known
Source locations	$\underline{\bar{r}}_i$	unknown†	—	
Source parameters	θ_i, ϕ_i, and ρ_i	unknown	—	
Transformation matrices	$\mathbb{T}_i$	unknown	—	
Rotation matrices	$\mathbb{Q}_{xi}$, $\mathbb{Q}_{yi}$, and $\mathbb{Q}_{zi}$	unknown	—	
Euler angles	α_i, β_i, and γ_i	unknown†	—	

†These unknowns are to be estimated.

the channel symbol $\mathrm{a}_i[q]$ is weighted using a transmit beamforming weight vector $\underline{\bar{w}}_i[\ell] \in \mathcal{C}^{\bar{N}\times 1}$ as $\underline{\bar{w}}_i[\ell]\,\mathrm{a}_i[q]$. Furthermore, the concatenation of all the weight vectors during a channel symbol period, which is given as

$$\bar{\mathbb{W}}_i = \left[\underline{\bar{w}}_i[0]\,, \underline{\bar{w}}_i[1]\,, \ldots, \underline{\bar{w}}_i\left[\bar{N}-1\right]\right] \in \mathcal{C}^{\bar{N}\times\bar{N}}, \tag{4.11}$$

is designed to form a distinct unitary matrix; i.e., $\bar{\mathbb{W}}_i$ and $\bar{\mathbb{W}}_j$ are randomly chosen for the i-th and j-th source where $i \neq j$ such that $\bar{\mathbb{W}}_i\bar{\mathbb{W}}_i^H = \mathbb{I}_{\bar{N}}$ and $\bar{\mathbb{W}}_i\bar{\mathbb{W}}_j^H \neq \pm\mathbb{I}_{\bar{N}}$. The weighted channel symbols are sent to a DAC and the output continuous waveform of the $\bar{N}$ emitters is denoted as $\underline{m}_i(t) \in \mathcal{C}^{\bar{N}\times 1}$.

Since the sensors form a distributed array, the spherical wave propagation model needs to be considered and the source can follow either the NBA or WBA. (Localisation under the WBA will be scrutinised in Chapter 5 as well.) Nevertheless, since the aperture of the sensors inside a group is small, spherical wave propagation can be approximated as plane wave propagation and the NBA is generally valid.

Based on the above assumptions, the received signal vector can be modelled as

$$\underline{x}(t) = \sum_{i=1}^{M} \begin{bmatrix} \mathring{S}_{i1}\underline{S}_{i1}\bar{\underline{S}}_{i1}^H\underline{m}_i(t-\tau_{i1}) \\ \mathring{S}_{i2}\underline{S}_{i2}\bar{\underline{S}}_{i2}^H\underline{m}_i(t-\tau_{i2}) \\ \vdots \\ \mathring{S}_{iB}\underline{S}_{iB}\bar{\underline{S}}_{iB}^H\underline{m}_i(t-\tau_{iB}) \end{bmatrix} + \underline{n}(t) \tag{4.12}$$

where, for the i-th source and the b-th group (namely, the b-th subvector in the bracket), $\underline{S}_{ib} \in \mathcal{C}^{N_b\times 1}$ represents the corresponding plane wave array manifold vector of the array of sensors in the group, and is given as

$$\underline{S}_{ib} \triangleq \underline{S}(\theta_{ib}, \phi_{ib}) = \exp\left(-j2\pi\frac{F_c}{c}\left[\underline{r}_{xb}, \underline{r}_{yb}, \underline{r}_{zb}\right]\underline{u}_{ib}\right) \tag{4.13}$$

with θ_{ib} and ϕ_{ib} denoting the azimuth and elevation with respect to the b-th secondary array reference point (see Figure 4.3 for reference). Likewise, $\underline{\bar{S}}_{ib} \in \mathcal{C}^{\bar{N}\times 1}$ represents the plane wave array manifold vector of the transmitter array and is given as

$$\underline{\bar{S}}_{ib} \triangleq \underline{\bar{S}}\left(\bar{\theta}_{ib}, \bar{\phi}_{ib}\right) = \exp\left(j2\pi \frac{F_c}{c}\left[\underline{\bar{R}}_{Xi}, \underline{\bar{R}}_{Yi}, \underline{\bar{R}}_{Zi}\right]\bar{u}_{ib}\right) \tag{4.14}$$

with $\bar{\theta}_{ib}$ and $\bar{\phi}_{ib}$ denoting the corresponding DODs. The term τ_{ib} represents the relative delay between the primary array reference point and the b-th secondary array reference point. Note that $\tau_{i1} = 0$ for $i = 1, 2, \ldots, M$ as it is associated with the primary array reference point.

Finally, the subvectors of all the groups are glued together by the spherical wave array manifold vector $\mathring{\underline{S}}_i \in \mathcal{C}^{B\times 1}$ associated with all the secondary reference

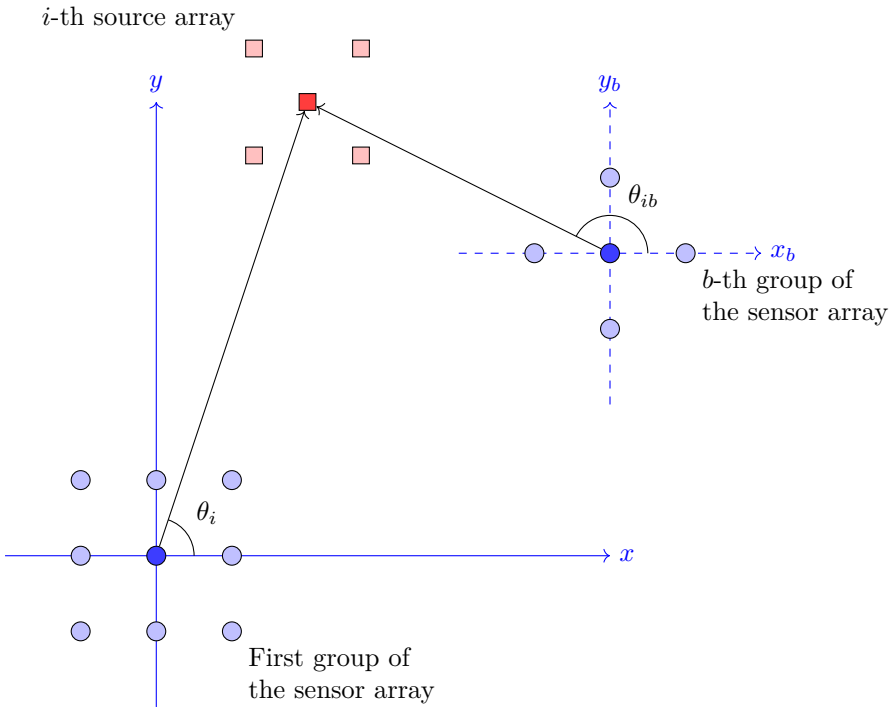

Figure 4.3: DOA with respect to a secondary array reference point. It is measured under the coordinate system $x_b y_b$, which is the translated version of the sensor coordinate system xy from its origin to the b-th secondary reference point.

points with respect to the primary reference point; it is defined as [13]

$$\begin{aligned}\mathring{\underline{S}}_i &= \left[\mathring{S}_{i1}, \mathring{S}_{i2}, \ldots, \mathring{S}_{iB}\right]^T \\ &\triangleq \mathring{\underline{S}}(\theta_i, \phi_i, \rho_i) \\ &= \rho_i^a \underline{\rho}^{-a}(\theta_i, \phi_i, \rho_i) \odot \exp\left(-j2\pi \frac{F_c}{c}\left(\rho_i \underline{1}_B - \underline{\rho}(\theta_i, \phi_i, \rho_i)\right)\right)\end{aligned} \tag{4.15}$$

with

$$\underline{\rho}(\theta_i, \phi_i, \rho_i) = \sqrt{\rho_i^2 \underline{1}_B + \mathring{\underline{r}}_x^2 + \mathring{\underline{r}}_y^2 + \mathring{\underline{r}}_z^2 - 2\rho_i \left[\mathring{\underline{r}}_x, \mathring{\underline{r}}_y, \mathring{\underline{r}}_z\right] \underline{u}_i} \in \mathcal{R}^{B\times 1} \tag{4.16}$$

$$\left[\mathring{\underline{r}}_x, \mathring{\underline{r}}_y, \mathring{\underline{r}}_z\right] = [\underline{r}_1, \underline{r}_2, \ldots, \underline{r}_B]^T \in \mathcal{R}^{B\times 3} \tag{4.17}$$

where a is the known path loss exponent. Furthermore, $\underline{n}(t) \in \mathcal{C}^{N\times 1}$ is the complex AWGN of zero mean and covariance $\sigma_n^2 \mathbb{I}_N$.

The received signal vector is sampled at the sampling frequency $1/\bar{T}$ using TDLs of length $2\bar{N}$. The received data can be represented as a cube as shown in Figure 4.4(a), where the q-th page $\mathbb{X}[q]$ denotes the samples associated with two consecutive channel symbol periods starting from the q-th channel symbol period.

4.2 Design of the Estimation Approach

The objective of the estimation problem is to find the location and orientation of the sources. Initially, the location of all the sources are estimated in terms of their directions and ranges. Thereafter, their orientations are estimated using two different approaches with the employment of the source beamforming weight vectors. The estimation procedure is carried out in the following three phases.

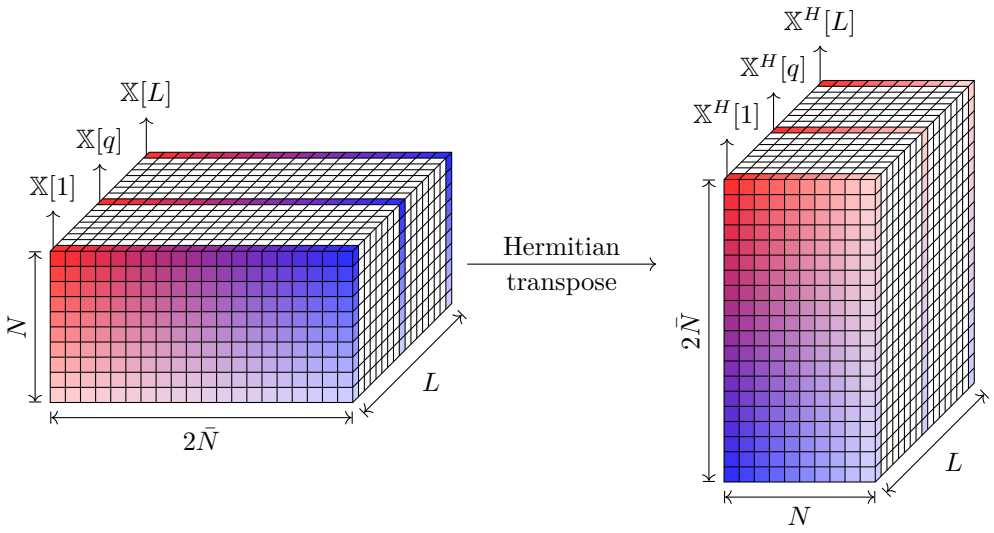

Figure 4.4: Signal rearrangement. (a) Received data cube. The q-th page $\mathbb{X}[q]$ consists of $2\bar{N}$ snapshots received at N sensors. (b) Rearranged signal matrix. The q-th interval $\mathbb{X}^H[q]$ is the Hermitian transposed version of $\mathbb{X}[q]$.

4.2.1 Direction Estimation

The covariance matrix of the received signal is

$$\mathbb{R}_{xx} = \mathcal{E}\Big\{\mathbb{X}[q]\,\mathbb{X}^H[q]\Big\} \in \mathcal{C}^{N\times N}. \tag{4.18}$$

Define a selection matrix $\mathbb{F}_b \in \mathcal{Z}^{N_b\times N}$ that extracts the subcovariance matrix associated with the b-th group as

$$\mathbb{F}_b = \Big[\mathbb{O}_{N_b\times(N_1+N_2+\cdots+N_{b-1})}, \mathbb{I}_{N_b}, \mathbb{O}_{N_b\times(N_{b+1}+N_{b+2}+\cdots+N_B)}\Big]. \tag{4.19}$$

Using the selection matrix of the first group, the corresponding subcovariance matrix is obtained as

$$\mathbb{R}_{x_1x_1} = \mathbb{F}_1\mathbb{R}_{xx}\mathbb{F}_1^T. \tag{4.20}$$

The azimuth and elevation can be estimated by a two-dimensional search of

$$\xi(\theta,\phi) = \frac{\underline{S}_1^H(\theta,\phi)\,\underline{S}_1(\theta,\phi)}{\underline{S}_1^H(\theta,\phi)\,\mathbb{E}_{n_1}\mathbb{E}_{n_1}^H\underline{S}_1(\theta,\phi)} \tag{4.21}$$

where $\underline{S}_1(\theta,\phi) \in \mathcal{C}^{N_1\times 1}$ is the array manifold vector associated with the first group and $\mathbb{E}_{n_1} \in \mathcal{C}^{N_1\times(N_1-M)}$ denotes the noise subspace of $\mathbb{R}_{x_1x_1}$.

4.2.2 Range Estimation

Subsequently, the range ρ is estimated upon completion of the estimation of the azimuth $\hat{\theta}$ and elevation $\hat{\phi}$. In order to estimate the range, the received signal vector of all the groups is to be employed.

With reference to Equ. (4.12), if the sources are assumed to be uncorrelated, it can be derived that the trace of the subcovariance matrix associated with the b-th group is given as

$$\mathrm{tr}\Big(\mathbb{F}_b\mathbb{R}_{xx}\mathbb{F}_b^T\Big) = N_b\left(\left(\underline{K}_b^{2a}\right)^T\underline{P} + \sigma_n^2\right). \tag{4.22}$$

In Equ. (4.22), the vector $\underline{K}_b \in \mathcal{R}^{M\times 1}$ is a vector of the ranges of all the sources associated with the first group and the b-th group, and is given as

$$\underline{K}_b = \left[\frac{\rho_{11}}{\rho_{1b}}, \frac{\rho_{21}}{\rho_{2b}}, \ldots, \frac{\rho_{M1}}{\rho_{Mb}}\right]^T \tag{4.23}$$

with ρ_{ib} denoting the range between the i-th source and the b-th secondary array reference point. Moreover, $\underline{P} = [P_1, P_2, \ldots, P_M]^T \in \mathcal{R}^{M\times 1}$ with P_i denoting the signal power of the i-th source impinging on the primary array reference point. Note that in Equ. (4.22), the trace is measured from the received signal, the signal power can be estimated using the subspace beamformer presented in Chapter 2, and the noise power can be estimated by averaging the least significant eigenvalues

of the covariance matrix. Therefore, the only unknown is the vector $\underline{K}_b$ associated with the ranges.

Furthermore, let $\lambda_b = \text{tr}\left(\mathbb{F}_b \mathbb{R}_{xx} \mathbb{F}_b^T\right)/N_b - \sigma_n^2$. By stacking Equ. (4.22) for all the groups, a system of equations can be formed as

$$\mathbb{K}^{\odot 2a} \underline{P} = \underline{\lambda} \tag{4.24}$$

where

$$\mathbb{K} = [\underline{K}_1, \underline{K}_2, \ldots, \underline{K}_B]^T = \begin{bmatrix} \frac{\rho_{11}}{\rho_{11}}, & \frac{\rho_{21}}{\rho_{21}}, & \ldots & \frac{\rho_{M1}}{\rho_{M1}} \\ \frac{\rho_{11}}{\rho_{12}}, & \frac{\rho_{21}}{\rho_{22}}, & \ldots & \frac{\rho_{M1}}{\rho_{M2}} \\ \vdots & \vdots & \ddots & \vdots \\ \frac{\rho_{11}}{\rho_{1B}}, & \frac{\rho_{21}}{\rho_{2B}}, & \ldots & \frac{\rho_{MB}}{\rho_{Mb}} \end{bmatrix} \in \mathcal{R}^{B \times M} \tag{4.25}$$

and $\underline{\lambda} = [\lambda_1, \lambda_2, \ldots, \lambda_B]^T \in \mathcal{R}^{B \times 1}$. The i-th column of $\mathbb{K}$ is the a-th root of the magnitude of the array manifold vector associated with all the secondary array reference points given in Equ. (4.15). It can be written as a function of the unknown range ρ_i of the i-th source as

$$\begin{aligned} \rho_i \underline{\rho}^{-1}(\theta_i, \phi_i, \rho_i) &= \rho_i \left(\rho_i^2 \underline{1}_B + \mathring{\underline{r}}_x^2 + \mathring{\underline{r}}_y^2 + \mathring{\underline{r}}_z^2 - 2\rho_i \left[\mathring{\underline{r}}_x, \mathring{\underline{r}}_y, \mathring{\underline{r}}_z \right] \underline{u}_i \right)^{-\frac{1}{2}} \\ &= \left(\underline{1}_B + \rho_i^{-1} \underline{A}_i + \rho_i^{-2} \underline{B} \right)^{-\frac{1}{2}} \\ &= \left(\mathbb{G}_i \left[1, \rho_i^{-1}, \rho_i^{-2} \right]^T \right)^{-\frac{1}{2}} \end{aligned} \tag{4.26}$$

where

$$\underline{A}_i = -2 \left[\mathring{\underline{r}}_x, \mathring{\underline{r}}_y, \mathring{\underline{r}}_z \right] \underline{u}_i \in \mathcal{R}^{B \times 1}; \tag{4.27a}$$

$$\underline{B} = \mathring{\underline{r}}_x^2 + \mathring{\underline{r}}_y^2 + \mathring{\underline{r}}_z^2 \in \mathcal{R}^{B \times 1}; \tag{4.27b}$$

$$\mathbb{G}_i = [\underline{1}_B, \underline{A}_i, \underline{B}] \in \mathcal{R}^{B \times 3}. \tag{4.27c}$$

Note that $\mathbb{G}_i$ can be constructed from the known array geometry of the secondary array reference points and the estimated direction of the i-th source. Therefore, the vector $\rho_i \underline{\rho}^{-1}(\theta_i, \phi_i, \rho_i)$ is a function of ρ_i only. By using Equ. (4.26) of all the sources, Equ. (4.24) can then be rewritten as

$$\left([\mathbb{G}_1, \mathbb{G}_2, \ldots, \mathbb{G}_M] \left(\mathbb{I}_M \boxtimes \left[\underline{1}_M, \underline{\rho}^{-1}, \underline{\rho}^{-2} \right]^T \right) \right)^{\odot(-a)} \underline{P} = \underline{\lambda} \tag{4.28}$$

where $\underline{\rho} = [\rho_1, \rho_2, \ldots, \rho_M]^T \in \mathcal{R}^{M \times 1}$ is a vector containing the unknown ranges of all the sources. By solving Equ. (4.28), the source ranges can be uniquely identified.

4.2.3 Orientation Estimation Using Two Approaches

In addition to the location estimation, the orientations of all the sources can be estimated from their DOAs and DODs associated with all the B groups of the receiver array. The DOAs can be obtained from the estimated source locations and the known sensor array geometry, while the DODs can be estimated with the employment of the source beamforming weight vectors. Two approaches are proposed to estimate the DODs as follows.

Approach without Interference Cancellation

In this approach, the DODs are estimated in the presence of the interference of the other sources. The signal matrix $\mathbb{X}[q]$ can be rearranged (Hermitian transposed) as shown in Figure 4.4(b). The rearranged matrix $\mathbb{X}^H[q]$ can be partitioned into B submatrices as

$$\mathbb{X}^H[q] = \left[\mathbb{X}_1^H[q], \mathbb{X}_2^H[q], \ldots, \mathbb{X}_B^H[q] \right] \tag{4.29}$$

where $\mathbb{X}_b^H[q] \in \mathcal{C}^{2\bar{N} \times N_b}$ for $b = 1, 2, \ldots, B$ corresponds to the b-th group. Without loss of generality, assume that the DODs of the first source are to be estimated.

Define the preprocessing matrix for the first source associated with a range bin ℓ as

$$\mathbb{P}_{\ell} = \mathbb{C}_1 \left(\mathbb{J}_{2\bar{N}}^T \right)^{\ell} \in \mathcal{C}^{\bar{N} \times 2\bar{N}} \tag{4.30}$$

where $\mathbb{C}_1 = \left[\bar{\mathbb{W}}_1, \mathbb{O}_{\bar{N} \times \bar{N}} \right] \in \mathcal{C}^{\bar{N} \times 2\bar{N}}$. Since the location of the desired source has been estimated in the previous phase, all the range bins ℓ_{1b} for $b = 1, 2, \ldots, B$ associated with the desired source can be calculated from the estimated source location and the known receiver array geometry. Using the estimated range bins, apply the preprocessing matrices onto the rearranged signal matrix as

$$\bar{\mathbb{X}}[q] = \left[\mathbb{P}_{\ell_{11}} \mathbb{X}_1^H[q], \mathbb{P}_{\ell_{12}} \mathbb{X}_2^H[q], \ldots, \mathbb{P}_{\ell_{1B}} \mathbb{X}_B^H[q] \right] \in \mathcal{C}^{\bar{N} \times N}. \tag{4.31}$$

The eigenspace of the covariance matrix $\mathbb{R}_{\bar{x}\bar{x}}$ of $\bar{\mathbb{X}}[q]$ associated with its most significant eigenvalues is spanned by the source array manifold vectors $\underline{\bar{S}}_{1b}$ for $b = 1, 2, \ldots, B$, together with the transformed versions of the source array manifold vectors $\underline{\bar{S}}_{ib}$ for $i = 2, 3, \ldots, M$ and $b = 1, 2, \ldots, B$ (this transformation is governed by the preprocessing matrix). Since, in general, the transformed array manifold vectors do not lie on the original array manifold, the DODs of the desired source can then be estimated by a two-dimensional search of

$$\xi\left(\bar{\theta}, \bar{\phi}\right) = \frac{\underline{\bar{S}}_1^H\left(\bar{\theta}, \bar{\phi}\right) \underline{\bar{S}}_1\left(\bar{\theta}, \bar{\phi}\right)}{\underline{\bar{S}}_1^H\left(\bar{\theta}, \bar{\phi}\right) \mathbb{E}_{\bar{n}_1} \mathbb{E}_{\bar{n}_1}^H \underline{\bar{S}}_1\left(\bar{\theta}, \bar{\phi}\right)} \tag{4.32}$$

where $\underline{\bar{S}}_1\left(\bar{\theta}, \bar{\phi}\right) \in \mathcal{C}^{\bar{N} \times 1}$ denotes the array manifold vector associated with the desired source and $\mathbb{E}_{\bar{n}_1}$ denotes the noise subspace of $\mathbb{R}_{\bar{x}\bar{x}}$.

Approach with Interference Cancellation

In an alternative approach, interference from all the other sources is eliminated prior to the DOD estimation of the desired source.

With the utilisation of the subspace beamforming techniques, the receiver beamforming weight vector for the desired source can be defined as

$$\underline{w}_1 = \mathbb{P}^{\perp}_{\mathbb{E}_j} \underline{S}_1 \in \mathcal{C}^{N\times 1} \tag{4.33}$$

where $\mathbb{P}^{\perp}_{\mathbb{E}_j} \in \mathcal{C}^{N\times N}$ is the projection matrix onto the complementary subspace of the one spanned by the columns of $\mathbb{E}_j \in \mathcal{C}^{N\times B(M-1)}$, which is defined as

$$\mathbb{E}_j = [\mathbb{E}_2, \mathbb{E}_3, \ldots, \mathbb{E}_M] \tag{4.34}$$

where

$$\mathbb{E}_i = \begin{bmatrix} \underline{S}_{i1}, & \underline{0}_{N_1}, & \cdots & \underline{0}_{N_1} \\ \underline{0}_{N_2}, & \underline{S}_{i2}, & \cdots & \underline{0}_{N_2} \\ \vdots & \vdots & \ddots & \vdots \\ \underline{0}_{N_B}, & \underline{0}_{N_B}, & \cdots & \underline{S}_{iB} \end{bmatrix} \in \mathcal{C}^{N\times B}; \tag{4.35}$$

i.e., $\mathbb{E}_j$ is the concatenation of all $\mathbb{E}_i$ except for $i = 1$. The weight vector $\underline{w}_1$ is (right) applied onto the preprocessed signal matrix as

$$\underline{\bar{x}}[q] = \bar{\mathbb{X}}[q]\, \underline{w}_1. \tag{4.36}$$

Using the noise subspace of the covariance matrix of $\underline{\bar{x}}[q]$, the DODs of the desired source can be estimated using a cost function similar to Equ. (4.32), except that the dimension of the noise subspace is increased to $\bar{N} - B$.

Both approaches elaborated above have their respective advantages and disadvantages. The approach without interference cancellation can deliver successful estimates even when the sources follow the NBA among different groups of sensors, as the signals of different groups are processed individually; however, it requires a much higher dimensional observation space. By contrast, in the approach with

interference cancellation, the number of emitters required for each source is hugely reduced since the dimension of the signal subspace is reduced; nonetheless, this approach fails when (some of) the sources follow the NBA among (some of) the groups. (Potentially, spatial smoothing can be applied to solve this problem [110].)

Upon completion of the estimation of the DODs of the desired source, the rotation matrices from the sensor system to the source system can be estimated. With the DOD estimates $\hat{\bar{\theta}}_{1b}$ and $\hat{\bar{\phi}}_{1b}$ available, the DOD directional vectors $\underline{\hat{\bar{u}}}_{1b}$ can be derived. Similarly, from the DOA estimate $\hat{\theta}_1$ and $\hat{\phi}_1$, range estimate $\hat{\rho}_1$, and the known array geometry, the DOA directional vectors $\underline{\hat{u}}_{1b}$ can be constructed. In addition, the mapping from a DOA directional vector to its DOD counterpart is dictated by the rotation matrix $\mathbb{Q}_1$ as

$$\underline{\hat{\bar{u}}}_{1b} = -\mathbb{Q}_1 \underline{\hat{u}}_{1b} \tag{4.37}$$

since the LOS paths are considered only. Thus, the rotation matrix can be estimated as

$$\hat{\mathbb{Q}}_1 = -\bar{\mathbb{U}}_1 \mathbb{U}_1^{\#} \tag{4.38}$$

where $\mathbb{U}_1 \in \mathcal{R}^{3\times B}$ and $\bar{\mathbb{U}}_1 \in \mathcal{R}^{3\times B}$ are the matrices containing the estimated DOA and DOD directional vectors, respectively. Furthermore, the Euler angles α_1, β_1 and γ_1 can be derived from $\hat{\mathbb{Q}}_1$ as

$$\hat{\alpha}_1 = \arctan\left(\frac{\underline{F}_2^T \hat{\mathbb{Q}}_1 \underline{F}_3}{\underline{F}_3^T \hat{\mathbb{Q}}_1 \underline{F}_3}\right); \tag{4.39a}$$

$$\hat{\beta}_1 = -\arcsin\left(\underline{F}_1^T \hat{\mathbb{Q}}_1 \underline{F}_3\right); \tag{4.39b}$$

$$\hat{\gamma}_1 = \arctan\left(\frac{\underline{F}_1^T \hat{\mathbb{Q}}_1 \underline{F}_2}{\underline{F}_1^T \hat{\mathbb{Q}}_1 \underline{F}_1}\right) \tag{4.39c}$$

where $\underline{F}_p = \left[\underline{0}_{p-1}^T, 1, \underline{0}_{3-p}^T\right]^T \in \mathcal{Z}^{3\times 1}$ for $p = 1, 2, 3$.

In conclusion, the localisation and orientation estimation approach proposed for the transmitter arrays is summarised as the following steps.

Step 1: Construct the covariance matrix of the received signal vector of all the groups using Equ. (4.18). Obtain the subcovariance matrix associated with the first group using Equ. (4.20). Estimate the azimuth and elevation of all the sources by a two-dimensional search of Equ. (4.21).

Step 2: Obtain the subcovariance matrices associated with all the groups and compute their traces. Using the traces and the estimated source directions from Step 1, form a system of equations using Equ. (4.28). Estimate the source ranges by solving this system of equations.

Step 3: Rearrange the received signal matrix using Equ. (4.29). Preprocess the rearranged signal matrix using Equ. (4.31). If the approach with interference cancellation is utilised, eliminate the interference using Equ. (4.36) as an additional substep. Estimate the DODs by a two-dimensional search of Equ. (4.32). Derive the Euler angles from the estimated DOAs and DODs using Equs. (4.39a) to (4.39c).

Note that, similar to Chapter 3, if NLOS paths are in existence, then sequences can be employed to distinguish different sources and the LOS paths can be selected using the signal power.

4.3 Computer Simulation Studies

In this section, the performance of the location and orientation estimators of the transmitter arrays is assessed through computer simulation studies.

In the simulations, a 20-element receiver array of array aperture 707.18 m is utilised. It can be partitioned into four groups where each group is a five-element

cross array of 0.05 m (half-wavelength) intersensor spacing. The sensor array operates in the presence of two sources where each source is a 13-element transmitter cross array of 0.05 m (half-wavelength) intersensor spacing. Assume that the first source is the desired source to be estimated. In addition, the array geometries are given in Table 4.2. The geometry of the sources and the sensor arrays projected onto the xy-plane are also shown in Figure 4.5. Other array system parameters are given in Table 4.3. Furthermore, the parameters and derived parameters of the sources are listed in Tables 4.4 and 4.5.

Prior to the assessment of the proposed localisation and orientation estimation

Table 4.2: Array Geometries of Transmitter Estimation

Sensor	x	y	z	**Sensor**	x	y	z
1	−0.05 m	0.00 m	0.00 m	**11**	499.95 m	0.00 m	0.00 m
2	0.00 m	−0.05 m	0.00 m	**12**	500.00 m	−0.05 m	0.00 m
3	0.00 m	0.00 m	0.00 m	**13**	500.00 m	0.00 m	0.00 m
4	0.00 m	0.05 m	0.00 m	**14**	500.00 m	0.05 m	0.00 m
5	0.05 m	0.00 m	0.00 m	**15**	500.05 m	0.00 m	0.00 m
6	−0.05 m	500.00 m	0.00 m	**16**	499.95 m	500.00 m	0.00 m
7	0.00 m	499.95 m	0.00 m	**17**	500.00 m	499.95 m	0.00 m
8	0.00 m	500.00 m	0.00 m	**18**	500.00 m	500.00 m	0.00 m
9	0.00 m	500.05 m	0.00 m	**19**	500.00 m	500.05 m	0.00 m
10	0.05 m	500.00 m	0.00 m	**20**	500.05 m	500.00 m	0.00 m
Emitter	x	y	z	**Emitter**	x	y	z
1	−0.10 m	0.00 m	0.00 m	**8**	0.00 m	0.00 m	0.05 m
2	−0.05 m	0.00 m	0.00 m	**9**	0.00 m	0.00 m	0.10 m
3	0.00 m	−0.10 m	0.00 m	**10**	0.00 m	0.05 m	0.00 m
4	0.00 m	−0.05 m	0.00 m	**11**	0.00 m	0.10 m	0.00 m
5	0.00 m	0.00 m	−0.10 m	**12**	0.05 m	0.00 m	0.00 m
6	0.00 m	0.00 m	−0.05 m	**13**	0.10 m	0.00 m	0.00 m
7	0.00 m	0.00 m	0.00 m				

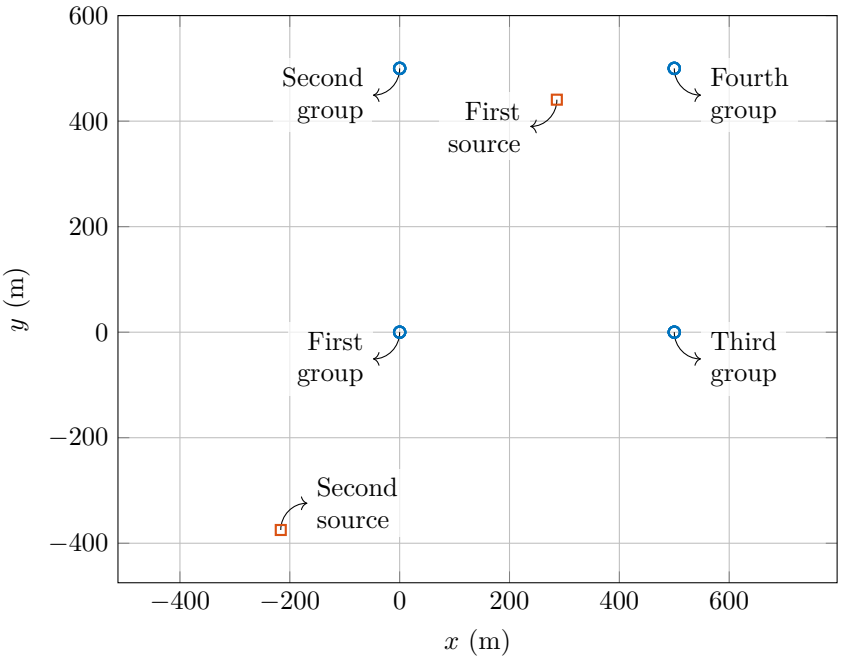

Figure 4.5: Source and sensor array geometry. The geometry is projected onto the xy-plane and the z-coordinates are not shown. Note that there are five sensors in each group; however, they seem to overlap in the figure as the intersensor spacing is relatively small compared with the array aperture.

Table 4.3: Array System Parameters

Parameter	Value
Carrier frequency	3 GHz
Sampling frequency	30 MHz
Number of snapshots	200
SNR	20 dB

Table 4.4: Simulation Parameters of Transmitter Estimation

Source	Azimuth θ	Elevation ϕ	Range ρ	Roll α	Pitch β	Yaw γ
1	57°	9°	532 m	−156°	22°	26°
2	240°	31°	505 m	17°	3°	171°

Table 4.5: Derived Parameters of the Desired Source

Group	DOA		DOD	
	Azimuth θ	Elevation ϕ	Azimuth $\bar{\theta}$	Elevation $\bar{\phi}$
1	57.00°	9.00°	91.45°	−22.42°
2	−11.71°	15.89°	157.84°	−2.71°
3	115.88°	9.64°	35.50°	−1.80°
4	−164.49°	20.56°	326.79°	46.87°

approaches, the direction-based localisation approach explained in [89] is evaluated first. It estimates the DOAs of all the sources from all the groups of the arrays with reference to a common direction reference. With the DOA estimates $\hat{\theta}_{ib}$ and $\hat{\phi}_{ib}$ available, the source locations can be estimated by solving a system of equations given as

$$\begin{bmatrix} (\underline{\bar{r}}_i - \underline{r}_1) - \|\underline{\bar{r}}_i - \underline{r}_1\| \, \underline{u}\left(\hat{\theta}_{i1}, \hat{\phi}_{i1}\right) \\ (\underline{\bar{r}}_i - \underline{r}_2) - \|\underline{\bar{r}}_i - \underline{r}_2\| \, \underline{u}\left(\hat{\theta}_{i2}, \hat{\phi}_{i2}\right) \\ \vdots \\ (\underline{\bar{r}}_i - \underline{r}_B) - \|\underline{\bar{r}}_i - \underline{r}_B\| \, \underline{u}\left(\hat{\theta}_{iB}, \hat{\phi}_{iB}\right) \end{bmatrix} = \underline{0}_B. \tag{4.40}$$

The estimated source locations projected onto the xy-plane are shown in Figure 4.6 for simplicity. The algorithm delivers multiple location estimates, two of which are in the vicinity of the source locations, while the rest are pseudo locations. All the estimated locations need to be evaluated with a geometry constraint in order to remove the pseudo locations.

Now, the proposed approaches are evaluated. The joint DOA azimuth and elevation estimation result is shown in Figure 4.7, where two peaks at the azimuths and elevations $(57°, 9°)$ and $(240°, 31°)$ can be observed, indicating a successful estimation of the azimuths and elevations. Based on the above direction estimates, by solving the system of equations given in Equ. (4.28), the ranges are estimated as 531.94 m and 507.11 m, with estimation errors of 6.50×10^{-2} m and

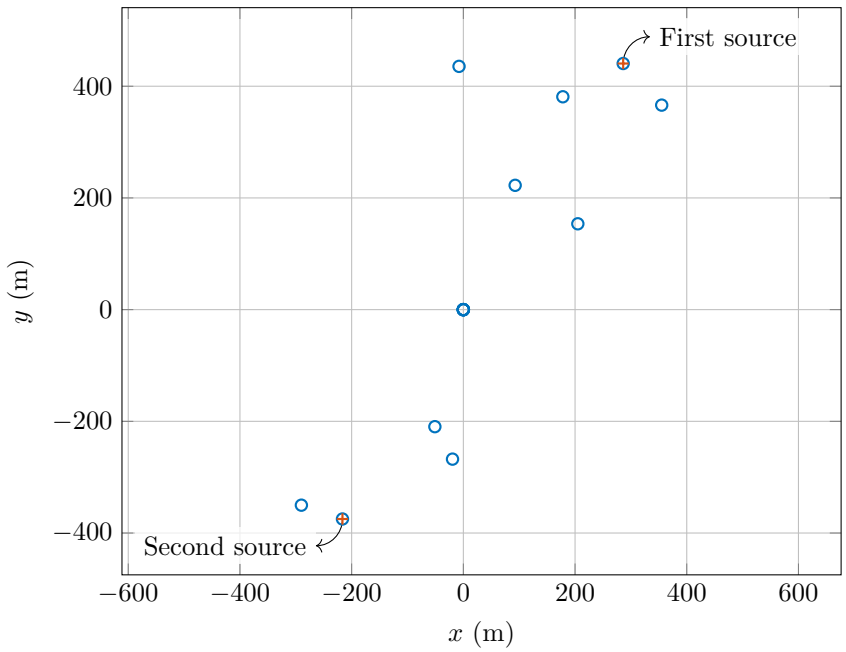

Figure 4.6: Pseudo locations of direction-based localisation. The estimation results (blue circles) are projected onto the xy-plane for simplicity. Only two of them are in the vicinity of the true locations (red pluses) while the others are pseudo locations.

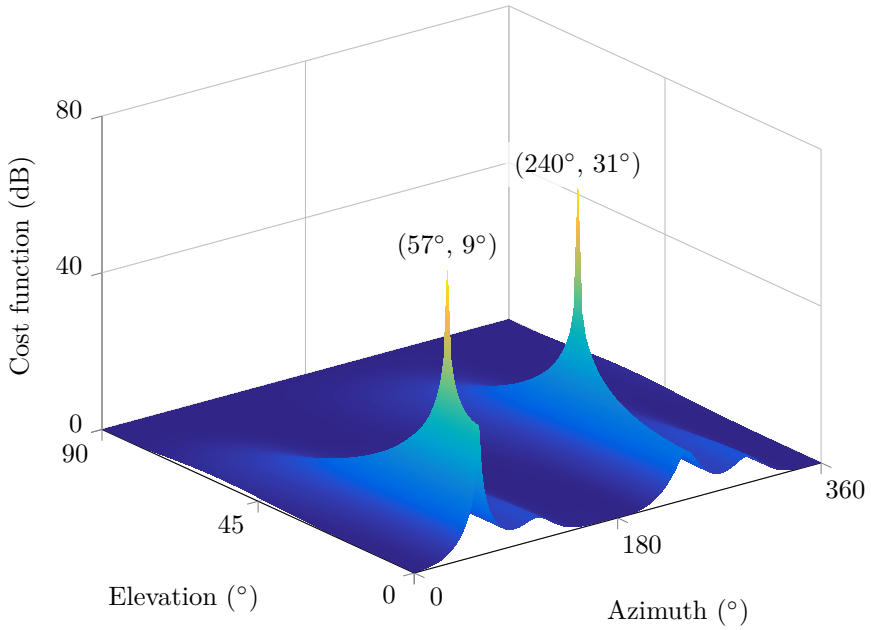

Figure 4.7: DOA azimuth and elevation estimation.

2.11 m, respectively. Thus, the source locations can be inferred from the azimuth, elevation, and range estimates. Subsequently, the orientation of the desired source is estimated. The joint DOD azimuth and elevation estimation results using the approaches without and with interference cancellation are shown in Figures 4.8 and 4.9, respectively, where four peaks at the azimuths and elevations $(91°, -22°)$, $(158°, -3°)$, $(36°, -2°)$, and $(327°, 47°)$ can be observed, indicating a successful estimation of the DODs. Note that there are estimation errors due to the search step size of 1°. The estimation errors can be further reduced by contracting the search space and decreasing the search step size. Based on the estimated DOAs and DODs, the Euler angles can be derived. The estimated Euler angles are $-156°$, 22°, and 26°, respectively, compliant with the parameters given in Table 4.4.

Furthermore, the performance of the estimators is assessed in terms of the estimation RMSE, which is shown in Figures 4.10 and 4.11. As shown, the estimator delivers very accurate estimation of the location and orientation of the sources.

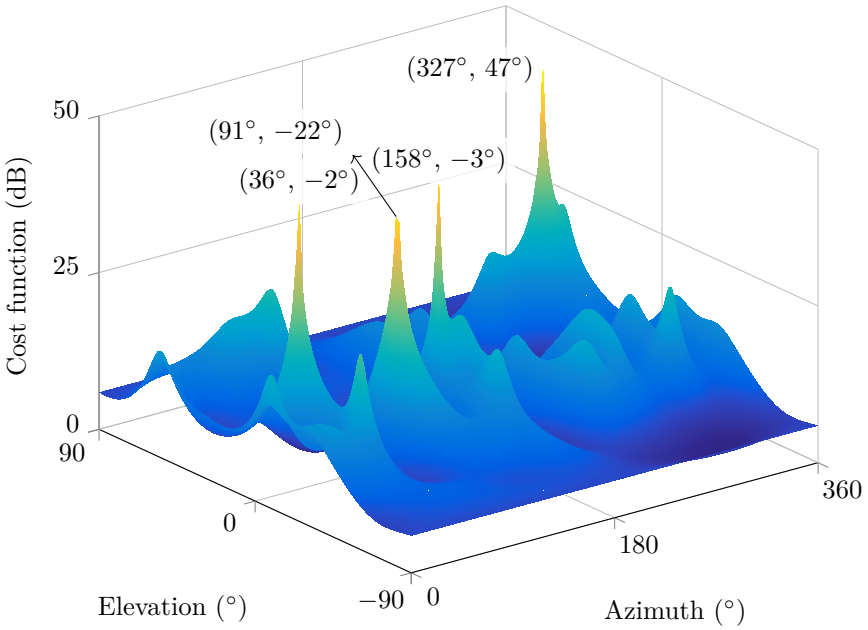

Figure 4.8: DOD azimuth and elevation estimation without interference cancellation.

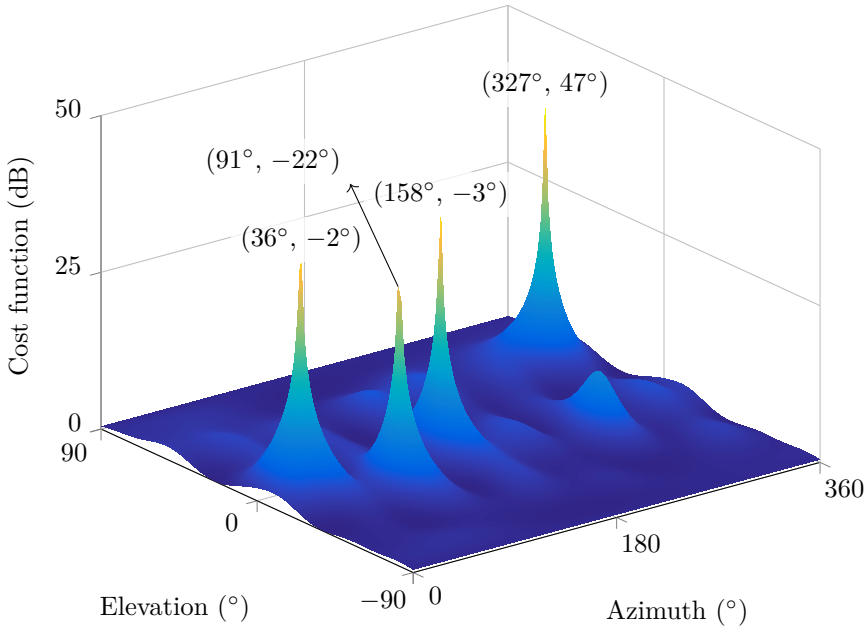

Figure 4.9: DOD azimuth and elevation estimation with interference cancellation.

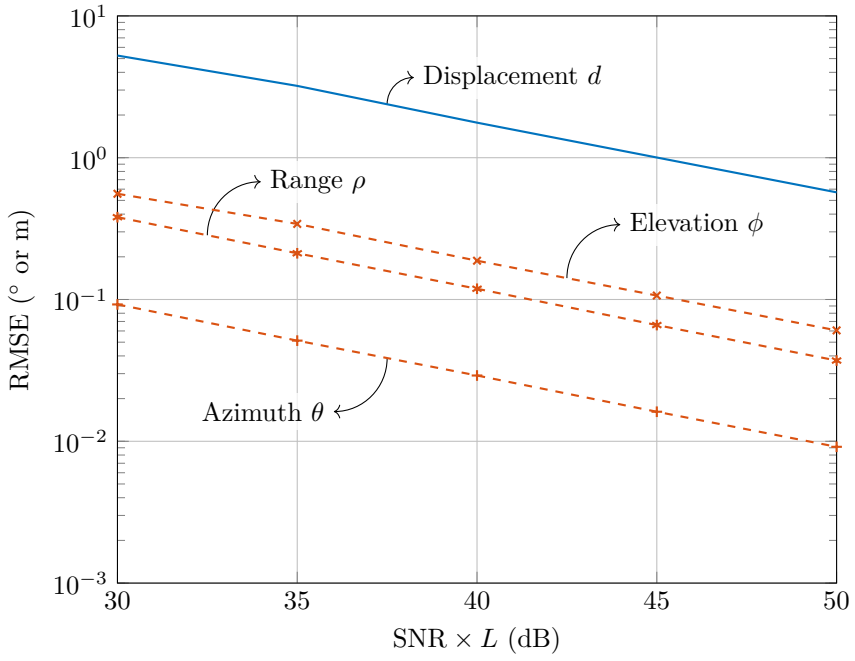

Figure 4.10: Transmitter localisation RMSE versus SNR and number of snapshots. The RMSEs of the displacement d, azimuth θ, elevation ϕ, and range ρ decrease as SNR × L increases. The results are averaged over 10 000 simulations.

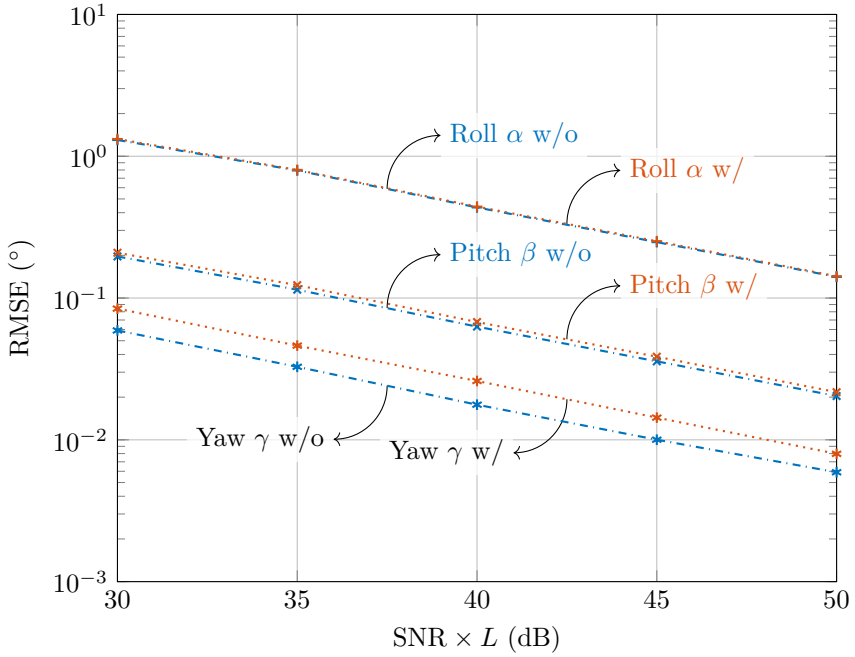

Figure 4.11: Transmitter orientation estimation RMSE versus SNR and number of snapshots. The RMSEs of the Euler angles α, β, and γ using the approaches without and with interference cancellation decrease as SNR $\times$ L increases. The results are averaged over 10 000 simulations.

Even at low SNR or small number of snapshots, the estimation errors are less than 1 m for the location and (almost) less than 1° for the Euler angles. Additionally, the two approaches to the orientation estimation deliver similar estimation errors of the Euler angles.

4.4 Summary

In this chapter, the approach to the estimation of the location and orientation of multiple sources is proposed. A distributed receiver array consisting of groups of small aperture sensor arrays is employed to estimate the location and orientation of multiple sources with each one being a transmitter array. The directions of the sources are estimated using subspace techniques like MUSIC first. Then, based on the direction estimates, the ranges are estimated by solving a system of equa-

tions. Thereafter, two approaches can be utilised to estimate the orientations with the employment of the source beamforming weight vectors. The approach without interference cancellation can correctly estimate source orientations even when the sources follow the NBA among all the groups of the receiver array; however, it generally requires more number of transmitter elements of each source as the dimension of the signal subspace, which contains interference, is higher. On the contrary, the approach with interference cancellation requires much less number of transmitter elements since the interference is eliminated; nonetheless, it fails to estimate source orientations when the sources follow the NBA. From the computer simulation results, the approaches proposed in this chapter are shown to estimate the source location and orientation with exceeding accuracy.

Chapter 5

Localisation under the Wideband Assumption

In array processing, subspace techniques like MUSIC are widely employed to solve the estimation problem. Despite the extensive researches of these algorithms in the literature, most of them assume that the wavefront of the impinging signal does not vary significantly when traversing through the sensors of the array, which is known as the NBA as shown in Figures 5.1(a) and 5.1(c) [1]. However, in a distributed array of sensors, the NBA may not be valid with a high probability due to the difference in the ranges between the source and the sensors, and the WBA, where the wavefront does vary significantly as shown in Figures 5.1(b) and 5.1(d), needs to be considered. Under the WBA, it is highly likely that the above subspace estimation algorithms fail to deliver correct estimates of the source parameters. Note that the concept of the NBA/WBA, where the overall geometry of the source and array plays a role, should not be confused with the narrowband/wideband signal,[1] as contrasted in Figure 5.1.

[1] A wideband source (large bandwidth) may be under the NBA for a particular location of the source and a given array geometry; however, if the source moves to another position in space and the array geometry remains the same, it may be under the WBA.

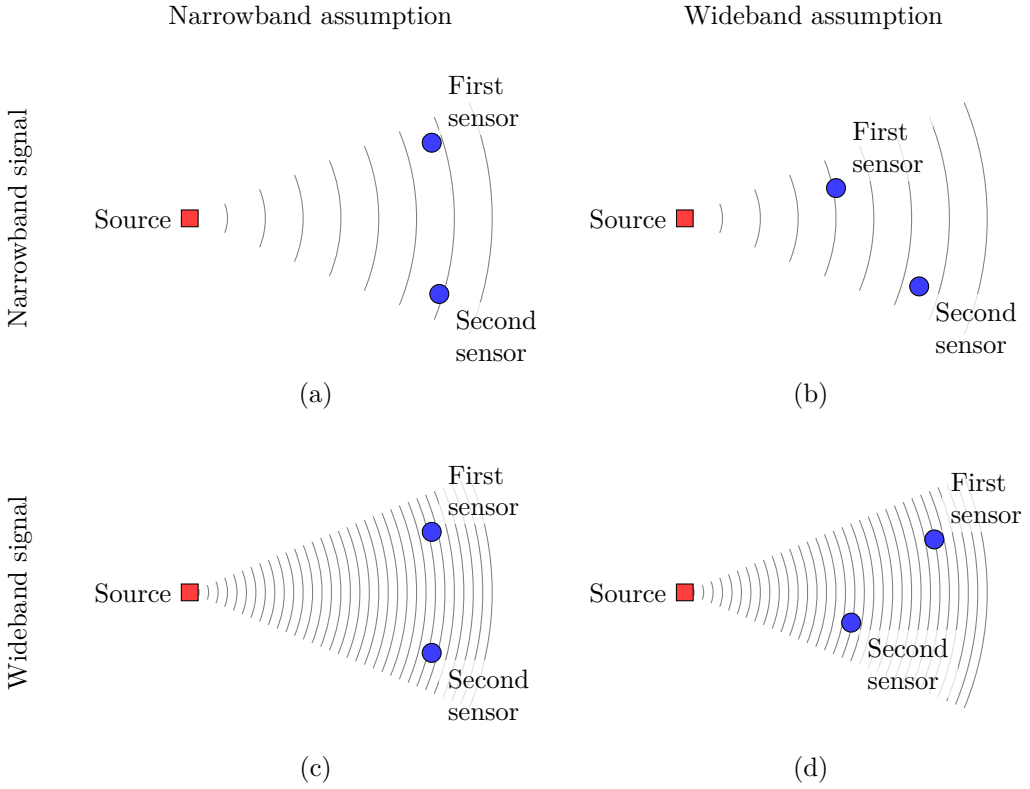

Figure 5.1: Wideband/narrowband assumption and wideband/narrowband signal. The density of the curves propagating from the source to the sensors represents the bandwidth of the baseband signal; i.e., the denser the curves are, the higher the bandwidth is. (a) Narrowband signal under narrowband assumption. (b) Narrowband signal under wideband assumption. (c) Wideband signal under narrowband assumption. (d) Wideband signal under wideband assumption.

In this chapter, two approaches are proposed to address the localisation problems under the WBA. In the first subcovariance-based (SCB) approach, the subcovariance of the received signal vector is utilised to estimate the source locations. In the second reference-rotation-based (RRB) approach, the rotation of the array reference point is employed to transform the WBA problem to its NBA counterpart so that localisation algorithms under the NBA are readily applicable. Through computer simulation studies, these two approaches are shown to estimate the source locations with outstanding accuracy.

The rest of this chapter is organised as follows. In Section 5.1, the signal model under the WBA is presented. In Sections 5.2 and 5.3, the SCB and RRB

approaches to the localisation problem are explained, respectively. In Section 5.4, computer simulation studies are carried out to investigate the performance of the SCB and RRB approaches in various scenarios. Last, in Section 5.5, the chapter is summarised.

5.1 Signal Model under the Wideband Assumption

Consider an array of N widely distributed sensors of a known array geometry. The array receives the signals from M sources via the LOS paths only with $M < N$. The geometry of the array and i-th source is shown in Figure 5.2, where the sensors are represented by the blue circles and the i-th source is represented by the red

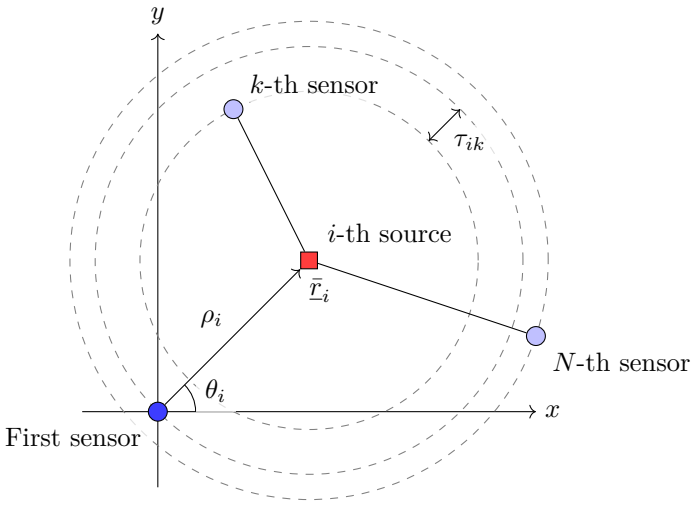

Figure 5.2: Spherical wave propagation from the i-th source to an array of sensors. The sensors of the array are represented by the blue circles with the array reference point denoted by the darker one. The source is represented by the red square. The location of the source is parameterised by its azimuth θ_i and range ρ_i. The delay τ_{ik} is the relative delay of the i-th source between the array reference point and the k-th sensor.

square. The array geometry can be described as

$$[\underline{r}_1, \underline{r}_2, \ldots, \underline{r}_N] = \left[\underline{r}_x, \underline{r}_y, \underline{r}_z\right]^T \in \mathcal{R}^{3\times N} \tag{5.1}$$

where $\underline{r}_k = [x_k, y_k, z_k]^T \in \mathcal{R}^{3\times 1}$ is the Cartesian coordinates of the k-th sensor and $\underline{r}_x$, $\underline{r}_y$, and $\underline{r}_z \in \mathcal{R}^{N\times 1}$ contain the coordinates of the x-, y-, and z-axis of all the sensors, respectively. Without loss of generality, the first sensor is located at the origin of the coordinate system and is selected as the array reference point. In addition, assume that the elevation $\phi_i = 0^\circ$ for all the sources. Hence, the location of the i-th source can be expressed in terms of its azimuth θ_i and range ρ_i as

$$\bar{\underline{r}}_i \triangleq \bar{\underline{r}}(\theta_i, \rho_i) = \rho_i \underline{u}_i \in \mathcal{R}^{3\times 1} \tag{5.2}$$

with

$$\underline{u}_i \triangleq \underline{u}(\theta_i) = [\cos\theta_i, \sin\theta_i, 0]^T \in \mathcal{R}^{3\times 1} \tag{5.3}$$

being a unit vector pointing from the array reference point towards the i-th source.

Since the array aperture is considerably larger than the carrier wavelength, spherical wave propagation needs to be considered. The spherical wave array manifold vector of the i-th source is given as [13]

$$\underline{S}_i \triangleq \underline{S}(\theta_i, \rho_i) = \rho_i^a \underline{\rho}^{-a}(\theta_i, \rho_i) \odot \exp\left(-j2\pi \frac{F_c}{c}\left(\rho_i \underline{1}_N - \underline{\rho}(\theta_i, \rho_i)\right)\right) \in \mathcal{C}^{N\times 1} \tag{5.4}$$

with

$$\underline{\rho}(\theta_i, \rho_i) = \sqrt{\rho_i^2 \underline{1}_N + \underline{r}_x^2 + \underline{r}_y^2 + \underline{r}_z^2 - 2\rho_i \left[\underline{r}_x, \underline{r}_y, \underline{r}_z\right] \underline{u}_i} \in \mathcal{R}^{N\times 1} \tag{5.5}$$

where a is the known path loss exponent.

If the messages $m_i(t)$ of all the sources follow the NBA, then the baseband

signal vector received at the array is

$$\underline{x}(t) = [x_1(t)\,, x_2(t)\,, \ldots, x_N(t)]^T = \sum_{i=1}^{M} \underline{S}_i m_i(t) + \underline{n}(t) \in \mathcal{C}^{N\times 1} \tag{5.6}$$

where $\underline{n}(t)$ represents the complex AWGN of zero mean and covariance $\sigma_n^2 \mathbb{I}_N$. Equation (5.6) can be rewritten in a more compact matrix format as

$$\underline{x}(t) = \mathbb{S}\underline{m}(t) + \underline{n}(t) \tag{5.7}$$

where

$$\mathbb{S} = [\underline{S}_1, \underline{S}_2, \ldots, \underline{S}_M] \in \mathcal{C}^{N\times M}; \tag{5.8}$$

$$\underline{m}(t) = [m_1(t)\,, m_2(t)\,, \ldots, m_M(t)] \in \mathcal{C}^{M\times 1}. \tag{5.9}$$

Since the messages and noise are assumed to be uncorrelated, the covariance matrix of the received signal vector $\underline{x}(t)$ is

$$\begin{aligned}
\mathbb{R}_{xx} &= \mathcal{E}\Big\{\underline{x}(t)\,\underline{x}^H(t)\Big\} \\
&= \mathcal{E}\Big\{\mathbb{S}\underline{m}(t)\,\underline{m}^H(t)\,\mathbb{S}^H\Big\} + \mathcal{E}\Big\{\underline{n}(t)\,\underline{n}^H(t)\Big\} \\
&= \mathbb{S}\underbrace{\mathcal{E}\Big\{\underline{m}(t)\,\underline{m}^H(t)\Big\}}_{=\mathbb{R}_{mm}}\mathbb{S}^H + \underbrace{\mathcal{E}\Big\{\underline{n}(t)\,\underline{n}^H(t)\Big\}}_{=\mathbb{R}_{nn}} \\
&= \mathbb{S}\mathbb{R}_{mm}\mathbb{S}^H + \mathbb{R}_{nn} \in \mathcal{C}^{N\times N}
\end{aligned} \tag{5.10}$$

where $\mathbb{R}_{mm} \in \mathcal{C}^{M\times M}$ and $\mathbb{R}_{nn} = \sigma_n^2 \mathbb{I}_N \in \mathcal{R}^{N\times N}$ are the covariance matrices of the messages and noise, respectively.

According to the structure of $\mathbb{R}_{xx}$ given in Equ. (5.10), the number of its most significant eigenvalues is determined by rank($\mathbb{R}_{mm}$), which is equal to the number of sources M. Equivalently, its minimum eigenvalue is σ_n^2 and its multiplicity is

$N-M$, which can then be utilised to infer the number of sources as $N-(N-M)$. Furthermore, the subspace spanned by the eigenvectors corresponding to the minimum eigenvalues is known as the noise subspace, which is complementary to the signal subspace spanned by the manifold vectors of the sources. Therefore, by using projection operators, the manifold vectors orthogonal to the noise subspace as well as their parameters (i.e., locations in terms of azimuths and ranges) can be estimated.

In contrast to the NBA, if at least one message follows the WBA, the received signal vector needs to be modelled as

$$\underline{x}(t) = \sum_{i=1}^{M} \underline{S}_i \odot \underline{m}_i(t) + \underline{n}(t) \in \mathcal{C}^{N\times 1} \tag{5.11}$$

where $\underline{m}_i(t) \in \mathcal{C}^{N\times 1}$ contains the delayed copies of the i-th message given as

$$\underline{m}_i(t) = \left[m_i(t-\tau_{i1}), m_i(t-\tau_{i2}), \ldots, m_i(t-\tau_{iN})\right]^T \tag{5.12}$$

with τ_{ik} denoting the relative delay of the i-th source between the array reference point and the k-th sensor. Equation (5.11) can also be rewritten in a matrix format as

$$\underline{x}(t) = (\mathbb{S} \odot \mathbb{M}(t))\, \underline{1}_M + \underline{n}(t) \tag{5.13}$$

where

$$\mathbb{S} = [\underline{S}_1, \underline{S}_2, \ldots, \underline{S}_M] \in \mathcal{C}^{N\times M}; \tag{5.14}$$

$$\mathbb{M}(t) = [\underline{m}_1(t), \underline{m}_2(t), \ldots, \underline{m}_M(t)] \in \mathcal{C}^{N\times M}. \tag{5.15}$$

In a similar fashion, since the messages and noise are uncorrelated, the covari-

ance matrix of the received signal vector is

$$\begin{aligned}
\mathbb{R}_{xx} &= \mathcal{E}\Big\{\underline{x}(t)\,\underline{x}^H(t)\Big\} \\
&= \mathcal{E}\Big\{(\mathbb{S}\odot\mathbb{M}(t))\,\underline{1}_M\underline{1}_M^T\,(\mathbb{S}\odot\mathbb{M}(t))^H\Big\} + \mathcal{E}\Big\{\underline{n}(t)\,\underline{n}^H(t)\Big\} \\
&= \bar{\mathbb{S}}\,\underbrace{\mathcal{E}\Big\{\mathrm{vec}(\mathbb{M}(t))\,\mathrm{vec}^H(\mathbb{M}(t))\Big\}}_{=\mathbb{R}_{mm}}\bar{\mathbb{S}}^H + \underbrace{\mathcal{E}\Big\{\underline{n}(t)\,\underline{n}^H(t)\Big\}}_{=\mathbb{R}_{nn}} \\
&= \bar{\mathbb{S}}\mathbb{R}_{mm}\bar{\mathbb{S}}^H + \mathbb{R}_{nn} \in \mathcal{C}^{N\times N}
\end{aligned} \tag{5.16}$$

where $\bar{\mathbb{S}} = [\mathrm{diag}(\underline{S}_1), \mathrm{diag}(\underline{S}_2), \ldots, \mathrm{diag}(\underline{S}_M)] \in \mathcal{C}^{N\times MN}$ and $\mathbb{R}_{mm} \in \mathcal{C}^{MN\times MN}$ denotes the covariance matrix of the delayed messages. Note that the number of the most significant eigenvalues of $\mathbb{R}_{xx}$ is determined by $\mathrm{rank}(\mathbb{R}_{mm})$ but bounded from above by N. In addition, $M < \mathrm{rank}(\mathbb{R}_{mm}) \leq MN$ if the messages of different sources are incoherent and at least one source follows the WBA. Therefore, the number of the most significant eigenvalues is between $M+1$ and N, inclusively. If $\mathrm{rank}(\mathbb{R}_{mm}) \geq N$, then the signal subspace of $\mathbb{R}_{xx}$ spans the entire observation space and the dimension of the noise subspace is zero. In this case, subspace estimation techniques like MUSIC fail to estimate the source parameters.

In order to address this issue, two approaches to source localisation under the WBA are proposed in the following sections.

5.2 Subcovariance-Based Approach

In this section, the SCB approach under the WBA is explained. It uses the subcovariance matrix of the received signal vector and its singular value decomposition to estimate the source locations.

Note that for some location (θ, ρ), its corresponding relative delay vector can

be derived from the known array geometry as

$$\underline{\tau}(\theta,\rho) = [\tau_1(\theta,\rho), \tau_2(\theta,\rho), \ldots, \tau_N(\theta,\rho)]^T = \frac{1}{c}\Big(\rho \underline{1}_N - \underline{\rho}(\theta,\rho)\Big). \tag{5.17}$$

Hereafter, the arguments θ and ρ of $\underline{\tau}(\theta,\rho)$ and its elements are omitted for simplicity unless otherwise noted. The received signal vector $\underline{x}(t)$ can be reversely delayed using $\underline{\tau}$ as

$$\bar{\underline{x}}(t) = [x_1(t+\tau_1), x_2(t+\tau_2), \ldots, x_N(t+\tau_N)]^T \in \mathcal{C}^{N\times 1} \tag{5.18}$$

and, consequently, the corresponding reversely delayed message vector of the i-th source is

$$\bar{\underline{m}}_i(t) = [m_i(t-\tau_{i1}+\tau_1), m_i(t-\tau_{i2}+\tau_2), \ldots, m_i(t-\tau_{iN}+\tau_N)]^T \in \mathcal{C}^{N\times 1}. \tag{5.19}$$

There are the following two cases with regards to the reversely delayed i-th message vector.

- If there exists exactly one i such that $\theta_i = \theta$ and $\rho_i = \rho$, then $\tau_{ik} = \tau_k$ for $k = 1, 2, \ldots, N$ and all the elements of $\bar{\underline{m}}_i(t)$ are aligned at delay zero; i.e., $\bar{\underline{m}}_i(t) = m_i(t)\,\underline{1}_N$. Furthermore, it is assumed that different sources do not share the same relative delay at the same sensor other than the array reference point; thus, $\tau_{jk} \neq \tau_k$ for $j \neq i$ and $k = 2, 3, \ldots, N$. This implies that the reversely delayed i-th message follows the NBA, whereas the other sources still remain under the WBA.

- Otherwise, if $\theta_i \neq \theta$ and $\rho_i \neq \rho$ $\forall i$, then all the sources still remain under the WBA.

Hold that thought and now examine the subcovariance matrix of the reversely

delayed received signal vector given in Equ. (5.18). Define two selection matrices associated with two nonoverlapping (but possibly interlacing) subvectors of $\underline{\bar{x}}(t)$. Without loss of generality, assume that the two subvectors contain the first N_A and last N_B elements, respectively, with $N = N_A + N_B$. Thus, the selection matrices can be defined as

$$\mathbb{F}_A = [\mathbb{I}_{N_A}, \mathbb{O}_{N_A \times N_B}] \in \mathcal{Z}^{N_A \times N}; \tag{5.20a}$$

$$\mathbb{F}_B = [\mathbb{O}_{N_B \times N_A}, \mathbb{I}_{N_B}] \in \mathcal{Z}^{N_B \times N}. \tag{5.20b}$$

Using the selection matrices, the corresponding subcovariance matrix can be retrieved from the covariance matrix of $\underline{\bar{x}}(t)$ as

$$\begin{aligned}
\mathbb{R}_{\bar{x}_A \bar{x}_B} &= \mathbb{F}_A \mathcal{E}\Big\{\underline{\bar{x}}(t)\, \underline{\bar{x}}^H(t)\Big\} \mathbb{F}_B^T \\
&= \sum_{i=1}^{M} \mathbb{F}_A \underline{S}_i \underline{S}_i^H \mathbb{F}_B^T \odot \mathbb{F}_A \mathcal{E}\Big\{\underline{\bar{m}}_i(t)\, \underline{\bar{m}}_i^H(t)\Big\} \mathbb{F}_B^T + \mathbb{F}_A \mathcal{E}\Big\{\underline{\bar{n}}(t)\, \underline{\bar{n}}^H(t)\Big\} \mathbb{F}_B^T \\
&= \sum_{i=1}^{M} \underline{S}_{iA} \underline{S}_{iB}^H \odot \underbrace{\mathcal{E}\Big\{\underline{\bar{m}}_{iA}(t)\, \underline{\bar{m}}_{iB}^H(t)\Big\}}_{=\mathbb{R}_{\bar{m}_{iA}\bar{m}_{iB}}} + \underbrace{\mathcal{E}\Big\{\underline{\bar{n}}_A(t)\, \underline{\bar{n}}_B^H(t)\Big\}}_{=\mathbb{R}_{\bar{n}_A\bar{n}_B}} \\
&= \sum_{i=1}^{M} \underline{S}_{iA} \underline{S}_{iB}^H \odot \mathbb{R}_{\bar{m}_{iA}\bar{m}_{iB}} + \mathbb{R}_{\bar{n}_A\bar{n}_B} \in \mathcal{C}^{N_A \times N_B}
\end{aligned} \tag{5.21}$$

where the associated subvectors of the array manifold vector $\underline{S}_i$, reversely delayed i-th message vector $\underline{\bar{m}}_i(t)$, and reversely delayed noise vector $\underline{\bar{n}}(t)$ are denoted by the subscripts A and B, respectively.

If the reversely delayed i-th message vector follows the NBA, the associated message subvectors are simplified to $\underline{\bar{m}}_{iA}(t) = m_i(t)\, \underline{1}_{N_A}$ and $\underline{\bar{m}}_{iB}(t) = m_i(t)\, \underline{1}_{N_B}$, which suggests that

$$\begin{aligned}
\mathbb{R}_{\bar{m}_{iA}\bar{m}_{iB}} &= \mathcal{E}\Big\{m_i(t)\, \underline{1}_{N_A} m_i^*(t)\, \underline{1}_{N_B}^T\Big\} \\
&= \mathcal{E}\{m_i(t)\, m_i^*(t)\}\, \underline{1}_{N_A} \underline{1}_{N_B}^T
\end{aligned}$$

$$= P_i \underline{1}_{N_A} \underline{1}_{N_B}^T. \tag{5.22}$$

Otherwise, if it follows the WBA, then its elements are uncorrelated since they are not aligned at delay zero, and the transmitted message is assumed to have a sharp autocovariance. Therefore, the subcovariance matrix of the reversely delayed i-th message vector is $\mathbb{R}_{\bar{m}_{iA}\bar{m}_{iB}} = \mathbb{O}_{N_A \times N_B}$. In summary, this matrix has the following format

$$\mathbb{R}_{\bar{m}_{iA}\bar{m}_{iB}} = \begin{cases} P_i \underline{1}_{N_A} \underline{1}_{N_B}^T, & \theta_i = \theta \wedge \rho_i = \rho; \quad (5.23a) \\ \mathbb{O}_{N_A \times N_B}, & \theta_i \neq \theta \vee \rho_i \neq \rho. \quad (5.23b) \end{cases}$$

In a similar fashion, the subcovariance matrix of the reversely delayed noise vector is $\mathbb{R}_{\bar{n}_A \bar{n}_B} = \mathbb{O}_{N_A \times N_B}$.

Based on the above analysis as well as the two cases explained before, the subcovariance matrix of the reversely delayed received signal is

$$\mathbb{R}_{\bar{x}_A \bar{x}_B} = \begin{cases} P_i \underline{S}_{iA} \underline{S}_{iB}^H, & \exists i : \theta_i = \theta \wedge \rho_i = \rho; \quad (5.24a) \\ \mathbb{O}_{N_A \times N_B}, & \forall i : \theta_i \neq \theta \vee \rho_i \neq \rho. \quad (5.24b) \end{cases}$$

In the first case, $\mathbb{R}_{\bar{x}_A \bar{x}_B}$ is a rank one matrix and is completely determined by the subvectors of the array manifold vector $\underline{S}_i$. Its singular value decomposition can be written as

$$\mathbb{R}_{\bar{x}_A \bar{x}_B} = \mathbb{U}_{\bar{x}_A} \mathbb{D}_{\bar{x}_A \bar{x}_B} \mathbb{V}_{\bar{x}_B}^H \tag{5.25}$$

where $\mathbb{U}_{\bar{x}_A} \in \mathcal{C}^{N_A \times N_A}$ is a unitary matrix containing the left singular vectors, $\mathbb{D}_{\bar{x}_A \bar{x}_B} \in \mathcal{R}^{N_A \times N_B}$ is a rectangular diagonal matrix containing the singular values on its diagonal, and $\mathbb{V}_{\bar{x}_B} \in \mathcal{C}^{N_B \times N_B}$ is a unitary matrix containing the right singular

vectors. Besides, the structure of the matrix containing the singular values is

$$\mathbb{D}_{\bar{x}_A\bar{x}_B} = \begin{bmatrix} P_i \left\|\underline{S}_{iA}\right\| \left\|\underline{S}_{iB}\right\|, & \underline{0}_{N_B-1}^T \\ \underline{0}_{N_A-1}, & \mathbb{O}_{(N_A-1)\times(N_B-1)} \end{bmatrix}. \tag{5.26}$$

In other words, among the $\min(N_A, N_B)$ singular values, there is only one nonzero singular value, which is referred to as the most significant singular value. Further, the left singular vector corresponding to this most singular value spans the same subspace as $\underline{S}_{iA}$ and, similarly, this applies to the right singular vector and $\underline{S}_{iB}$. Moreover, in the second case, $\mathbb{R}_{\bar{x}_A\bar{x}_B}$ is a zero matrix and its "most significant" singular vector does not span the same subspace as the array manifold vector of any source. Therefore, the parameters of (the subvectors of) the array manifold vectors can be estimated using the most significant singular vector of $\mathbb{R}_{\bar{x}_A\bar{x}_B}$, regardless of the assumption the sources follow before the received signal is reversely delayed.

According to the theory explained above, the localisation algorithm in practice is designed as follows. Suppose that the received signal is collected at the sampling frequency F_s and sampling period $T_s = 1/F_s$. It is also assumed that the sampling frequency is high enough so that the autocovariance properties of the message signals of all the sources can be recovered. Suppose that L snapshots are collected at the array, which can be written in a matrix format as

$$\mathbb{X} = [\underline{x}(t_1), \underline{x}(t_2), \ldots, \underline{x}(t_L)] = [\underline{x}_1, \underline{x}_2, \ldots, \underline{x}_N]^T \in \mathcal{C}^{N\times L} \tag{5.27}$$

where $t_\ell = \ell T_s$ is the ℓ-th time instance and $\underline{x}_k \in \mathcal{C}^{L\times 1}$ contains all the L snapshots collected at the k-th sensor starting from the first time instance. In order to estimate the source locations in terms of their parameters θ and ρ, a cost function of these two parameters is to be maximised by a two-dimensional search of them over the parameter space. Note that, in contrast to the MUSIC algorithm in [19],

the null subspace in the SCB approach is parameter dependent. Based on the received signal matrix given in Equ. (5.27), the estimation procedure is described as follows [111].

First, for a particular (θ, ρ), calculate the discrete relative delay vector based on Equ. (5.17) as

$$\underline{\ell}(\theta,\rho) = [\ell_1(\theta,\rho), \ell_2(\theta,\rho), \ldots, \ell_N(\theta,\rho)]^T = \lfloor F_s \underline{\tau}(\theta,\rho) \rfloor \in \mathcal{Z}^{N\times 1} \tag{5.28}$$

where $\ell_k(\theta,\rho)$ denotes its k-th element. Then, reversely delay the signal received at the k-th sensor (i.e., the k-th row of $\mathbb{X}$, in the format of a column vector) using $\ell_k(\theta,\rho)$ as

$$\underline{\bar{x}}_k(\theta,\rho) = \mathbb{J}_L^{-\ell_k(\theta,\rho)+L} \underline{\bar{x}}_k \in \mathcal{C}^{L\times 1} \tag{5.29}$$

where

$$\mathbb{J}_L = \begin{bmatrix} \underline{0}_{L-1}^T, & 0 \\ \mathbb{I}_{L-1}, & \underline{0}_{L-1} \end{bmatrix} \in \mathcal{Z}^{L\times L} \tag{5.30}$$

is the L-dimensional lower shift matrix. By repeating this reversely delaying step for $k = 1, 2, \ldots, N$ (i.e., all the rows of $\mathbb{X}$), the reversely delayed received signal matrix associated with this (θ, ρ) can be formed as

$$\bar{\mathbb{X}}(\theta,\rho) = [\underline{\bar{x}}_1(\theta,\rho), \underline{\bar{x}}_2(\theta,\rho), \ldots, \underline{\bar{x}}_N(\theta,\rho)]^T \in \mathcal{C}^{N\times L}. \tag{5.31}$$

In addition, the subcovariance matrix of $\bar{\mathbb{X}}(\theta,\rho)$ associated with the N_A and N_B sensors can be obtained as

$$\mathbb{R}_{\bar{x}_A\bar{x}_B}(\theta,\rho) = \frac{1}{L}\mathbb{F}_A \bar{\mathbb{X}}(\theta,\rho)\, \bar{\mathbb{X}}^H(\theta,\rho)\, \mathbb{F}_B \in \mathcal{C}^{N_A\times N_B}. \tag{5.32}$$

Subsequently, estimate the null subspace of $\mathbb{R}_{\bar{x}_A\bar{x}_B}(\theta,\rho)$ using its singular value decomposition. Take its left singular vectors as an example; its null subspace,

which is denoted as $\mathbb{E}_n(\theta, \rho) \in \mathcal{C}^{N_A \times (N_A - 1)}$, consists of its left singular vectors corresponding to its $N_A - 1$ least significant singular values. With the employment of the null subspace, evaluate the following cost function

$$\xi(\theta, \rho) = \frac{\underline{S}_A^H(\theta, \rho)\, \underline{S}_A(\theta, \rho)}{\underline{S}_A^H(\theta, \rho)\, \mathbb{E}_n(\theta, \rho)\, \mathbb{E}_n^H(\theta, \rho)\, \underline{S}_A(\theta, \rho)} \tag{5.33}$$

where $\underline{S}_A(\theta, \rho)$ contains the first N_A elements of the array manifold vector parameterised by θ and ρ.

The above procedure from Equs. (5.28) to (5.33) is repeated for all θ and ρ in the parameter space to find the source locations (θ, ρ) at which Equ. (5.33) is maximised.

In conclusion, the proposed SCB localisation approach is summarised as the following steps.

Step 1: For a particular (θ, ρ) calculate the discrete relative delay vector using Equ. (5.28).

Step 2: Reversely delay the signals received at all the sensors using Equ. (5.29). Form the reversely delayed signal matrix using Equ. (5.31).

Step 3: Calculate the subcovariance matrix using Equ. (5.32).

Step 4: Find the null subspace of the subcovariance matrix as its left or right singular vectors corresponding to its least significant singular values.

Step 5: Evaluate the cost function Equ. (5.33).

Step 6: Repeat Steps 1 to 5 for all θ and ρ in the parameter space to estimate the source locations.

5.3 Reference-Rotation-Based Approach

On top of the SCB approach described in Section 5.2, the source locations can be estimated under the WBA by exploiting the concept of the rotation of the array reference point.

As explained in Section 5.1, the first sensor is selected as the array reference point without loss of generality. This is defined as the primary reference point, utilising which the manifold vector associated with the i-th source is $\underline{S}_i$. Now, consider that the array reference point changes to the k-th sensor. In this case, the new reference point is $\underline{r}_k$ and the array geometry together with the azimuths and ranges of all the sources is measured with respect to $\underline{r}_k$. Furthermore, the manifold vector of the i-th source under the new reference point is $S_{ik}^{-1}\underline{S}_i$ where S_{ik} is the k-th element of $\underline{S}_i$ [12, 13].

In the presence of M sources, the received signal vector at the array with the k-th sensor being the array reference point can be expressed as

$$\underline{x}_k(t) = \sum_{i=1}^{M} S_{ik}^{-1}\underline{S}_i \odot \underline{m}_i(t) + \underline{n}(t) \in \mathcal{C}^{N\times 1}. \tag{5.34}$$

Poll the reference point from the first sensor to the last and preprocess (concatenate and average) all the received signal vectors as

$$\begin{aligned}
\bar{\underline{x}}(t) &= \frac{1}{\sqrt{N}} \left(\mathbb{I}_N \otimes \underline{1}_N\right)^T \left[\underline{x}_1^T(t), \underline{x}_2^T(t), \ldots, \underline{x}_N^T(t)\right]^T \\
&= \frac{1}{\sqrt{N}} \left(\mathbb{I}_N \otimes \underline{1}_N\right)^T \left(\left(\left(\underline{1}_N\underline{1}_M \oslash \mathbb{S}\right) \boxtimes \left(\mathbb{S} \odot \mathbb{M}(t)\right)\right)\underline{1}_N + \underline{1}_N \otimes \underline{n}(t)\right) \\
&= \frac{1}{\sqrt{N}} \left(\left(\left(\underline{1}_N\underline{1}_M \oslash \mathbb{S}\right) \boxtimes \underline{1}_N^T \left(\mathbb{S} \odot \mathbb{M}(t)\right)\right)\underline{1}_N + \underline{1}_N \otimes \underline{1}_N^T\underline{n}(t)\right) \\
&= \frac{1}{\sqrt{N}} \left(\left(\underline{1}_N\underline{1}_M \oslash \mathbb{S}\right) \mathrm{diag}\left(\left(\mathbb{S} \odot \mathbb{M}(t)\right)^T \underline{1}_N\right)\underline{1}_N + \underline{1}_N\underline{1}_N^T\underline{n}(t)\right) \\
&= \frac{1}{\sqrt{N}} \left(\left(\underline{1}_N\underline{1}_M \oslash \mathbb{S}\right) \left(\mathbb{S} \odot \mathbb{M}(t)\right)^T \underline{1}_N + \underline{1}_N\underline{1}_N^T\underline{n}(t)\right)
\end{aligned}$$

$$= \underbrace{(\underline{1}_N \underline{1}_M \oslash \mathbb{S})}_{=\mathbb{A}} \underbrace{\frac{1}{\sqrt{N}} \left(\mathbb{S} \odot \mathbb{M}(t)\right)^T \underline{1}_N}_{=\underline{\bar{m}}(t)} + \underbrace{\frac{1}{\sqrt{N}} \underline{1}_N \underline{1}_N^T \underline{n}(t)}_{=\underline{\bar{n}}(t)}$$

$$= \mathbb{A}\underline{\bar{m}}(t) + \underline{\bar{n}}(t) \tag{5.35}$$

where $\mathbb{A}$, $\underline{\bar{m}}(t)$, and $\underline{\bar{n}}(t)$ are the preprocessed versions of the array manifold vectors, messages, and noise, respectively. (Recall that $\mathbb{S}$ and $\mathbb{M}(t)$ are the matrices containing the array manifold vectors and message vectors of all the sources, respectively.) The preprocessed signal model given in Equ. (5.35) has a similar format to the signal model given in Equ. (5.7) under the NBA, except that the manifold vectors are element-wise inverted. Therefore, the covariance matrix of the preprocessed signal vector $\underline{\bar{x}}(t)$ is given as

$$\begin{aligned}
\mathbb{R}_{\bar{x}\bar{x}} &= \mathcal{E}\left\{\underline{\bar{x}}(t)\, \underline{\bar{x}}^H(t)\right\} \\
&= \mathbb{A}\, \underbrace{\mathcal{E}\left\{\underline{\bar{m}}(t)\, \underline{\bar{m}}^H(t)\right\}}_{=\mathbb{R}_{\bar{m}\bar{m}}} \mathbb{A}^H + \underbrace{\mathcal{E}\left\{\underline{\bar{n}}(t)\, \underline{\bar{n}}^H(t)\right\}}_{=\mathbb{R}_{\bar{n}\bar{n}}} \\
&= \mathbb{A}\mathbb{R}_{\bar{m}\bar{m}}\mathbb{A}^H + \mathbb{R}_{\bar{n}\bar{n}} \in \mathcal{C}^{N\times N}
\end{aligned} \tag{5.36}$$

where $\mathbb{R}_{\bar{m}\bar{m}}$ and $\mathbb{R}_{\bar{n}\bar{n}}$ are the covariance matrices of the preprocessed messages and noise, respectively. The covariance matrix of the preprocessed messages is

$$\mathbb{R}_{\bar{m}\bar{m}} = \mathcal{E}\left\{ \frac{1}{\sqrt{N}} \left(\mathbb{S} \odot \mathbb{M}(t)\right)^T \underline{1}_N \underline{1}_N^T \left(\mathbb{S} \odot \mathbb{M}(t)\right)^* \frac{1}{\sqrt{N}} \right\} \in \mathcal{C}^{M\times M}, \tag{5.37}$$

which has a similar structure as Equ. (5.16). Also, its rank is assumed to be M; this is because for two incoherent signals, it is highly unlikely that the superposition of the delayed versions of one signal is coherent with such a superposition of the delayed versions of the other signal. In addition, the covariance matrix of the

preprocessed noise is

$$\begin{aligned}\mathbb{R}_{\bar{n}\bar{n}} &= \mathcal{E}\left\{\frac{1}{\sqrt{N}}\underline{1}_N\underline{1}_N^T\underline{n}(t)\,\underline{n}^H(t)\,\underline{1}_N\underline{1}_N^T\frac{1}{\sqrt{N}}\right\} \\ &= \frac{1}{N}\underline{1}_N\underline{1}_N^T\mathcal{E}\left\{\underline{n}(t)\,\underline{n}^H(t)\right\}\underline{1}_N\underline{1}_N^T \\ &= \frac{1}{N}\underline{1}_N\underline{1}_N^T\sigma_n^2\mathbb{I}_N\underline{1}_N\underline{1}_N^T \\ &= \sigma_n^2\underline{1}_N\underline{1}_N^T \in \mathcal{R}^{N\times N}, \end{aligned} \tag{5.38}$$

which is a rank one matrix. Thus, according to the structure of $\mathbb{R}_{\bar{x}\bar{x}}$, it has $M+1$ most significant eigenvalues associated with the preprocessed messages and noise, and the multiplicity of the zero eigenvalue is $N-M-1$. Further, the subspace spanned by the eigenvectors of $\mathbb{R}_{\bar{x}\bar{x}}$ corresponding to its most significant eigenvalues is $(M+1)$-dimensional. This subspace is known as the signal subspace and the related eigenvectors are denoted as $\mathbb{E}_s \in \mathcal{C}^{N\times(M+1)}$. The subspace spanned by the element-wise inverted manifold vectors is always a subspace of the signal subspace; i.e., $\mathcal{L}[\mathbb{A}] \subset \mathcal{L}[\mathbb{E}_s]$. Meanwhile, the complementary subspace of the signal subspace is associated with the zero eigenvalues and is $(N-M-1)$-dimensional. This subspace is known as the null subspace and the related eigenvectors are denoted as $\mathbb{E}_n \in \mathcal{C}^{N\times(N-M-1)}$. The subspace spanned by the columns of $\mathbb{A}$ is always orthogonal to the null subspace; that is, $\mathcal{L}[\mathbb{A}] \perp \mathcal{L}[\mathbb{E}_n]$. Thus, the null subspace can be used to estimate the source locations, using the subspace estimation techniques under the NBA.

In practice, the L snapshots collected at the array with the k-th sensor being the reference point can be denoted in a matrix format as $\mathbb{X}_k \in \mathcal{C}^{N\times L}$. Besides, the preprocessed signal matrix is formed as

$$\bar{\mathbb{X}} = \frac{1}{\sqrt{N}}\left(\mathbb{I}_N \otimes \underline{1}_N\right)^T\left[\mathbb{X}_1^T, \mathbb{X}_2^T, \ldots, \mathbb{X}_N^T\right]^T \in \mathcal{C}^{N\times L} \tag{5.39}$$

and its covariance matrix is constructed as

$$\mathbb{R}_{\bar{x}\bar{x}} = \frac{1}{L}\bar{\mathbb{X}}\bar{\mathbb{X}}^H \in \mathcal{C}^{N\times N}. \tag{5.40}$$

The null subspace is constructed from the eigendecomposition of $\mathbb{R}_{\bar{x}\bar{x}}$. Then the azimuths and ranges (i.e., source locations) can be estimated by a two-dimensional search of the following cost function

$$\xi(\theta,\rho) = \frac{\underline{A}^H(\theta,\rho)\,\underline{A}(\theta,\rho)}{\underline{A}^H(\theta,\rho)\,\mathbb{E}_n\mathbb{E}_n^H\,\underline{A}(\theta,\rho)} \tag{5.41}$$

where $\underline{A}(\theta,\rho) = \underline{S}^{-1}(\theta,\rho)$. Note that, in contrast to the SCB approach, the null subspace in the RRB approach is parameter independent. On top of that, since $\mathcal{L}[\underline{1}_N] \perp \mathcal{L}[\mathbb{E}_n]$, there is a risk of maximising the cost function at a wrong (θ,ρ) where the associated inverted manifold vector is $\underline{A}(\theta,\rho) = \underline{1}_N$. However, this can be circumvented by using an array of at least four sensors of a noncircular array geometry such that a location that is equidistant from all the sensors cannot be found.

In conclusion, the proposed RRB approach is summarised as the following steps.

Step 1: Poll the array reference point from the first sensor to the last and preprocess (concatenate and average) the received signal matrices using Equ. (5.39).

Step 2: Form the covariance matrix of the preprocessed signal using Equ. (5.40).

Step 3: Find the null subspace of the covariance matrix as its eigenvectors corresponding to its least significant eigenvalues.

Step 4: Estimate the source locations by evaluating Equ. (5.41).

5.4 Computer Simulation Studies

In this section, the performance of the proposed localisation algorithm using both the SCB and RRB approaches is assessed through computer simulation studies. In the simulations, a 10-element array of 300 m array aperture is utilised; the array geometry is given in Table 5.1. The array operates in the presence of three sources; their parameters are listed in Table 5.2. Note that their elevations are 0° and are not listed. The geometry of the sources and the array is also shown in Figure 5.3. Additionally, other array system parameters are listed in Table 5.3.

The joint azimuth and range (i.e., location) estimation results of the SCB, RRB, and NBA approaches are shown between Figures 5.4 and 5.6. In the SCB approach, the subvectors are chosen as two five-element vectors comprising alternating elements of the original received signal vector. The estimation result is shown in Figure 5.4, where three peaks at the azimuths and ranges $(122°, 560\,\text{m})$, $(53°, 549\,\text{m})$, and $(73°, 593\,\text{m})$ can be observed, indicating a successful estimation

Table 5.1: Array Geometry

Sensor	x	y	Sensor	x	y
1	0 m	0 m	**6**	0 m	300 m
2	88 m	29 m	**7**	−88 m	271 m
3	143 m	104 m	**8**	−143 m	196 m
4	143 m	196 m	**9**	−143 m	104 m
5	88 m	271 m	**10**	−88 m	29 m

Table 5.2: Simulation Parameters

Source	Azimuth θ	Range ρ
1	122°	560 m
2	53°	549 m
3	73°	593 m

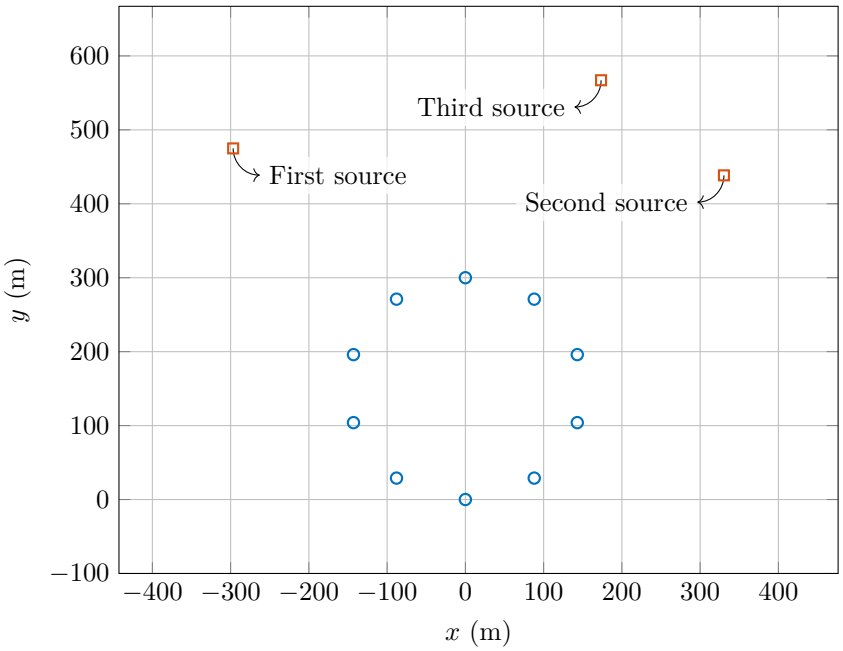

Figure 5.3: Sources and array geometry. The sensors are represented by the blue circles and the sources are represented by the red squares.

Table 5.3: Array System Parameters

Parameter	Value
Carrier frequency	3 GHz
Sampling frequency	30 MHz
Number of snapshots	200
SNR	20 dB

of the source locations. The same conclusion can be made for the RRB approach, which is shown in Figure 5.5. By contrast, no clear peaks can be observed in Figure 5.6 when the NBA approach is applied to the signals under the WBA; i.e., it fails to deliver correct estimates of the source locations.

Furthermore, the performance of the SCB and RRB approaches is compared to that of the eigenvalue-based (EVB) approach proposed in [13] in terms of the estimation RMSE using two different array geometries as listed in Table 5.4 and shown in Figure 5.7.

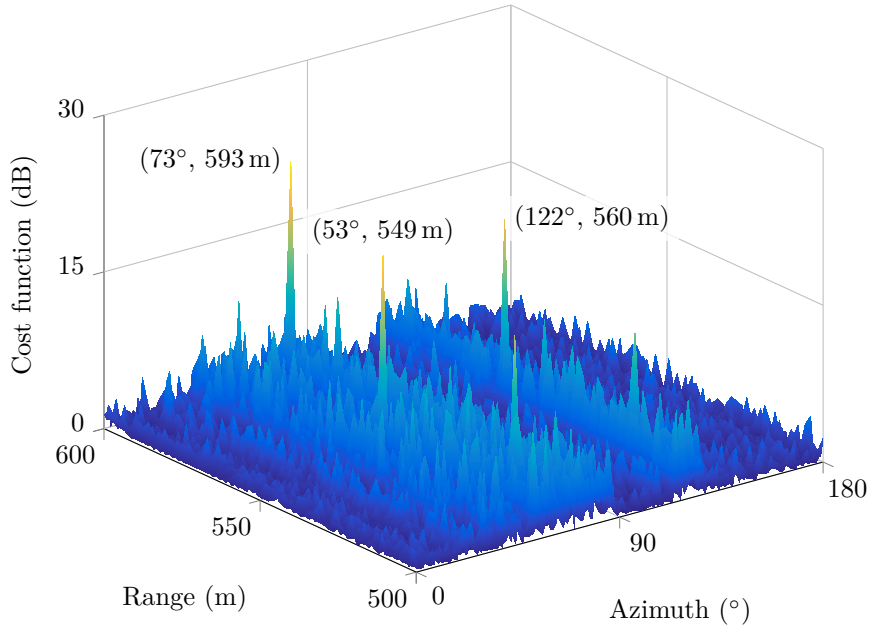

Figure 5.4: Azimuth and range estimation using the SCB approach.

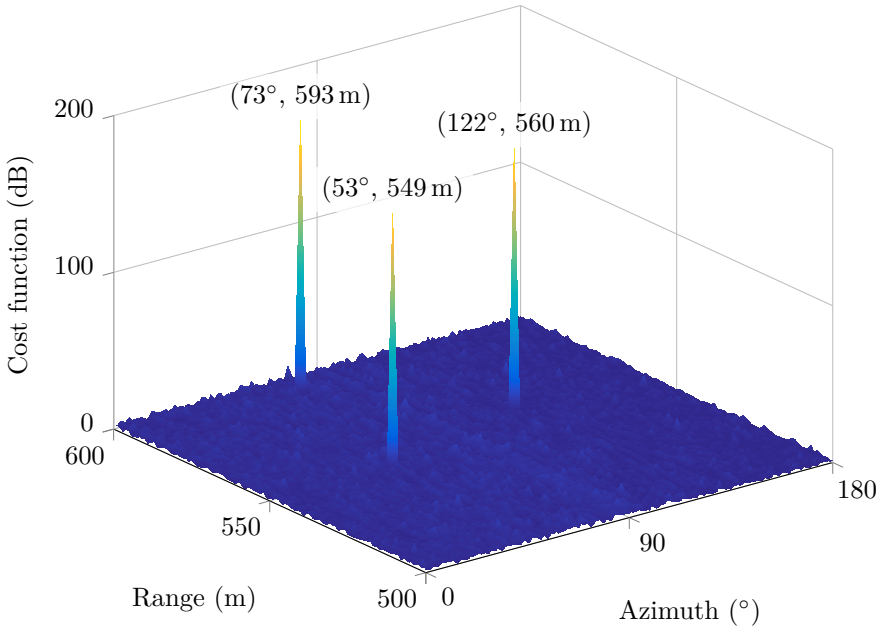

Figure 5.5: Azimuth and range estimation using the RRB approach.

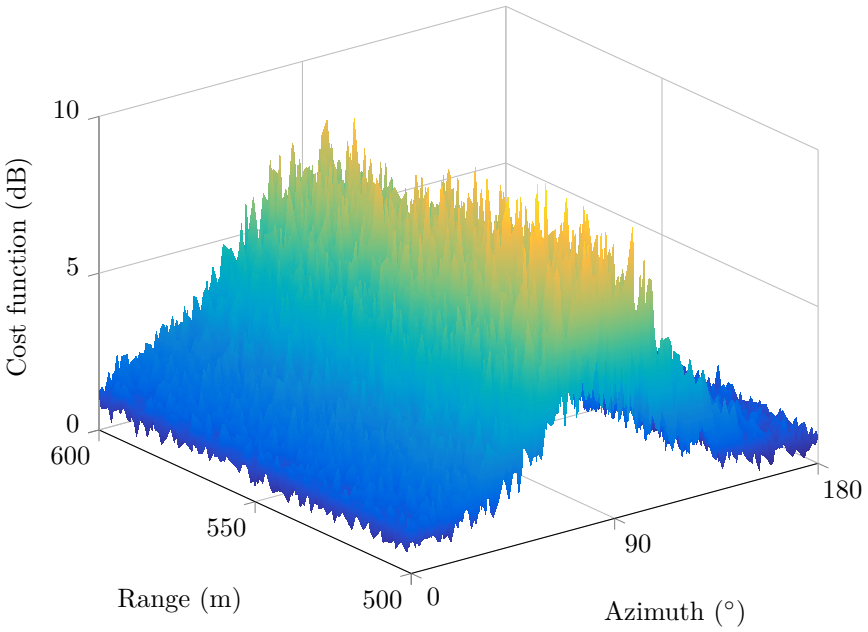

Figure 5.6: Azimuth and range estimation using the NBA approach.

Table 5.4: "Good" and "Bad" Array Geometries

Sensor	"Good"		"Bad"	
	x	y	x	y
1	0 m	0 m	0 m	0 m
2	100 m	150 m	150 m	150 m
3	0 m	300 m	0 m	300 m
4	−75 m	135 m	−150 m	150 m

First, the "good" geometry is examined. The azimuth and range of the source are 81° and 145 m, respectively. This configuration is similar to the "good" geometry in [13]. On top of that, the angles between the focusing vectors (the definition and computation of the focusing vectors can be found in [13]) are 120.47°, 117.05°, and 122.48°, respectively. Since the three angles are approximately 120°, this is a "good" geometry in the metric fusion phase and leads to good estimation accuracy [13]. The RMSE curves of the azimuth, range, and location estimates using the SCB, RRB, and EVB approaches are shown in Figure 5.8. The RMSE curves of the EVB and SCB approaches decline as SNR $\times$ L grows. For the SCB ap-

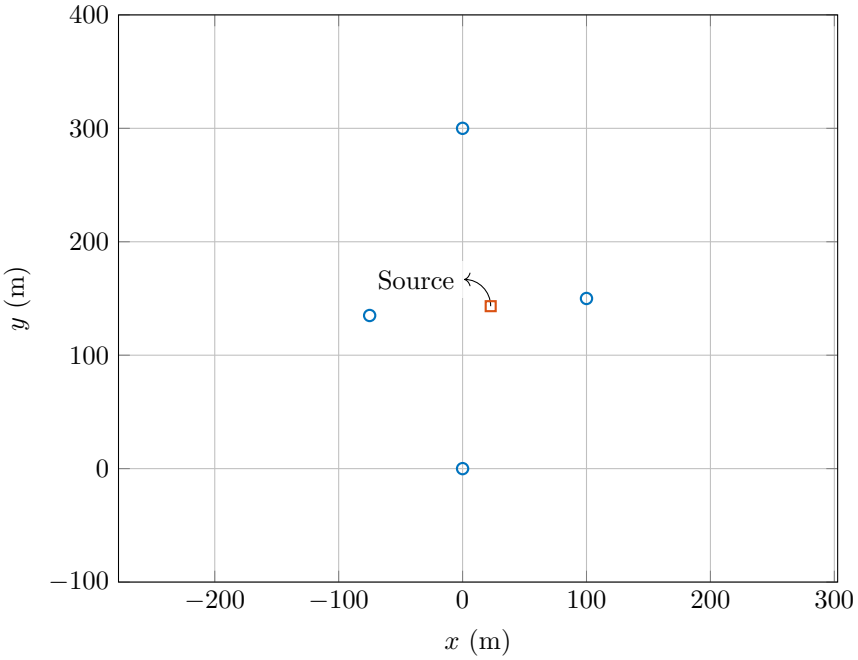

(a)

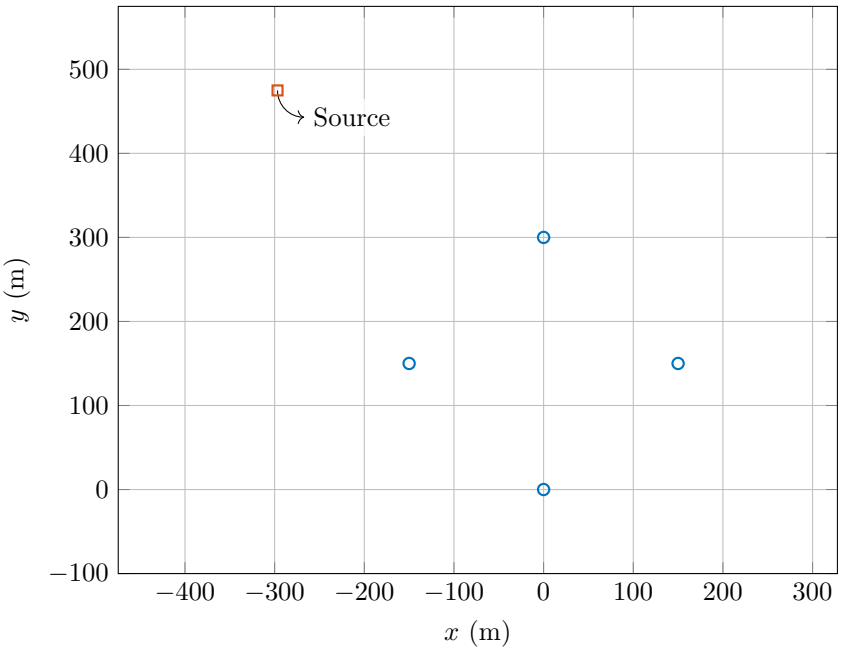

(b)

Figure 5.7: Source and "good" and "bad" array geometries. The sensors are represented by the blue circles and the source is represented by the red square. (a) "Good" array geometry. (b) "Bad" array geometry.

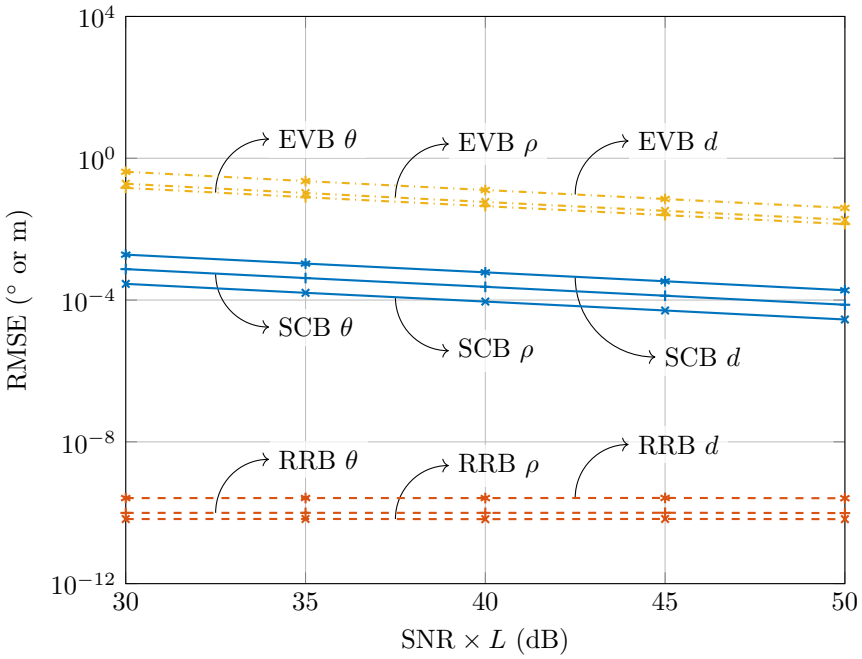

Figure 5.8: Estimation RMSE versus SNR and number of snapshots with the "good" array geometry. The RMSEs of the azimuth θ, range ρ and displacement d of the SCB and EVB approaches decrease as SNR $\times$ L increases while those of the RRB approach remains constant. The results are averaged over 10 000 simulations.

proach, the reason is that the noise effect cannot be perfectly eliminated using its subcovariance property in practice with a finite number of snapshots. Consequently, the signal subspace can be more accurately estimated with either higher SNR or more number of snapshots. Furthermore, the RRB approach enjoys very small and constant RMSE curves regardless of SNR $\times$ L. The reason is that the preprocessed noise does not contribute to the null subspace, which can then be perfectly estimated irrespective of the SNR or number of snapshots. In addition, the performance of the SCB approach is worse than the RRB approach due to the residual of the noise in the subcovariance matrix in a practical scenario. However, both the proposed SCB and RRB approaches perform much better than the EVB approach.

Second, the "bad" geometry is examined. The azimuth and range of the source are 122° and 560 m, respectively. Besides, the angles between the three focusing

vectors are 39.49°, 119.67°, and 80.18°. This is a "bad" geometry in the metric fusion phase as the first angle is too small [13]. The RMSE curves of the azimuth, range and location estimates using the three approaches are shown in Figure 5.9. The RMSE of the EVB approach is huge and stays constant with a "bad" geometry, reaching the order of magnitude of 1×10^2. This indicates that the source location cannot be correctly estimated using the EVB approach when a "bad" geometry is employed, even with higher SNR or more number of snapshots. Quite the contrary, the RMSE curves of the SCB and RRB approaches remain similar to the "good" geometry case. This implies that they are robust to "bad" geometries with small angles between focusing vectors as the metric fusion phase is circumvented.

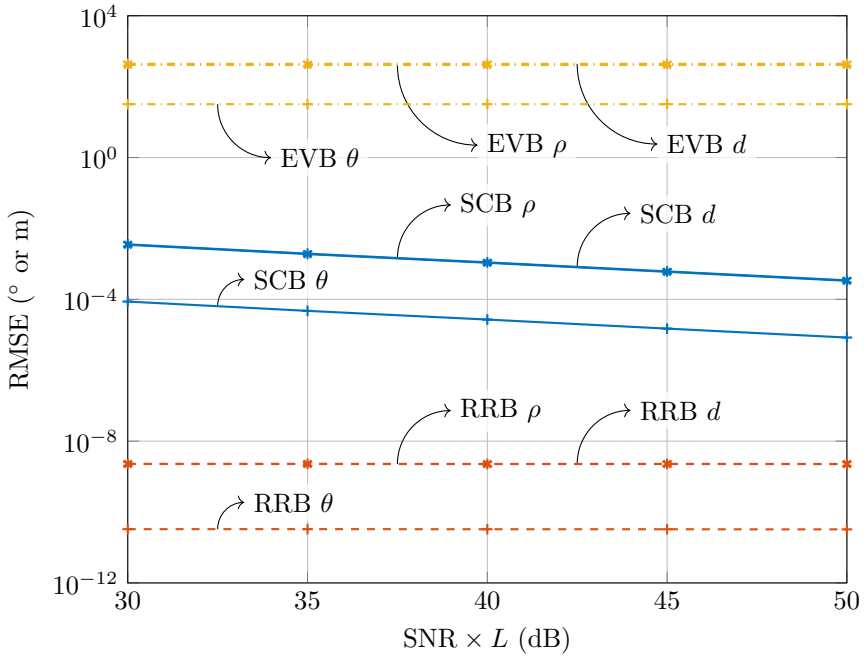

Figure 5.9: Estimation RMSE versus SNR and number of snapshots with the "bad" array geometry. The RMSEs of the SCB and RRB approaches are similar to the "good" array geometry case while those of the EVB approach are significantly big. The results are averaged over 10 000 simulations.

5.5 Summary

In this chapter, the localisation of multiple sources are examined under the WBA, where the wavefront of an impinging signal varies significantly when traversing through the sensors of an array. In the first SCB approach, the subcovariance matrix of the received signal vector, together with its singular value decomposition, is exploited to reconstruct a parameter-dependent signal subspace and estimate the source locations. In the second RRB approach, the concept of the rotation of the array reference point is employed to transform the WBA problem to its NBA counterpart so that the NBA subspace approaches are readily applicable. Through computer simulation studies, these two approaches are shown to deliver accurate estimates of source locations under the WBA. Moreover, they are robust to "bad" array geometries as the metric fusion phase is avoided.

Chapter 6

Conclusions and Further Work

In this thesis, the localisation problem in array processing is studied and the main technical chapters are summarised as follows.

In Chapter 2, multi-source indoor MIMO OWC is studied in a parametric approach. A major task in such an environment is the elimination of the interference. In order to achieve this, a parametric model that employs the geometries of the source and sensor arrays is presented for indoor MIMO OWC. Based on this model, a localisation approach, which is employed as a blind channel estimator, is proposed. It estimates parameters including the DOAs, range bins, and path gains of all the paths of the desired source in a three-step procedure, with the incorporation of cone angle parameterisation. Furthermore, two subspace multi-beam beamformers that exploit the STAR manifold vectors are presented, which effectively combine all the paths of the desired source based on the channel parameter estimates. In contrast to the traditional OWC system where the ISI and MAI are generally alleviated by adjusting the position and directivity of the sources and sensors, the beamformers presented in this chapter achieve complete interference cancellation without any restrictions on the physical configuration of the system. Their performance amounts to the optimal decorrelating receiver in terms of the

output SNIR, without the requirement of full channel knowledge.

In Chapter 3, the estimation of the locations and orientations of the receiver arrays is studied. A sensor array is exploited to estimate the location and orientation of its own with respect to a global coordinate system based on the signals transmitted from multiple sources of known locations. First, the DOAs of the sources are estimated using subspace estimation techniques. Subsequently, based on the DOA estimates and the known locations of the sources, the ranges of the sources are estimated by solving a system of quadratic equations. Finally, based on the estimates from the above steps, the location and orientation (in terms of the Euler angles) of the sensor array are estimated by solving two systems of linear equations. Moreover, a simplified approach for two-dimensional space where the elevations of the sources are negligible is proposed. It directly estimates the sensor array location and orientation from the DOA estimates without the estimation of the source ranges. As the range estimation is either derived from DOA estimates or completely discarded, the proposed approaches do not require the knowledge of the transmitted waveforms at the receiver side for estimating source ranges.

In Chapter 4, the estimation of the locations and orientations of the transmitter arrays is studied. A distributed receiver array comprising multiple compact sensor arrays is employed to estimate the locations and orientations of multiple sources with each one being a transmitter array of a known array geometry. First, the DOAs of the sources are estimated using subspace techniques based on the signals received at the primary group of the receiver array. Then, the ranges are estimated using the signals received at all the groups of the receiver array by solving a system of equations. Subsequently, two approaches without and with interference cancellation can be utilised to estimate the DODs of the sources, from which their orientations can be derived. The DOD estimation approaches make use of the format of the source beamforming weight vectors to extract the information

conveyed in the transmitter array manifold vectors. In particular, the approach without interference cancellation can handle messages under the NBA across all the groups of the sensor array; however, it requires a higher dimension of the observation space and, hence, more number of elements of each source. By contrast, the approach with interference cancellation requires a much lower dimension of the observation space; nevertheless, since the spatial information has been used for interference cancellation at the receiver, only the sources under the WBA are distinguishable among the groups of the sensor array.

In Chapter 5, the WBA, where the wavefront of a baseband signal varies significantly when traversing through the sensors of an array, is studied in distributed arrays, with the incorporation of the spherical wave propagation model. Under this assumption, NBA subspace approaches to the estimation of source locations fail to deliver correct estimation results. Two novel approaches are proposed to solve the localisation problem under the WBA. The first SCB approach employs the subcovariance of the received signal vector to estimate the source locations. Specifically, when examining a particular location in the parameter space, the relative delays associated with this location are utilised to reversely delay the received signal vector so that the source at this location follows the NBA, while others remain under the WBA. The subcovariance of the reversely delayed received signal vector is evaluated to mitigate the contribution of the sources under the WBA, and its singular value decomposition is employed to estimate the source location. In addition, the second RRB approach is based on the rotation of the array reference point. By concatenating and averaging the signal vectors received with different sensors being the array reference point, an NBA-like signal model can be obtained under the WBA. Hence, NBA localisation algorithms can be readily applied to estimate the source locations.

6.1 List of Contributions

The contributions presented in this thesis is summarised as the following list.

- Development of the localisation approach that is exploited as a blind channel estimator for location and path gain estimation for multi-source indoor MIMO OWC systems.
- Development of subspace multibeam beamformers that effectively use all the paths of the desired source.
- Development of the localisation and orientation estimation approach for a receiver array using multiple sources of known locations for both three- and two-dimensional space.
- Development of the localisation and orientation estimation approach for transmitter arrays using a distributed sensor array comprising small aperture arrays and the source beamforming weight vectors.
- Investigation of the structure of the covariance matrix of the received signal vector under the WBA.
- Development of the SCB approach to source localisation under the WBA using the subcovariance matrix of the received signal vector.
- Development of the RRB approach to source localisation under the WBA with the employment of the rotation of the array reference point.

6.2 Suggestions for Further Work

The work presented in this thesis addresses the challenges posed in the localisation problem in array processing. In this section, possible tasks incentivised by this

work are outlined.

Quantum effect. The OWC signal model presented in this thesis is developed under classic physics. However, when the size of photoemitters and photosensors becomes significantly small (e.g., on the nanoscale), quantum effects that cannot be explained by classic physics comes into play. For example, quantum noise expresses the uncertainty in transmitted and received signals due to the quantum origin of photoemitters and photosensors. A type of quantum noise is shot noise, which is brought by the discrete nature of electric charge and can be modelled by a Poisson process. Such quantum effects can be considered to further enhance the OWC signal model.

Diffuse reflection. In the OWC signal model presented in this thesis, only specular reflection of multipaths is considered. Diffuse reflection from the walls, ceiling, and floor of indoor environments can also be incorporated to extend the signal model. Diffuse multipaths are a cluster of rays that are inseparable in space and time [112]. In array processing, the array manifold vector of diffuse multipaths can be modelled using the first order Taylor series approximation about the nominal DOA of the paths [113].

Array ambiguity. An array of large intersensor spacing generally suffers from array ambiguity, which is the collinearity of the array manifold vectors associated with a set of distinct parameters. When such a distributed array is utilised to estimate the source locations under the WBA using subspace techniques, pseudo peaks are expected to appear due to the collinearity. This degrades the accuracy of the subspace estimator. Array ambiguities can be resolved by associating two sets of MUSIC estimates [114], by estimating signal power of true and ambiguous directions [115], or by observing the array pattern of beamformers [116]

Detection under WBA. Source detection under the WBA is an interesting problem to be investigated, apart from source localisation. Since the snapshots are not independent under the WBA, source detection algorithms such as AIC and MDL, based on maximising the likelihood of sample noise being a multivariate Gaussian, cannot be directly applied to infer the number of sources [18]. This could be potentially solved using hypothesis testing in combination with the autocorrelation and cross-correlation properties of the signals.

References

[1] A. Manikas, *Differential Geometry in Array Processing*. London, UK: Imperial College Press, 2004.

[2] S. Anderson, M. Millnert, M. Viberg, and B. Wahlberg, "An adaptive array for mobile communication systems," *IEEE Transactions on Vehicular Technology*, vol. 40, no. 1, pp. 230–236, Feb. 1991.

[3] A. J. Paulraj and C. B. Papadias, "Space–time processing for wireless communications," *IEEE Signal Processing Magazine*, vol. 14, no. 6, pp. 49–83, Nov. 1997.

[4] W. C. Knight, R. G. Pridham, and S. M. Kay, "Digital signal processing for sonar," *Proceedings of the IEEE*, vol. 69, no. 11, pp. 1451–1506, Nov. 1981.

[5] S. Zhou and P. Willett, "Submarine location estimation via a network of detection-only sensors," *IEEE Transactions on Signal Processing*, vol. 55, no. 6, pp. 3104–3115, Jun. 2007.

[6] I. Bekkerman and J. Tabrikian, "Target detection and localization using MIMO radars and sonars," *IEEE Transactions on Signal Processing*, vol. 54, no. 10, pp. 3873–3883, Oct. 2006.

[7] J. Li and P. Stoica, "MIMO radar with colocated antennas," *IEEE Signal Processing Magazine*, vol. 24, no. 5, pp. 106–114, Oct. 2007.

[8] J. C. Chen, K. Yao, and R. E. Hudson, "Source localization and beamforming," *IEEE Signal Processing Magazine*, vol. 19, no. 2, pp. 30–39, Mar. 2002.

[9] J. C. Chen, L. Yip, J. Elson, H. Wang, D. Maniezzo, R. E. Hudson, K. Yao, and D. Estrin, "Coherent acoustic array processing and localization on wireless sensor networks," *Proceedings of the IEEE*, vol. 91, no. 8, pp. 1154–1162, Aug. 2003.

[10] S. Gezici, Z. Tian, G. B. Giannakis, H. Kobayashi, A. F. Molisch, H. V. Poor, and Z. Sahinoglu, "Localization via ultra-wideband radios: A look at positioning aspects for future sensor networks," *IEEE Signal Processing Magazine*, vol. 22, no. 4, pp. 70–84, Jul. 2005.

[11] N. Patwari, J. N. Ash, S. Kyperountas, A. O. Hero, R. L. Moses, and N. S. Correal, "Locating the nodes: Cooperative localization in wireless sensor networks," *IEEE Signal Processing Magazine*, vol. 22, no. 4, pp. 54–69, Jul. 2005.

[12] A. Manikas, Y. I. Kamil, and P. Karaminas, "Positioning in wireless sensor networks using array processing," in *IEEE Global Telecommunications Conference*, New Orleans, LA, Nov./Dec. 2008, pp. 1–5.

[13] A. Manikas, Y. I. Kamil, and M. Willerton, "Source localization using sparse large aperture arrays," *IEEE Transactions on Signal Processing*, vol. 60, no. 12, pp. 1977–1989, Dec. 2012.

[14] M. S. Bartlett, "A note on the multiplying factors for various χ^2 approximations," *Journal of the Royal Statistical Society*, vol. 16, no. 2, pp. 296–298, Oct. 1954.

[15] D. N. Lawley, "Tests of significance for the latent roots of covariance and correlation matrices," *Biometrika*, vol. 43, no. 1/2, pp. 128–136, Jun. 1956.

[16] H. Akaike, "Information theory and an extension of the maximum likelihood principle," in *Proceeding of the Second International Symposium on Information Theory*, Tsahkadsor, USSR, Sep. 1971, pp. 267–281.

[17] J. Rissanen, "Modeling by shortest data description," *Automatica*, vol. 14, no. 5, pp. 465–471, Sep. 1978.

[18] M. Wax and T. Kailath, "Detection of signals by information theoretic criteria," *IEEE Transactions on Acoustics, Speech, and Signal Processing*, vol. 33, no. 2, pp. 387–392, Apr. 1985.

[19] R. O. Schmidt, "Multiple emitter location and signal parameter estimation," *IEEE Transactions on Antennas and Propagation*, vol. 34, no. 3, pp. 276–280, Mar. 1986.

[20] M. A. Doron and E. Doron, "Wavefield modeling and array processing, part II—algorithms," *IEEE Transactions on Signal Processing*, vol. 42, no. 10, pp. 2560–2570, Oct. 1994.

[21] F. Belloni, A. Richter, and V. Koivunen, "DoA estimation via manifold separation for arbitrary array structures," *IEEE Transactions on Signal Processing*, vol. 55, no. 10, pp. 4800–4810, Oct. 2007.

[22] J. Zhuang and A. Manikas, "Fast root-MUSIC for arbitrary arrays," *Electronics Letters*, vol. 46, no. 2, pp. 174–176, Jan. 2010.

[23] R. Roy and T. Kailath, "ESPRIT—estimation of signal parameters via rotational invariance techniques," *IEEE Transactions on Acoustics, Speech, and Signal Processing*, vol. 37, no. 7, pp. 984–995, Jul. 1989.

[24] M. S. Bartlett, "Smoothing periodograms from time-series with continuous spectra," *Nature*, vol. 161, no. 4096, pp. 686–687, May 1948.

[25] H. Cox, "Resolving power and sensitivity to mismatch of optimum array processors," *The Journal of the Acoustical Society of America*, vol. 54, no. 3, pp. 771–785, Sep. 1973.

[26] J. Capon, "High-resolution frequency-wavenumber spectrum analysis," *Proceedings of the IEEE*, vol. 57, no. 8, pp. 1408–1418, Aug. 1969.

[27] R. T. Lacoss, "Data adaptive spectral analysis methods," *Geophysics*, vol. 36, no. 4, pp. 661–675, Aug. 1971.

[28] D. J. Sadler and A. Manikas, "Blind reception of multicarrier DS-CDMA using antenna arrays," *IEEE Transactions on Wireless Communications*, vol. 2, no. 6, pp. 1231–1239, Nov. 2003.

[29] M. A. Khalighi and M. Uysal, "Survey on free space optical communication: A communication theory perspective," *IEEE Communications Surveys & Tutorials*, vol. 16, no. 4, pp. 2231–2258, Jun. 2014.

[30] J. M. Kahn and J. R. Barry, "Wireless infrared communications," *Proceedings of the IEEE*, vol. 85, no. 2, pp. 265–298, Feb. 1997.

[31] L. C. Andrews and R. L. Phillips, *Laser Beam Propagation through Random Media*. Bellingham, WA: SPIE Press, 2005.

[32] M. Razavi and J. H. Shapiro, "Wireless optical communications via diversity reception and optical preamplification," *IEEE Transactions on Wireless Communications*, vol. 4, no. 3, pp. 975–983, May 2005.

[33] W. O. Popoola and Z. Ghassemlooy, "BPSK subcarrier intensity modulated free-space optical communications in atmospheric turbulence," *Journal of Lightwave Technology*, vol. 27, no. 8, pp. 967–973, Apr. 2009.

[34] M. A. Khalighi, N. Schwartz, N. Aitamer, and S. Bourennane, "Fading reduction by aperture averaging and spatial diversity in optical wireless systems," *IEEE/OSA Journal of Optical Communications and Networking*, vol. 1, no. 6, pp. 580–593, Nov. 2009.

[35] P. Polynkin, A. Peleg, L. Klein, T. Rhoadarmer, and J. Moloney, "Optimized multiemitter beams for free-space optical communications through turbulent atmosphere," *Optics Letters*, vol. 32, no. 8, pp. 885–887, Apr. 2007.

[36] J. A. Anguita, M. A. Neifeld, and B. V. Vasic, "Spatial correlation and irradiance statistics in a multiple-beam terrestrial free-space optical communication link," *Applied Optics*, vol. 46, no. 26, pp. 6561–6571, Sep. 2007.

[37] B. Castillo-Vazquez, A. Garcia-Zambrana, and C. Castillo-Vazquez, "Closed-form BER expression for FSO links with transmit laser selection over exponential atmospheric turbulence channels," *Electronics Letters*, vol. 45, no. 23, pp. 1185–1187, Nov. 2009.

[38] E. J. Lee and V. W. S. Chan, "Part 1: Optical communication over the clear turbulent atmospheric channel using diversity," *IEEE Journal on Selected Areas in Communications*, vol. 22, no. 9, pp. 1896–1906, Nov. 2004.

[39] S. G. Wilson, M. Brandt-Pearce, Q. Cao, and J. H. Leveque, "Free-space optical MIMO transmission with Q-ary PPM," *IEEE Transactions on Communications*, vol. 53, no. 8, pp. 1402–1412, Aug. 2005.

[40] S. G. Wilson, M. Brandt-Pearce, Q. Cao, and M. Baedke, "Optical repetition MIMO transmission with multipulse PPM," *IEEE Journal on Selected Areas in Communications*, vol. 23, no. 9, pp. 1901–1910, Sep. 2005.

[41] S. M. Navidpour, M. Uysal, and M. Kavehrad, "BER performance of free-space optical transmission with spatial diversity," *IEEE Transactions on Wireless Communications*, vol. 6, no. 8, pp. 2813–2819, Aug. 2007.

[42] N. Cvijetic, S. G. Wilson, and M. Brandt-Pearce, "Performance bounds for free-space optical MIMO systems with APD receivers in atmospheric turbulence," *IEEE Journal on Selected Areas in Communications*, vol. 26, no. 3, pp. 3–12, Apr. 2008.

[43] N. Letzepis, I. Holland, and W. Cowley, "The Gaussian free space optical MIMO channel with Q-ary pulse position modulation," *IEEE Transactions on Wireless Communications*, vol. 7, no. 5, pp. 1744–1753, May 2008.

[44] L. Zeng, D. C. O'Brien, H. L. Minh, G. E. Faulkner, K. Lee, D. Jung, Y. Oh, and E. T. Won, "High data rate multiple input multiple output (MIMO) optical wireless communications using white LED lighting," *IEEE Journal on Selected Areas in Communications*, vol. 27, no. 9, pp. 1654–1662, Dec. 2009.

[45] T. A. Tsiftsis, H. G. Sandalidis, G. K. Karagiannidis, and M. Uysal, "Optical wireless links with spatial diversity over strong atmospheric turbulence channels," *IEEE Transactions on Wireless Communications*, vol. 8, no. 2, pp. 951–957, Feb. 2009.

[46] E. Bayaki, R. Schober, and R. K. Mallik, "Performance analysis of MIMO free-space optical systems in Gamma–Gamma fading," *IEEE Transactions on Communications*, vol. 57, no. 11, pp. 3415–3424, Nov. 2009.

[47] R. Mesleh, R. Mehmood, H. Elgala, and H. Haas, "Indoor MIMO optical wireless communication using spatial modulation," in *IEEE International*

Conference on Communications, Cape Town, South Africa, May 2010, pp. 1–5.

[48] N. D. Chatzidiamantis, M. Uysal, T. A. Tsiftsis, and G. K. Karagiannidis, "Iterative near maximum-likelihood sequence detection for MIMO optical wireless systems," *Journal of Lightwave Technology*, vol. 28, no. 7, pp. 1064–1070, Apr. 2010.

[49] C. Abou-Rjeily, "On the optimality of the selection transmit diversity for MIMO-FSO links with feedback," *IEEE Communications Letters*, vol. 15, no. 6, pp. 641–643, Jun. 2011.

[50] H. Hashemi, G. Yun, M. Kavehrad, F. Behbahani, and P. A. Galko, "Indoor propagation measurements at infrared frequencies for wireless local area networks applications," *IEEE Transactions on Vehicular Technology*, vol. 43, no. 3, pp. 562–567, Aug. 1994.

[51] J. M. Kahn, W. J. Krause, and J. B. Carruthers, "Experimental characterization of non-directed indoor infrared channels," *IEEE Transactions on Communications*, vol. 43, no. 2/3/4, pp. 1613–1623, Feb./Mar./Apr. 1995.

[52] J. R. Barry, J. M. Kahn, W. J. Krause, E. A. Lee, and D. G. Messerschmitt, "Simulation of multipath impulse response for indoor wireless optical channels," *IEEE Journal on Selected Areas in Communications*, vol. 11, no. 3, pp. 367–379, Apr. 1993.

[53] T. Komine and M. Nakagawa, "Fundamental analysis for visible-light communication system using LED lights," *IEEE Transactions on Consumer Electronics*, vol. 50, no. 1, pp. 100–107, Feb. 2004.

[54] D. Kedar and S. Arnon, "Urban optical wireless communication networks: The main challenges and possible solutions," *IEEE Communications Magazine*, vol. 42, no. 5, pp. S2–S7, May 2004.

[55] H. Elgala, R. Mesleh, and H. Haas, "Indoor optical wireless communication: Potential and state-of-the-art," *IEEE Communications Magazine*, vol. 49, no. 9, pp. 56–62, Sep. 2011.

[56] T. Fath and H. Haas, "Performance comparison of MIMO techniques for optical wireless communications in indoor environments," *IEEE Transactions on Communications*, vol. 61, no. 2, pp. 733–742, Feb. 2013.

[57] J. B. Carruthers and P. Kannan, "Iterative site-based modeling for wireless infrared channels," *IEEE Transactions on Antennas and Propagation*, vol. 50, no. 5, pp. 759–765, May 2002.

[58] J. B. Carruthers, S. M. Carroll, and P. Kannan, "Propagation modelling for indoor optical wireless communications using fast multi-receiver channel estimation," *IEE Proceedings - Optoelectronics*, vol. 150, no. 5, pp. 473–481, Oct. 2003.

[59] C. Gong and Z. Xu, "Channel estimation and signal detection for optical wireless scattering communication with inter-symbol interference," *IEEE Transactions on Wireless Communications*, vol. 14, no. 10, pp. 5326–5337, Oct. 2015.

[60] X. Chen and M. Jiang, "Adaptive statistical Bayesian MMSE channel estimation for visible light communication," *IEEE Transactions on Signal Processing*, vol. 65, no. 5, pp. 1287–1299, Mar. 2017.

[61] T. Foggi, G. Colavolpe, E. Forestieri, and G. Prati, "Channel estimation algorithms for MLSD in optical communication systems," *IEEE Photonics Technology Letters*, vol. 18, no. 19, pp. 1984–1986, Oct. 2006.

[62] W. Chung, "Channel estimation methods based on Volterra kernels for MLSD in optical communication systems," *IEEE Photonics Technology Letters*, vol. 22, no. 4, pp. 224–226, Feb. 2010.

[63] P. A. Haigh, Z. Ghassemlooy, S. Rajbhandari, I. Papakonstantinou, and W. Popoola, "Visible light communications: 170 mb/s using an artificial neural network equalizer in a low bandwidth white light configuration," *Journal of Lightwave Technology*, vol. 32, no. 9, pp. 1807–1813, May 2014.

[64] J. Hightower and G. Borriello, "Location systems for ubiquitous computing," *Computer*, vol. 34, no. 8, pp. 57–66, Aug. 2001.

[65] J. J. Caffery and G. L. Stuber, "Overview of radiolocation in CDMA cellular systems," *IEEE Communications Magazine*, vol. 36, no. 4, pp. 38–45, Apr. 1998.

[66] N. Bulusu, J. Heidemann, and D. Estrin, "GPS-less low-cost outdoor localization for very small devices," *IEEE Personal Communications*, vol. 7, no. 5, pp. 28–34, Oct. 2000.

[67] A. H. Sayed, A. Tarighat, and N. Khajehnouri, "Network-based wireless location: Challenges faced in developing techniques for accurate wireless location information," *IEEE Signal Processing Magazine*, vol. 22, no. 4, pp. 24–40, Jul. 2005.

[68] A. Boukerche, H. A. B. F. Oliveira, E. F. Nakamura, and A. A. F. Loureiro, "Localization systems for wireless sensor networks," *IEEE Wireless Communications*, vol. 14, no. 6, pp. 6–12, Dec. 2007.

[69] R. Chellappa and S. Theodoridis, Eds., *Academic Press Library in Signal Processing: Volume 3—Array and Statistical Signal Processing.* Waltham, MA: Academic Press, 2014.

[70] T. S. Rappaport, J. H. Reed, and B. D. Woerner, "Position location using wireless communications on highways of the future," *IEEE Communications Magazine*, vol. 34, no. 10, pp. 33–41, Oct. 1996.

[71] C. Savarese, J. M. Rabaey, and J. Beutel, "Location in distributed ad-hoc wireless sensor networks," in *IEEE International Conference on Acoustics, Speech, and Signal Processing*, Salt Lake City, UT, May 2001, pp. 2037–2040.

[72] V. Seshadri, G. V. Zaruba, and M. Huber, "A Bayesian sampling approach to in-door localization of wireless devices using received signal strength indication," in *Third IEEE International Conference on Pervasive Computing and Communications*, Kauai Island, HI, Mar. 2005, pp. 75–84.

[73] C.-L. Wang, Y.-S. Chiou, and S.-C. Yeh, "A location algorithm based on radio propagation modeling for indoor wireless local area networks," in *IEEE 61st Vehicular Technology Conference*, Stockholm, Sweden, May/Jun. 2005, pp. 1–5.

[74] X. Li, "RSS-based location estimation with unknown pathloss model," *IEEE Transactions on Wireless Communications*, vol. 5, no. 12, pp. 3626–3633, Dec. 2006.

[75] P. Tarrio, A. M. Bernardos, and J. R. Casar, "An RSS localization method based on parametric channel models," in *International Conference on Sensor Technologies and Applications*, Valencia, Spain, Oct. 2007, pp. 265–270.

[76] K. Whitehouse, C. Karlof, and D. Culler, "A practical evaluation of radio signal strength for ranging-based localization," *Mobile Computing and Communications Review*, vol. 11, no. 1, pp. 41–52, Jan. 2007.

[77] M. I. Silventoinen and T. Rantalainen, "Mobile station emergency locating in GSM," in *IEEE International Conference on Personal Wireless Communications*, New Delhi, India, Feb. 1996, pp. 232–238.

[78] J.-Y. Lee and R. A. Scholtz, "Ranging in a dense multipath environment using an UWB radio link," *IEEE Journal on Selected Areas in Communications*, vol. 20, no. 9, pp. 1677–1683, Dec. 2002.

[79] J. Benesty, J. Chen, and Y. Huang, "Time-delay estimation via linear interpolation and cross correlation," *IEEE Transactions on Speech and Audio Processing*, vol. 12, no. 5, pp. 509–519, Sep. 2004.

[80] C. Knapp and G. Carter, "The generalized correlation method for estimation of time delay," *IEEE Transactions on Acoustics, Speech, and Signal Processing*, vol. 24, no. 4, pp. 320–327, Aug. 1976.

[81] J. Smith and J. Abel, "Closed-form least-squares source location estimation from range-difference measurements," *IEEE Transactions on Acoustics, Speech, and Signal Processing*, vol. 35, no. 12, pp. 1661–1669, Dec. 1987.

[82] H. Schau and A. Robinson, "Passive source localization employing intersecting spherical surfaces from time-of-arrival differences," *IEEE Transactions on Acoustics, Speech, and Signal Processing*, vol. 35, no. 8, pp. 1223–1225, Aug. 1987.

[83] Y. T. Chan and K. C. Ho, "A simple and efficient estimator for hyperbolic location," *IEEE Transactions on Signal Processing*, vol. 42, no. 8, pp. 1905–1915, Aug. 1994.

[84] M. S. Brandstein, J. E. Adcock, and H. F. Silverman, "A closed-form location estimator for use with room environment microphone arrays," *IEEE Transactions on Speech and Audio Processing*, vol. 5, no. 1, pp. 45–50, Jan. 1997.

[85] K. J. Krizman, T. E. Biedka, and T. S. Rappaport, "Wireless position location: Fundamentals, implementation strategies, and sources of error," in *IEEE 47th Vehicular Technology Conference*, Phoenix, AZ, May 1997, pp. 919–923.

[86] S. Tekinay, "Wireless geolocation systems and services," *IEEE Communications Magazine*, vol. 36, no. 4, p. 28, Apr. 1998.

[87] F. Gustafsson and F. Gunnarsson, "Positioning using time-difference of arrival measurements," in *IEEE International Conference on Acoustics, Speech, and Signal Processing*, Hong Kong, Hong Kong, Apr. 2003, pp. 553–556.

[88] L. Yang and K. C. Ho, "An approximately efficient TDOA localization algorithm in closed-form for locating multiple disjoint sources with erroneous sensor positions," *IEEE Transactions on Signal Processing*, vol. 57, no. 12, pp. 4598–4615, Dec. 2009.

[89] M. Gavish and A. J. Weiss, "Performance analysis of bearing-only target location algorithms," *IEEE Transactions on Aerospace and Electronic Systems*, vol. 28, no. 3, pp. 817–828, Jul. 1992.

[90] L. M. Kaplan, Q. Le, and N. Molnar, "Maximum likelihood methods for bearings-only target localization," in *IEEE International Conference on Acoustics, Speech, and Signal Processing*, Salt Lake City, UT, May 2001, pp. 3001–3004.

[91] H.-J. Shao, X.-P. Zhang, and Z. Wang, "Efficient closed-form algorithms for AOA based self-localization of sensor nodes using auxiliary variables," *IEEE Transactions on Signal Processing*, vol. 62, no. 10, pp. 2580–2594, May 2014.

[92] J. Werner, J. Wang, A. Hakkarainen, N. Gulati, D. Patron, D. Pfeil, K. Dandekar, D. Cabric, and M. Valkama, "Sectorized antenna-based DoA estimation and localization: Advanced algorithms and measurements," *IEEE Journal on Selected Areas in Communications*, vol. 33, no. 1, pp. 2272–2286, Nov. 2015.

[93] P. Stoica and A. Nehorai, "MUSIC, maximum likelihood, and Cramer–Rao bound: Further results and comparisons," *IEEE Transactions on Acoustics, Speech, and Signal Processing*, vol. 38, no. 12, pp. 2140–2150, Dec. 1990.

[94] H. Zamiri-Jafarian, M. M. Mirsalehi, I. Ahadi-Akhlaghi, and H. Keshavarz, "A neural network-based mobile positioning with hierarchical structure," in *The 57th IEEE Semiannual Vehicular Technology Conference*, Jeju, Korea, Apr. 2003, pp. 2003–2007.

[95] W. Jung, W. Woo, and S. Lee, "Orientation tracking exploiting ubiTrack," in *The Seventh International Conference on Ubiquitous Computing*, Tokyo, Japan, Sep. 2005, pp. 47–50.

[96] N. B. Priyantha, A. K. L. Miu, H. Balakrishnan, and S. Teller, "The cricket compass for context-aware mobile applications," in *The Seventh Annual International Conference on Mobile Computing and Networking*, Rome, Italy, Jul. 2001, pp. 1–14.

[97] J. R. Gonzalez and C. J. Bleakley, "High-precision robust broadband ultrasonic location and orientation estimation," *IEEE Journal of Selected Topics in Signal Processing*, vol. 3, no. 5, pp. 832–844, Oct. 2009.

[98] R. L. Moses, D. Krishnamurthy, and R. M. Patterson, "A self-localization method for wireless sensor networks," *EURASIP Journal on Advances in Signal Processing*, vol. 2003, no. 4, pp. 348–358, Dec. 2003.

[99] H. Krim and M. Viberg, "Two decades of array signal processing research: The parametric approach," *IEEE Signal Processing Magazine*, vol. 13, no. 4, pp. 67–94, Aug. 1996.

[100] A. Manikas, Ed., *Beamforming: Sensor Signal Processing for Defence Applications*. London, UK: Imperial College Press, 2015.

[101] A. Manikas and M. Sethi, "A space–time channel estimator and single-user receiver for code-reuse DS-CDMA systems," *IEEE Transactions on Signal Processing*, vol. 51, no. 1, pp. 39–51, Jan. 2003.

[102] P. Karaminas and A. Manikas, "Super-resolution broad null beamforming for cochannel interference cancellation in mobile radio networks," *IEEE Transactions on Vehicular Technology*, vol. 49, no. 3, pp. 689–697, May 2000.

[103] A. Manikas and L. K. Huang, "STAR channel estimation in DS-CDMA communication systems," *IEE Proceedings - Communications*, vol. 151, no. 4, pp. 387–393, Aug. 2004.

[104] D. J. Sadler and A. Manikas, "MMSE multiuser detection for array multicarrier DS-CDMA in fading channels," *IEEE Transactions on Signal Processing*, vol. 53, no. 7, pp. 2348–2358, Jul. 2005.

[105] D. Estrin, L. Girod, G. Pottie, and M. Srivastava, "Instrumenting the world with wireless sensor networks," in *IEEE International Conference on Acoustics, Speech, and Signal Processing*, Salt Lake City, UT, May 2001, pp. 2033–2036.

[106] Z. Fang and A. Manikas, "Arrayed space optical communications: Localization of the ground station," in *IEEE International Conference on Communications*, Paris, France, May 2017, pp. 1–6.

[107] E. Venieris and A. Manikas, "Near–far field multipath spatial–temporal localisation," in *IEEE International Conference on Communications*, Paris, France, May 2017, pp. 1–6.

[108] A. Ward, A. Jones, and A. Hopper, "A new location technique for the active office," *IEEE Personal Communications*, vol. 4, no. 5, pp. 42–47, Oct. 1997.

[109] J. R. Lowell, "Military applications of localization, tracking, and targeting," *IEEE Wireless Communications*, vol. 18, no. 2, pp. 60–65, Apr. 2011.

[110] T.-J. Shan, M. Wax, and T. Kailath, "On spatial smoothing for direction-of-arrival estimation of coherent signals," *IEEE Transactions on Acoustics, Speech, and Signal Processing*, vol. 33, no. 4, pp. 806–811, Aug. 1985.

[111] Z. Fang and A. Manikas, "DOA and range estimation of multiple sources under the wideband assumption," in *IEEE Global Communications Conference*, Washington, D.C., Dec. 2016, pp. 1–6.

[112] K. I. Pedersen, P. E. Mogensen, and B. H. Fleury, "A stochastic model of the temporal and azimuthal dispersion seen at the base station in outdoor propagation environments," *IEEE Transactions on Vehicular Technology*, vol. 49, no. 2, pp. 437–447, Mar. 2000.

[113] F. Rashid and A. Manikas, "Arrayed MC-CDMA reception in space–time diffused multipath vector channels," *Wireless Communications and Mobile Computing*, vol. 8, no. 5, pp. 575–584, Jun. 2007.

[114] Y. I. Abramovich, N. K. Spencer, and A. Y. Gorokhov, "Positive-definite Toeplitz completion in DOA estimation for nonuniform linear antenna arrays—Part II: Partially augmentable arrays," *IEEE Transactions on Signal Processing*, vol. 47, no. 6, pp. 1502–1521, Jun. 1999.

[115] ——, "Resolving manifold ambiguities in direction-of-arrival estimation for nonuniform linear antenna arrays," *IEEE Transactions on Signal Processing*, vol. 47, no. 10, pp. 2629–2643, Oct. 1999.

[116] S. Supakwong, A. Manikas, and A. G. Constantinides, "Resolving manifold ambiguities in direction finding systems," in *15th European Signal Processing Conference*, Poznan, Poland, Sep. 2007, pp. 95–99.